GA-A16764
UC-77

RADIOCHEMICAL ANALYSIS OF THE FIRST PLATEOUT PROBE FROM THE FORT ST. VRAIN HIGH-TEMPERATURE GAS-COOLED REACTOR

by
R. D. BURNETTE

Work supported in part by
Department of Energy
Contract DE-AT03-76ET35300
and in part by
Public Service Company of Colorado
Purchase Order Number N-2240

JUNE 1982

GENERAL ATOMIC COMPANY

DISCLAIMER

Printed in the United States of America
Available from
National Technical Information Service
U.S. Department of Commerce
5285 Port Royal Road
Springfield, VA. 22161

NTIS price codes
Printed copy: A06
Microfiche copy: A01

GA-A16764
UC-77

RADIOCHEMICAL ANALYSIS OF THE FIRST PLATEOUT PROBE FROM THE FORT ST. VRAIN HIGH-TEMPERATURE GAS-COOLED REACTOR

by
R. D. BURNETTE

Work supported in part by
Department of Energy
Contract DE-AT03-76ET35300
and in part by
Public Service Company of Colorado
Purchase Order Number N-2240

GENERAL ATOMIC PROJECT 6400 AND 2970
JUNE 1982

GENERAL ATOMIC COMPANY

FOREWORD

The analysis reported herein was sponsored jointly by the Public Service Company of Colorado and by the U.S. Department of Energy. The Public Service Company of Colorado sponsored the work on iodine, strontium, and sulfur isotopes. The Department of Energy sponsored the analysis of all other radionuclides.

ABSTRACT

This report presents the analysis of radioactive elements on the first plateout probe from the Fort St. Vrain high-temperature gas-cooled reactor. The plateout probe is a device which samples the primary coolant for condensible fission products. Circuit inventories of individual radionuclides are estimated from the probe analysis. The analysis shows that the radioactive contamination in the primary circuit is remarkably low, with activation product concentrations much greater than that of fission products. The analysis demonstrates that the concentrations of the key fission products I-131 and Sr-90 are far below the limits allowed by the technical specification.

CONTENTS

FIGURES

FIGURES (Continued)

TABLES

TABLES (Continued)

1. SUMMARY AND MAIN CONCLUSIONS

Radiochemical analysis of the first plateout probe from the Fort St. Vrain (FSV) high-temperature gas-cooled reactor (HTGR) is complete. The main conclusion of this analysis is that the concentrations of I-131 and Sr-90 in the primary circuit are far below the allowable limits specified in Technical Specification LCO 4.2.8. This conclusion is reached even though the probe may not have quantitatively sampled iodine. Other available data on iodine behavior, including the iodine monitor and grab sample xenon release rate/birthrate (R/B) measurements can be used at present to show compliance with the iodine specification.

Another important finding is that, to date, little or no barium, cesium, or strontium was directly released from the core. Rather, these volatile metals were released only via their gaseous precursors xenon and krypton. Once in the primary circuit, a large fraction of these metals apparently affix to small dust or aerosol particles and are thereby transported around the circuit. In addition, the concentrations of Ba-140 and Sr-90 show that the R/B of short half-life xenon and krypton isotopes can be accurately estimated by straight-line extrapolation of the R/B versus half-life ($t^{1/2}$) curve. Finally, the concentration of H_2S in the helium coolant is apparently below that required for deleterious sulphidation corrosion.

2. INTRODUCTION

This report presents a radiochemical analysis of the first plateout probe from FSV. The probe was removed from the reactor following shutdown on November 9, 1981 after 408 equivalent full power days of operation. Prior to shutdown, the reactor had attained 100% power for the first time. Figure 2-1 shows a plot of reactor power history in 1981. The probe had been in place sampling the helium coolant since reactor startup in July 1976. This report collects all the radiochemical data obtained. These data are required to assure compliance with the requirements for Sr-90 and I-131 concentrations given in Technical Specification LCO 4.2.8.

2.1. OBJECTIVES OF THE PLATEOUT PROBE

The plateout probe samples the hot primary coolant gas for condensible fission products. It allows the amount of circulating and condensed key fission products in the circuit to be calculated. Fort St. Vrain Technical Specification LCO 4.2.8 limits the concentrations of I-131 and Sr-90. The probe is intended to be the primary means of demonstrating compliance with LCO 4.2.8. However, this device can also meet other objectives:

1. Assure compliance with LCO 4.2.8 for I-131 and Sr-90.

2. Measure vapor pressure of sulfur.

3. Determine extent of metallic corrosion.

4. Measure concentrations of other fission products.

5. Determine chemical species of condensed products and mode of transport to tubes.

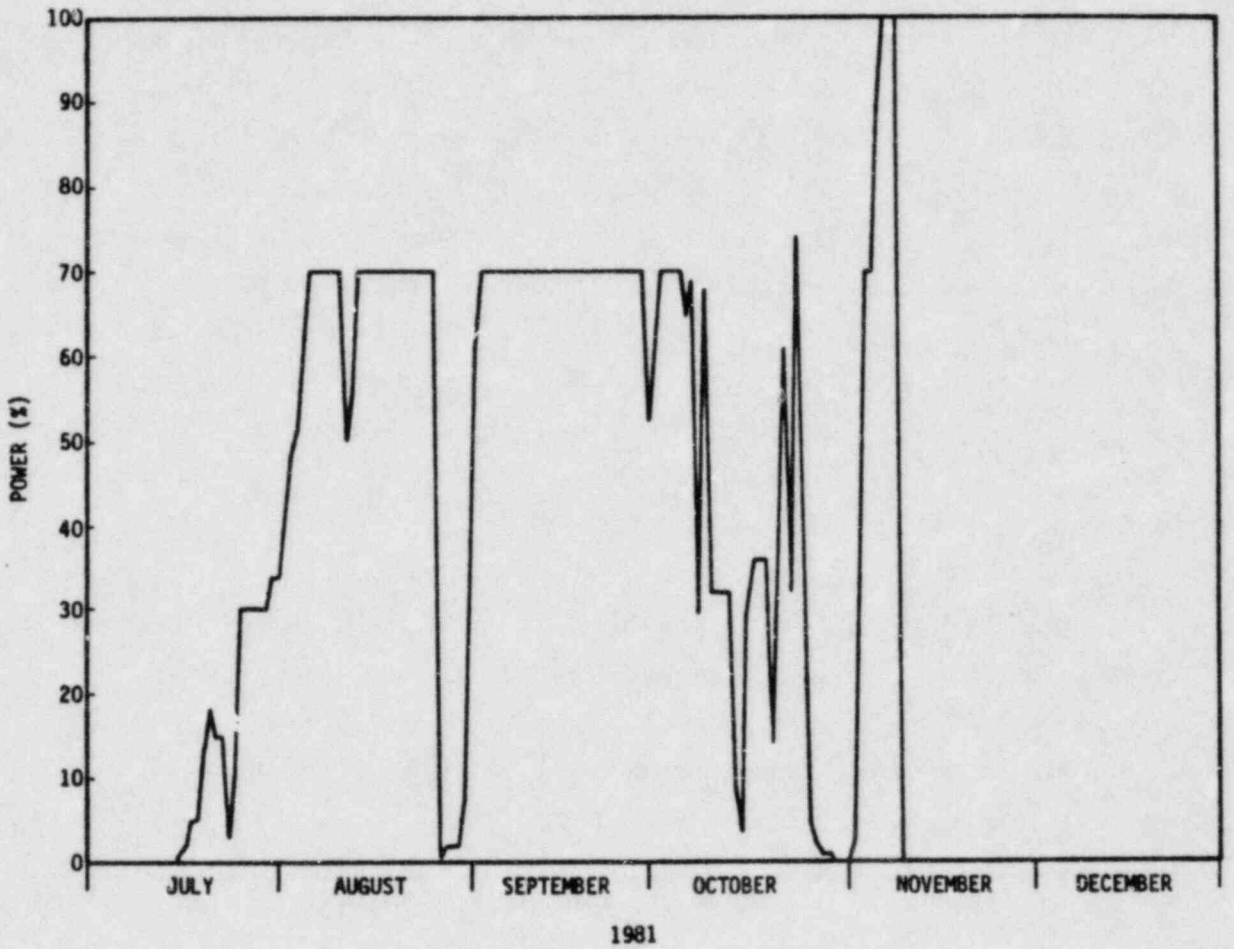

Fig. 2-1. Fort St. Vrain reactor power history in 1981

6. Measure neutron flux at the probe from analysis of activation products.

2.1.1. Compliance With Technical Specification LCO 4.2.8

Because circulating and plated-out fission products are the initial source terms for certain accident scenarios, technical specifications have been established to assure that the 10CFR100 dose limits would not be exceeded in the event of a design basis depressurization accident (FSV design basis accident No. 2). Technical Specification LCO 4.2.8 established the following limits and described their basis:

1. The product of primary coolant noble gas beta plus gamma activity times $\bar{E}$ shall not exceeed 1.09 Ci-MeV/kg (2.40 Ci-MeV/lb) (where $\bar{E}$ is the weighted average of the beta and gamma energies per disintegration in MeV), when measured 15 min after sampling.

2. The primary coolant circulating halogen inventory shall not exceed an I-131 thyroid dose equivalent of 24 Ci.

3. The plateout halogen inventory shall not exceed an I-131 thyroid dose equivalent of 5000 Ci/loop (10,000 total).

4. The plateout Sr-90 inventory shall not exceed a Sr-90 bone dose equivalent of 140 Ci/loop (280 Ci total).

5. Determination of $\bar{E}$ will be performed at least once a month, and in any event, will be performed each time that the primary coolant radioactivity concentration changes by 25% from the previous measurement.

To enable compliance with Technical Specification LCO 4.2.8, analytical instrumentation has been installed in FSV to directly measure fission products in the primary coolant circuit. This instrumentation includes a continuous circulating activity monitor; gas sampling systems to measure

fission gases, including iodine isotopes; and plateout probes to measure condensible species, especially Sr-90 and I-131. This report is intended to describe the radiochemical data and analysis of the first plateout probe in detail.

The various measurements and predictions of fission product activity are complementary and must be interpreted collectively to obtain the best estimate of the total circuit inventory. For example, essentially all of the Sr-90 in the primary circuit was expected to arise from decay of its short-lived gaseous precursor Kr-90 (32 s half-life). Obviously, the most straightforward way to determine the amount of Sr-90 so produced is by directly measuring the Kr-90 inventory in the primary circuit. The concentration of Kr-90 has been too low for direct measurement. Therefore, the Kr-90 release rate from the core has been determined by extrapolating the measured release rates of longer lived krypton isotopes, since the functional relationship between the R/B of the fission gases from coated particle fuel and their half-lives is well established. In the case of Sr-90 directly released from the core, mechanistic transport calculations and plateout probe measurements must be relied upon. Section 2.3.1 gives details on strontium analyses.

A similar situation exists for determining I-131 inventories. Experiments showed that the R/B value of an iodine isotope is equal to, or slightly less than, that of a xenon isotope of the same half-life. Therefore, the I-131 plateout inventory is easily determined by calculating its R/B, and hence release rate, by measuring the xenon isotopes in the primary coolant and conservatively assuming that all of the released I-131 is plated out. Plateout concentration of I-131 can also be inferred by directly measuring plateout of other iodine isotopes, I-135 and I-133, using a procedure which involves gamma counting coolant samples for the daughter Xe-135 and Xe-133 following reactor shutdown. This procedure has been used at FSV. The results show that iodine release to the primary circuit can be accurately calculated using the R/B of xenon at the half-life of the iodine isotope.

Directly measuring circulating iodine during reactor operation is more difficult. The plateout probe was designed specifically to collect iodine isotopes and therefore directly measure the concentration of I-131 in the coolant helium. In addition, the circulating I-131 concentration may be inferred from direct measurements of circulating I-135 and I-133 using the iodine monitor. Section 2.3.4 describes in detail all of these ancillary methods and results for iodine analysis, because they bear directly on the results obtained from the plateout probe.

2.1.2. Measurement of the Vapor Pressure of Gaseous Sulfur

In principle, the vapor pressure of sulfur (presumably H_2S) can be determined by analyzing the inventory of S-35 found in the diffusion tubes. It is important to determine whether corrosion can occur via the formation of metallic sulfides. Section 2.3.5 gives details on this analysis.

2.1.3. Extent of Metallic Corrosion

A special sleeve was added to the outside of the probe body expressly to provide samples for metallographic examination. The extent of corrosion by oxidation, carburization, and sulphidation has been determined in Ref. 1.

2.1.4. Concentration of Other Fission Products and Mode of Transport

The distribution of all fission products in the primary circuit can be inferred from the concentrations found on and inside the plateout probe. Moreover, by analyzing the axial profiles of the fission products in the diffusion tubes, the chemical species or mode of transport can be determined. Possible modes include (1) gaseous (atomic or molecular) transport (i.e., iodine vapor, H_2S vapor, cesium vapor), (2) gaseous precursor transport (i.e., Kr-90 → Sr-90), and (3) transport of nuclides attached to dust or aerosol particles. The concentrations and modes of transport are discussed in the sections on individual nuclides.

2.1.5. Neutron Flux at the Probe

By measuring the concentration of nuclides formed by direct neutron activation, estimates of the neutron flux at this point in the circuit can be checked. This is important to accurately assess the formation of activation products in the primary circuit at locations where maintenance is important. Section 4.4 discusses the activation products.

2.2. DESIGN OF THE PLATEOUT PROBE

The design of the probe was first described in Ref. 2. Later, Ref. 3 amplified this report and provided details on the analysis and interpreted results. Portions of those documents are excerpted below.

Figure 2-2 is a cross section of the reactor vessel showing the location of the plateout probes. One sample stream is taken from each coolant loop at the inlet to the steam generator and exhausted to the inlet of the circulator. A second sample stream is taken from the return coolant and is also exhausted to the circulator inlet. Figure 2-3 shows the details of the plateout probes. These probes are inserted through a nozzle in the prestressed concrete reactor vessel (PCRV) and into a penetration through the wall of the steam generator. Thus, they extend into the high-temperature gas at the inlet to the steam generator.

The probe is clamped into the steam generator penetration with a bayonet-type lock. Four diffusion tube sample streams are taken from the hot-gas stream inside the steam generator and a fifth is taken from the cold return gas on the outside of the steam generator. All of these flows exhaust into a collection plenum located between the two metal O-ring seals. From there, the flow is taken out of the port located on top of the steam generator penetration and routed down through the lower cavity floor to the inlet to the circulators (as indicated in Fig. 2-2). Thus, the flows are driven by the normal pressure differences of the reactor circuit [approximately 17 kPa (2.5 psi) for the hot gas samples and 34 kPa (5 psi) for the cold gas sample]. These pressure drops are essentially the pressure drop

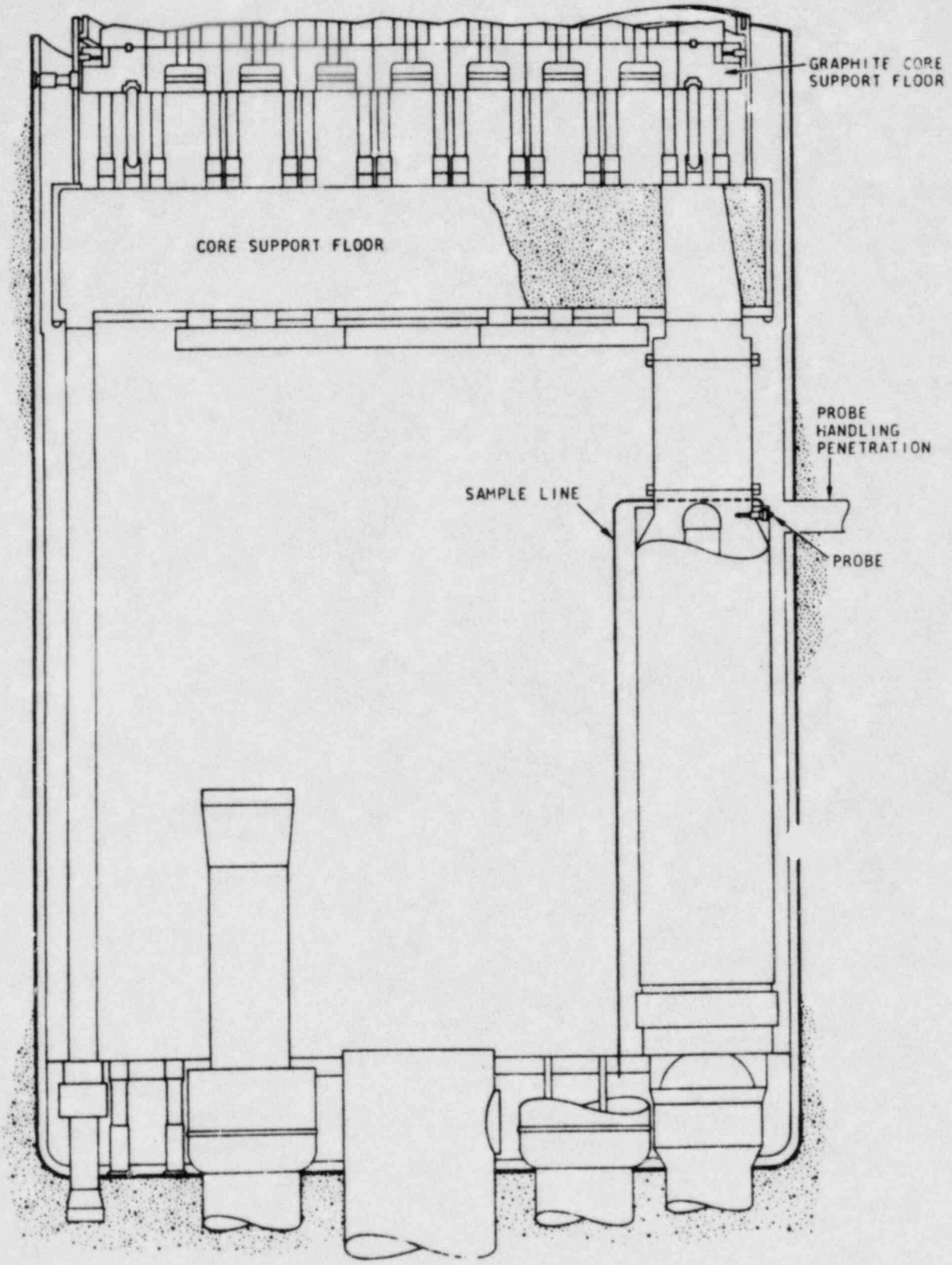

Fig. 2-2. Fission product plateout probe axial location

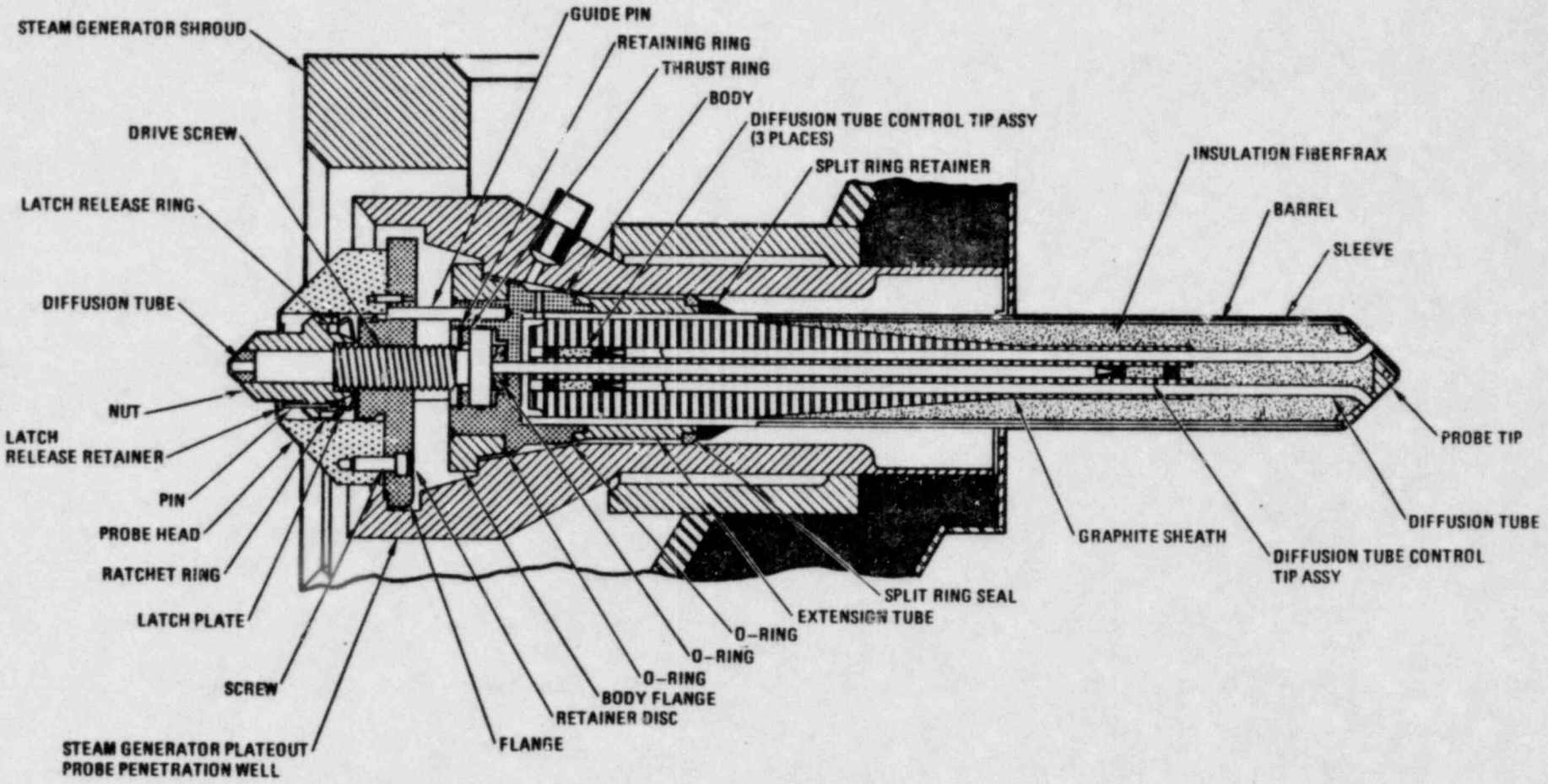

Fig. 2-3. Plateout probe

across the steam generator and across the entire primary circuit, respectively. The quoted values are approximate averages for 70% power, where almost all of the operation to date has occurred.

Each individual diffusion tube is approximately 33 cm (13 in.) long and contains a series of filters: two fiberfrax filters for removing excess particulate matter, an activated charcoal filter for removing all sorbable fission products, and finally a porous metal filter. Figure 2-4 shows the overall assembly. Note that the leading fiberfrax filter has a conical indentation in its frontal face to increase the amount of surface area to minimize the effect of dust buildup. The porous metal filter overwhelmingly offers the largest flow resistance so that the loading of the upstream fiberfrax and charcoal filters with particulate matter (construction debris, carbon dust, etc.) should not appreciably increase the total flow resistance (which would, of course, result in a decreased volumetric flow rate). Figure 2-5 is a photograph of an as-manufactured probe. All individual diffusion probes were calibrated with flowing helium prior to the assembly of the overall probe. Upon removal from the reactor, all tubes were flow tested to check the initial calibration. If the flow resistance had increased, the core release rate of important fission products could still be conservatively estimated by assuming that the end-of-life flow rate (i.e., the minimum flow rate) prevailed for the entire operating period.

For ease of identification, the tubes are labeled with a letter indicating their position when the probe is viewed from the locking mechanism end of the probe (that is, Top, Center, Bottom, Left, and Right). Each of these tubes has a slightly different function. The T, B, and R tubes were designed to provide information about the larger dust particles in the reactor circuit; their collection efficiency for the larger dust particles was thought to be influenced by the entrance configuration of the tube, in contrast to the smaller dust particles which will be collected equally by all of the diffusion tubes. The T tube faces upstream and will collect more large particles than the R tube, which faces perpendicular to the flow, and the B tube, which faces downstream.

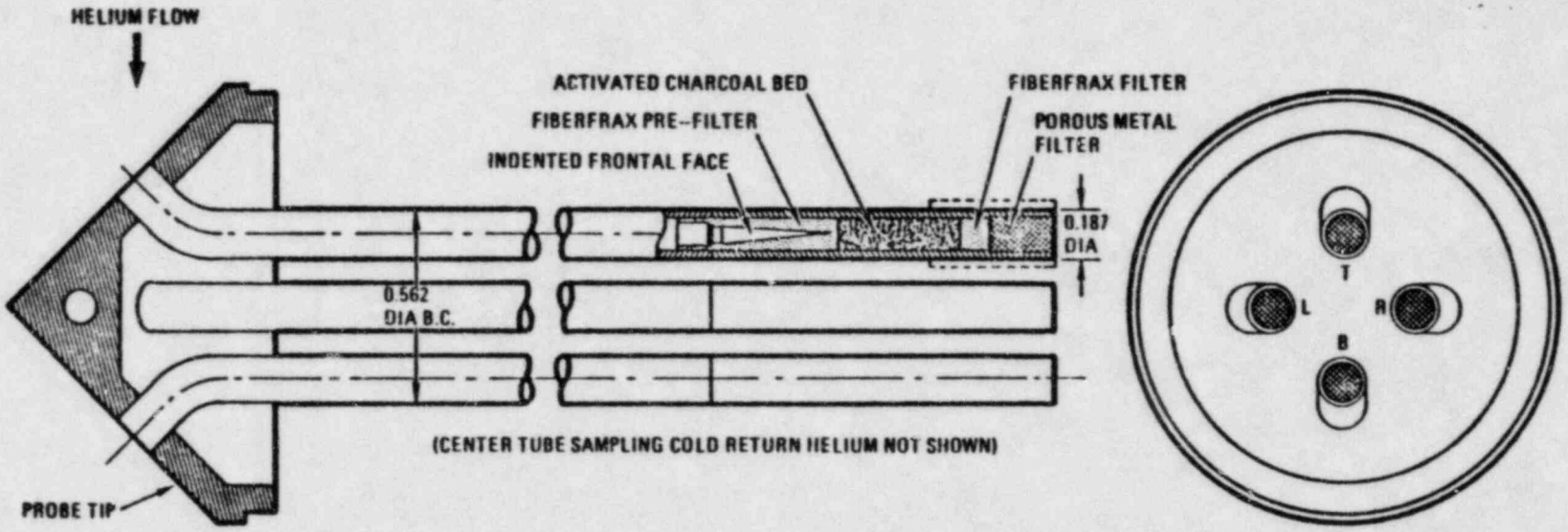

Fig. 2-4. Diffusion probe details

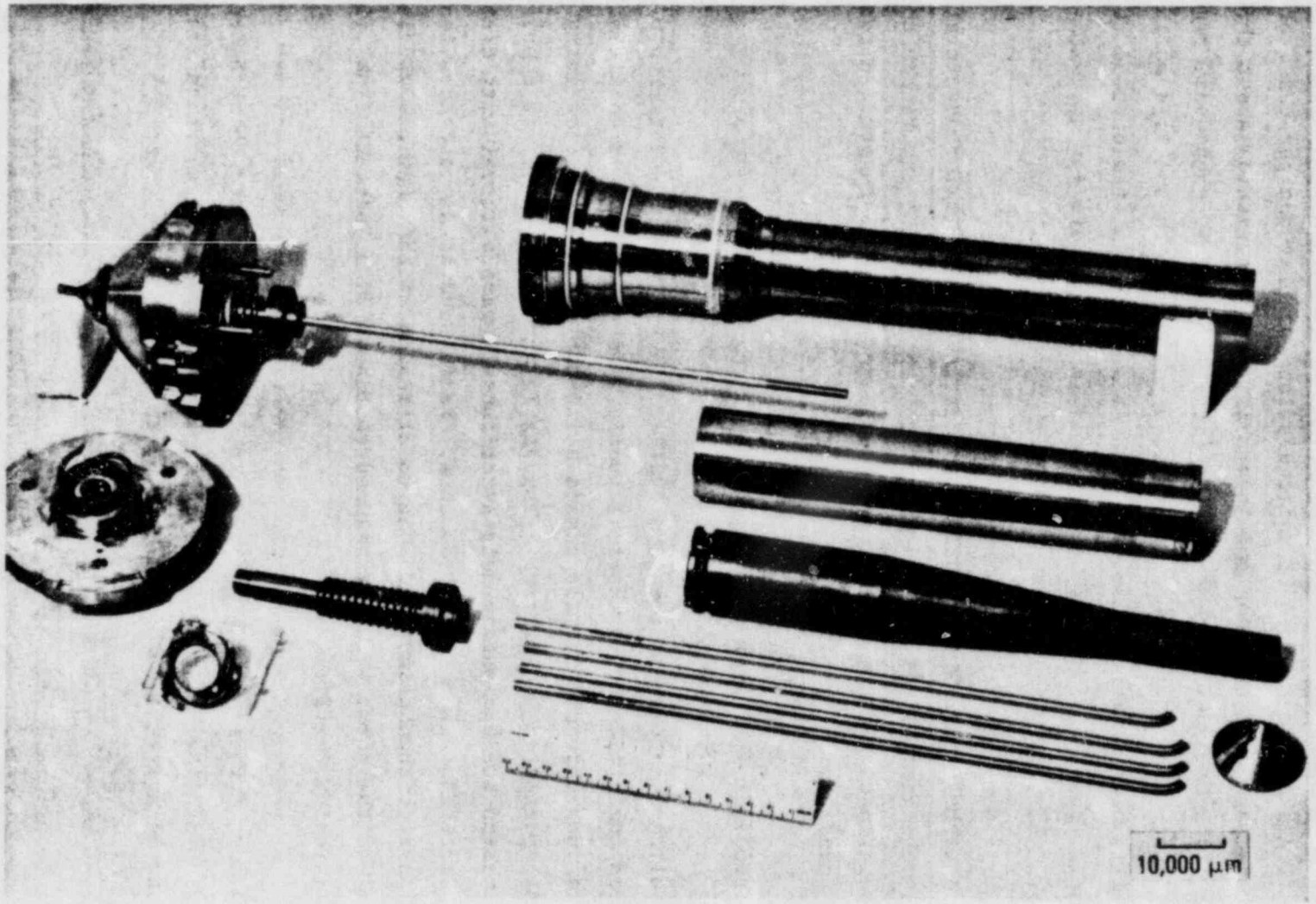

Fig. 2-5. As-manufactured probe parts

The C tube processes a sample of the return coolant gas and provides information about the amount of recirculation (or plateout per pass) of fission products around the loop and thus additional information about the physical form of the different species (e.g., elemental, compounds, precursor, or dust-borne). The L tube is also a Low flow tube and is specifically designed to help distinguish between dust and noble gas fission product transport. These points will be discussed in more detail in the next section.

The probe has an arrangement of insulation and thermal conductors to maintain the greater part of the diffusion tube length at the return coolant gas temperature. Figure 2-6 shows the expected temperature profile for 100% power operation.

2.3. THEORY OF DIFFUSION TUBES

A diffusion tube, as the name implies, is a device for determining the diffusion coefficient of a chemical species. Essentially, it consists of a reactive tube through which is passed a laminar flow of gas containing the chemical species to be analyzed. The gas is assumed to enter at a uniform concentration and instantaneously establishes a parabolic velocity distribution across the diameter of the tube. Radial and axial concentration distributions are then established due to diffusion of the chemical species to the wall of the tube, which is assumed to behave as a "perfect sink" (i.e., a unit sticking coefficient).

Various investigators (Refs. 4 through 7) have treated this theoretical problem. In terms of the axial surface distribution, the solution can be expressed as a variation of the Gormley-Kennedy equation (Ref. 5):

$$A(Z) = \frac{A_T D}{Q} \left(9.4106e^{-11.489DZ/Q} + 6.8309e^{-70.06DZ/Q} + 5.8198e^{-179.07DZ/Q} + \ldots\right) , \qquad (2\text{-}1)$$

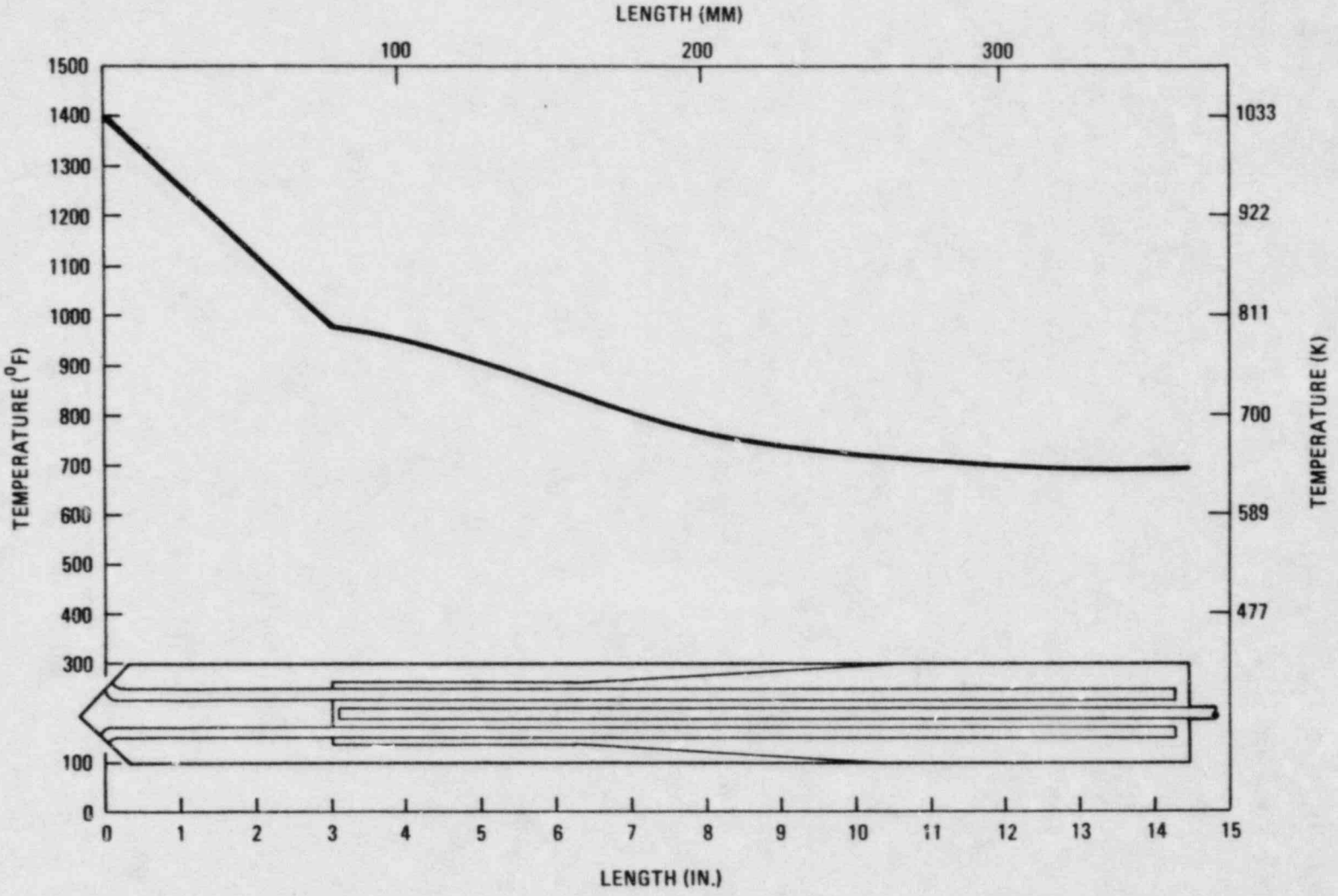

Fig. 2-6. Diffusion tube temperature profile

where A(Z) = activity on the surface per centimeter of tube length (μCi/cm),

A_T = total amount that has entered the tube (μCi),

D = diffusion coefficient (cm^2/s),

Q = volumetric flow rate (cm^3/s),

Z = distance from the entrance of tube (cm).

If the flow rate is sufficiently low, the higher order terms are much smaller than the first term in the series. On the other hand, for low values of D, which is the case for aerosol particles, the entire equation must be used.

2.3.1. Condensible Metallic Species

Figure 2-7 is a plot showing profiles to be expected in the L tube for (1) condensible elements, (2) gaseous precursor, and (3) dust-borne species. The steep profile was calculated using the Gormley-Kennedy equation (Eq. 2-1), for a vapor species having a diffusion coefficient of 0.1 cm^2/s, which is approximately correct for strontium, cesium, and barium vapor species in helium at 4.7 MPa (46 atm). The calculated profiles in Fig. 2-7 are for isothermal conditions. In fact, the FSV diffusion tubes operated somewhat cooler and were not isothermal (see Fig. 2-6). Nevertheless, temperature is a "second order effect" in this case; a steep concentration profile will occur should metal vapor species arrive at the probe, regardless of the exact temperature.

The total amount, A_T, of gaseous (or "molecular") Sr-90 that has entered the diffusion tube can usually be determined by analyzing the diffusion tubes and outlet filters (with appropriate corrections for dust-borne and noble-gas-borne components as necessary). These filter units contain a fiberfrax section, a charcoal trap, and a 0.6-cm (1/4-in.) length of porous metal filter that are typically rated at 98% removal of >0.7-μm particles. These filter units should have removed essentially all of the fission products in the coolant stream. As an alternate (or check) to the filter measurements, the total amount of gaseous metallics that entered the filter

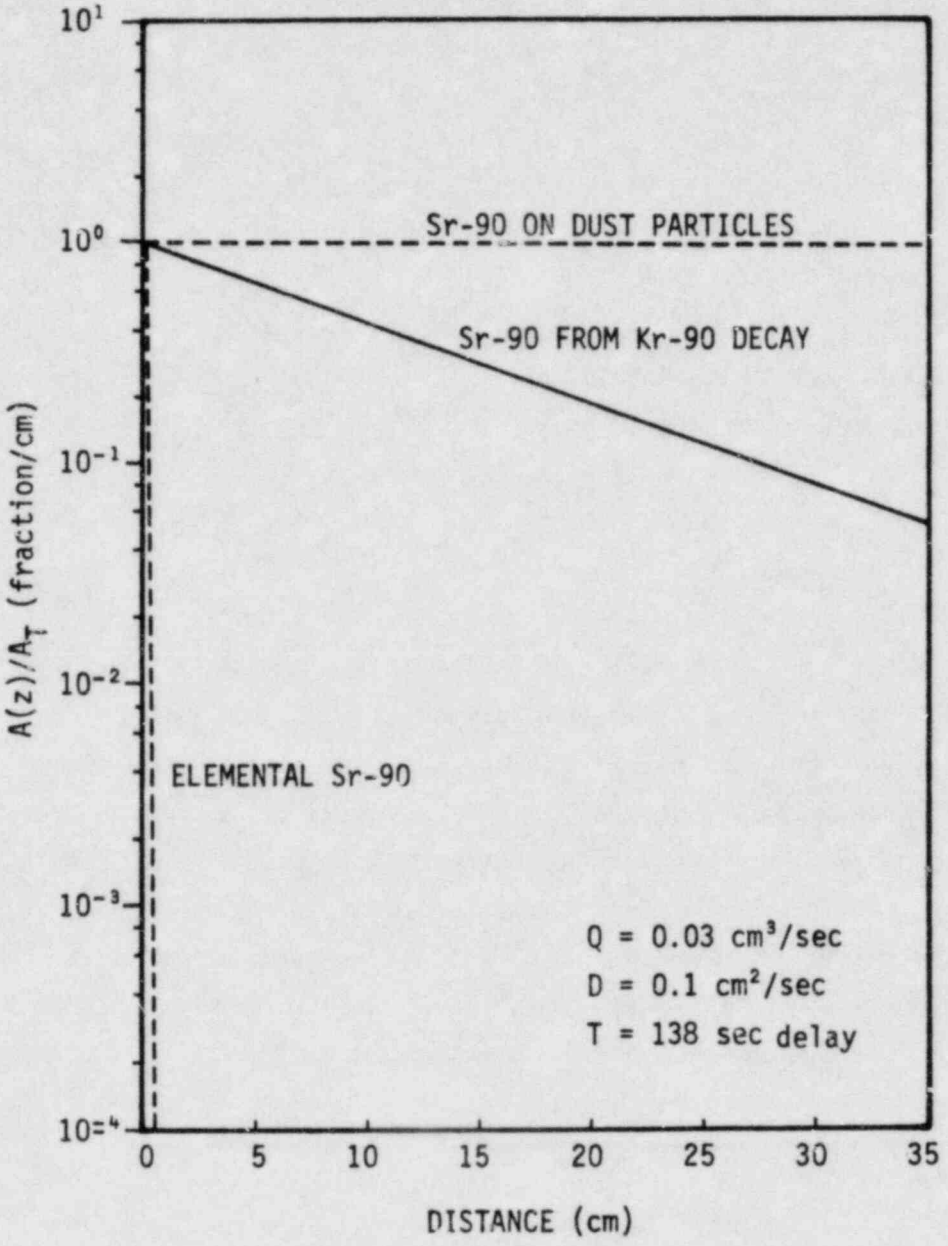

Fig. 2-7. Typical plateout profiles (normalized) in the low flow tube

can be estimated by integrating Eq. 2-1 to get the amount for an infinitely long tube. Assuming that only the first term is important, this results in

$$A_\infty = 0.0870\ A(L)\ \frac{Q}{D} \quad , \tag{2-2}$$

where A_∞ = the total amount which would be collected by an infinitely long tube (μCi),

$A(L)$ = the amount per unit length as recorded at the exit end of the tube of length L (μCi/cm),

Q = the flow rate (cm^3/s),

D = the diffusion coefficient (cm^2/s).

2.3.2. Dust-Borne Species

Some of the fission products in the reactor circuit may be sorbed on dust or other gas-borne particles. The theoretical distribution of these particles in the diffusion tubes will still be given by Eq. 2-1 if the walls of the tube approximate a "perfect sink." However, the diffusion coefficients for reasonably sized dust particles will be many decades smaller than the diffusion coefficients of elemental species. Thus, the concentration profile along the surface of the tube would be essentially flat at the contemplated flow rates. The total amount of fission products attached to dust particles in the circuit can be calculated from Eq. 2-3. If the concentration in the C tube is small or uncertain, the C tube term can be neglected to yield a conservative result.

$$M_{t(dust)} = \left[\frac{M_h(dust)}{f_h} - \frac{M_c(dust)}{f_c}\right] F_R \quad , \tag{2-3}$$

where $M_{t(dust)}$ = total metal in loop on dust (Ci),

$M_{h(dust)}$ = total metal in hot tube (minus precursor and metal vapor contribution) (Ci),

$M_{c(dust)}$ = total metal in cold tube (minus precursor and metal vapor contribution) (Ci),

f_h, f_c = flow rates in hot, cold tubes, respectively (cm^3/s),
F_R = flow rate in reactor (cm^3/s).

2.3.3. Noble-Gas Daughter Products

The source of some fission products of interest is primarily from short-lived noble-gas precursors, such as 14-s Xe-140, 32-s Kr-90, and 3.2-min Kr-89. In this case, the daughter-product concentration profile will be similar to the noble-gas parent profile in the diffusion tubes. With an inside diameter of the diffusion tubes of 0.304 cm and a length of 33 cm, the tube volume is 4.0 cm^3, giving a transit time of 3.6 s at a flow rate of 1 cm^3/s. Thus, there will be negligible attenuation by decay of the above listed noble gases in transit through the tube, and the daughter-product concentration profiles will be relatively flat. However, the L tube is a Low flow tube and there was approximately a 138-s transit time for this tube. Thus, there was significant decay of the noble-gas precursors during transit through the L tube.

The solid line on Fig. 2-7 illustrates the normalized concentration profile that might be expected for Sr-90 being deposited from its 32-s half-life Kr-90 parent in the L tube. If a dust component is present, a large amount of the dust should be found in the outlet filter, while a noble-gas precursor will have essentially no contribution to the filter activity, since the transit time through the filter is short.

The total amount of solid daughter produced by decay of its gaseous precursor during transit through the diffusion tube is given by

$$M_{gt} = G\,(1 - e^{-\lambda_m t_1})(e^{-\lambda_m t_2}) \quad , \tag{2-4}$$

$$M_{gx} = \frac{M_{gt} F_x}{\lambda_g V_\ell}\,(1 - e^{-\lambda_g \tau_x}) \quad , \tag{2-5}$$

where M_{gx} = total metal species in tube x (μCi) from decay of gaseous precursors,

M_{gt} = total metallic species in loop from decay of gaseous precursor, G,

$G = 0.85\ P\ \bar{\gamma}\ (R/B)$,

λ_g, λ_m = decay constants of gas and metal, respectively,

t_1, t_2 = time in reactor and time to shutdown, respectively,

F_x = tube flow rate,

V_ℓ = PCRV volume,

$\bar{\gamma}$ = yield of noble gas isotope,

τ_x = delay time in tube x.

2.3.4. Iodine Behavior

Table 2-1 lists the four methods available for obtaining information on iodine release and transport in the prim[illegible]uit.

The R/B and iodine monitor methods are used during reactor operation. The iodine decay and plateout probe methods are used following reactor shutdown. The plateout probe is the only device which measures circulating I-131 activity as specified in Technical Specification LCO 4.2.8. Compliance with Technical Specification LCO 4.2.8 can also be assured by other indirect methods. For example, the iodine decay and iodine monitor techniques measure only I-133 and I-135; consequently, I-131 concentration must be inferred when these methods are used. All of the methods are discussed below.

2.3.4.1. Iodine Release. At core temperatures, the transport behaviors of iodine and xenon are assumed to be identical. This has been verified by measurements at the General Atomic in-pile loop (GAIL) (Ref. 8), at Peach Bottom (Ref. 9), and recently at FSV (described below) using the iodine decay method. Consequently, the release of iodine can be calculated from its R/B, which is obtained from xenon R/B data. Section 4 gives the R/B of all the xenon and krypton isotopes and plots log R/B versus log $t^{1/2}$. For isotopes having half-lives of several minutes or more, the data tend to

TABLE 2-1
METHODS FOR IODINE SURVEILLANCE AT FSV

Method	What is Measured or Calculated
R/B	Total release of specific iodine isotopes obtained from xenon R/B versus $t^{1/2}$ line
Iodine decay	Total I-133, I-135 in primary circuit (or R/B) obtained from xenon data following shutdown
Iodine monitor	Concentration of I-133 and I-135 in helium coolant in lower plenum
Plateout probe	Concentration of I-131 in helium coolant at core outlet and inlet

group around a straight line whose slope is about 0.4. The R/B of any iodine isotope is obtained from the xenon line. The total activity of iodine released is then calculated from the following equation:

$$A_I = 0.85P\bar{\gamma}\ R/B\ (1 - e^{-\lambda t_1}) \quad , \tag{2-6}$$

where A_I = activity iodine of released (Ci),

P = thermal power (W), 8.5×10^8 x fractional power level,

$\bar{\gamma}$ = cumulative yield for specific isotope,

R/B = release rate of specific isotope obtained from xenon R/B versus $t^{1/2}$ curve (see Section 4),

λ = decay constant,

t_1 = time at power (s).

2.3.4.2. Iodine Decay. This technique is a direct measurement of total plateout of I-133 and I-135. The method has been used successfully at GAIL (Ref. 8), Peach Bottom (Ref. 9), and FSV. The specific activity of the decay daughter activities Xe-135 and Xe-133 from the main loop helium following a reactor shutdown must be monitored. The measurement requires that the purification system flow rate be maintained constant following a reactor shutdown for 6 to 10 h. This allows time for the fuel to cool and a sufficient cleanup time for the Xe-135 and Xe-133 in the main loop that originated from direct release from the fuel. The quantities of Xe-135 and Xe-133 that remain after several hours of cleanup are those originating from decay of I-135 and I-133 plateout inventories.

The iodine parent is calculated from the xenon data using the following equation for radioactive growth and decay:

$$I^o = \frac{Xe - Xe^o\ e^{-(\lambda_2 + r_s)t}}{[e^{-\lambda_1 t} - e^{-(\lambda_2 + r_s)t}]BR}\left(\frac{\lambda_2 + r_s - \lambda_1}{\lambda_2}\right) \quad , \tag{2-7}$$

where I^o = iodine at shutdown (Ci),

Xe^o = xenon at shutdown (Xe-133 = 12.8, Xe-135 = 48) (Ci),

Xe = xenon at time after shutdown (Ci),

λ_1 = decay constant iodine (I-133 = 9.3×10^{-6}, I-135 = 2.8×10^{-5}) (s^{-1}),

λ_2 = decay constant xenon (Xe-133 = 1.5×10^{-6}, Xe-135 = 2.1×10^{-5}) (s^{-1}),

t = time after shutdown (s),

r_s = purification constant (1.73×10^{-5} s^{-1}),

BR = branching ratio iodine to xenon (I-135 $\overset{0.70}{\rightarrow}$ Xe-135, I-133 $\overset{0.976}{\rightarrow}$ Xe-133).

Section 4.1.2 discusses the results of this test.

2.3.4.3. Iodine Monitor. The iodine monitor measures circulating iodine concentrations during reactor operation. It is located in the lower cavity at a penetration just below the level of the circulator outlet.

Figure 2-8 schematically depicts the iodine monitor. Briefly, the monitor collects iodine on a charcoal trap inside the PCRV and purges daughter xenon to a cold trap for counting. A clever arrangement of tube in tube and back sweeping of the inlet orifice keeps the xenon that is normally in the primary coolant from contaminating the cold trap. The concentration of gaseous iodine in the primary circuit is calculated by modifying the equation for radioactive growth and decay.

The iodine monitor measures only I-133 and I-135 isotopes which have convenient radioactive xenon daughters to trap and count. Consequently, the I-131 concentration must be extrapolated from the I-133 and I-135 data. The concentration of I-131 in the gas phase was calculated by using the following equations:

$$A_C = \frac{0.85\ P\ R/B\ \bar{\gamma}\ [1 - e^{-(\lambda + r_s + r_p)t}]}{1 + (r_s + r_p/\lambda)} \quad , \qquad (2\text{-}8)$$

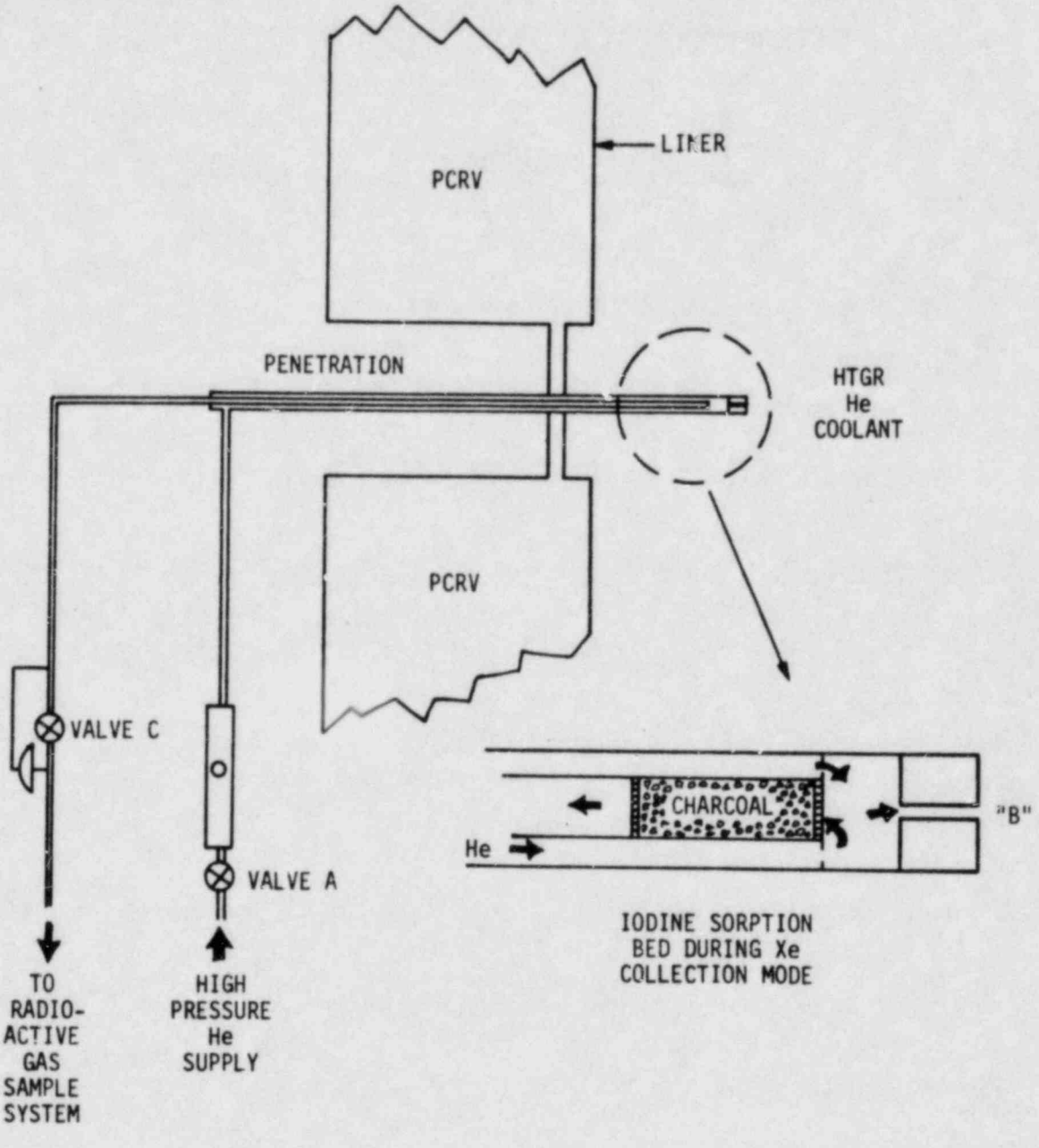

Fig. 2-8. HTGR iodine monitor

where A_c = circulating I-131 activity (Ci) (from monitor data),

A_i = iodine release (Ci) (from R/B data equation),

λ = decay constant (9.7×10^{-7}) (s^{-1}),

r_s = purification constant (s^{-1}),

r_p = plateout constant (s^{-1}).

At steady state, if $r_p >> r_s$ and λ and $A_i >> A_c$, then A_p, the plateout activity, is essentially equal to A_i, the amount released. Furthermore, at steady state, the term in brackets is 1.0 and by combining with Eq. 2-6 the following results:

$$r_p = \frac{A_p}{A_c} \lambda \quad , \tag{2-9}$$

and the plateout per pass is

$$\tau = 1 - e^{-r_p t_c} \quad , \tag{2-10}$$

where τ = plateout per pass (fraction),

t_c = cycle time (~13 s at 60% power and 10.3 s at 70% power).

At sorption equilibrium, A_p/A_c is a constant.

Equation 2-9 states that the plateout constant is a linear function of λ and therefore provides a means of extrapolating the I-133 and I-135 data to I-131.

2.3.4.4. Plateout Probe. The plateout probe is the primary device for determining I-131 concentration in the coolant helium. The probe samples hot helium (inlet to the steam generator) and cold return helium (exit of the circulator) and therefore can directly measure the fractional plateout per pass. The probe was originally designed to quantitatively remove iodine from the gas flowing into the tubes. Atomic or molecular iodine was expected to adsorb on the metal walls of the diffusion tube with an inverse temperature relationship (that is, the concentration should increase with

length of tube as the temperature decreases). The small activated carbon trap at the end of each tube was provided specifically to adsorb any iodine vapor that was not removed upstream.

The expected concentration of iodine in the diffusion tubes can be calculated from the following equation:

$$I_x = \frac{A_c f_x}{\lambda V_\ell} (1 - e^{-\lambda t_1}) e^{-\lambda t_2} \quad , \tag{2-11}$$

where I_x = total I-131 in tube x (μCi),

A_c = total I-131 in helium (μCi) (from iodine monitor data),

f_x = flow rate in tube x (cm^3/s),

V_ℓ = volume of loop (cm^3),

t_1 = time at power (s),

t_2 = decay time to shutdown (s).

Conversely, Eq. 2-11 can calculate A_c from measurements of I-131 in tube I_x.

The fractional plateout per pass of I-131 is calculated from iodine concentrations in the hot and cold tubes:

$$\tau = 1 - \frac{I_c/f_c}{I_h/f_h} \quad , \tag{2-12}$$

where τ = fractional plateout per pass,

I_c, I_h = concentration I-131 in the cold and hot tubes, respectively (μCi),

f_c, f_h = flow rate in cold and hot tubes, respectively (g/s).

Iodine atoms were anticipated to chemically react either in the fuel or in the primary circuit with fission product metal atoms such as cesium, barium, or strontium to form stable iodides, such as CsI, BaI, and SrI. These compounds are far less volatile than iodine and would be expected to

have a steep profile in the tube entrance similar to that shown in Fig. 2-7. Although atomic (gaseous) iodine would not be expected to be associated with dust particles, CsI or BaI, because of their low volatility, could be attached to dust particles, which would result in flat concentration profiles.

2.3.5. Sulfur Analysis

Metal sulphidation can be damaging because of the possible formation of low melting sulfides. Consequently, analyzing the plateout probe for sulfur contamination was deemed important, primarily to allow the vapor pressure of gaseous sulfur species to be calculated. (Reference 1 specifically addresses sulphidation corrosion of the outer probe sleeve.) Knowing the amount of sulfur trapped in a diffusion tube allows the sulfur concentration in the helium coolant to be calculated. (This calculation assumes that the diffusion tube quantitatively removed the sulfur from the gas stream; if not, then the calculation is for a lower limit value.)

The concentration of radioactive S-35 in the primary coolant can be calculated from the following equation:

$$\text{S-35(tot)} = \frac{\text{S-35}_x \lambda}{(1 - e^{-\lambda t})\, F_x} V_\ell \quad , \tag{2-13}$$

where S-35(tot) = total S-35 in helium (μCi),
S-35$_x$ = total S-35 in tube x (μCi),
V_ℓ = total helium, 2.1 x 10^{10} cm^3 (STP),
λ = decay constant S-35, 9.4 x 10^{-8} s^{-1},
t = time at power (s),
F_x = flow rate in tube x (cm^3/s) (STP).

The potential sources of sulfur in the circuit are fuel matrix and H-327 graphite and other graphite components (HLM and PGX). If the main source of sulfur is assumed to be the core (fuel matrix and H-327), then the concentration of natural sulfur can be calculated using Eqs. 2-13 and 2-14,

assuming that S-35 is a result of in-situ neutron activation of stable S-34 which comprises 4.2% of natural sulfur.*

$$\frac{N_S}{N_{S-35}} = \frac{\lambda}{nv f \sigma (1 - e^{-\lambda t})} \quad , \tag{2-14}$$

where N_S/N_{S-35} = ratio of natural sulfur atoms to S-35 atoms,

nv = neutron flux ~4×10^{13} n/cm^2 s,

σ = absorption cross section for S-34 n,γ S-35 = 0.23 b,

f = isotopic fraction S-34 = 0.0422.

$$P_{H_2S} = \left(\frac{N_S}{N_{S-35}}\right) \frac{\text{S-35 } (\mu\text{Ci/cm}^3)\ V_\ell \times 3.7 \times 10^4 \text{ (dps/}\mu\text{Ci)}\ P_{He}}{\lambda A I_{He}} \quad , \tag{2-15}$$

where P_{H_2S} = partial pressure of sulfur in the coolant (species is assumed to be H_2S) [MPa (atm)],

P_{He} = 4.6 MPa (46 atm),

A = 6×10^{23} atoms/g-mole,

I_{He} = helium inventory, 8.5×10^5 g-moles.

Sulfur contamination in graphite or fuel rod matrix (or plated out in the circuit) would be in the form of metallic sulfides such as NaS, SiS, FeS, NiS, etc. These sulfides would tend to hydrolyze in the presence of water vapor to form H_2S and the metal oxide* (Ref. 10):

$$MS + H_2O = MO + H_2S \quad ,$$

*The fuel matrix is believed to be the main sulfur source because of its higher sulfur concentration. In addition, the graphite components have been exposed to extremely high temperatures (>2600°C) for long times (several days) during their graphitization, which would have vaporized the more volatile sulfur species. The fuel rods were annealed at only about 1800°C for 1 h. In addition, tests on H_2S release from core materials were conducted at General Atomic. In these scoping tests, a gas mixture of 1% water vapor in helium was passed through fixed beds of pulverized fuel matrix and PGX graphite at 800°C. H_2S was continuously released from the matrix over several days of exposure. H_2S was not released from the PGX graphite at any time during the 30 days of exposure.

where M = metal (Na, Ni, Si, Fe, etc.)

In addition, since the concentration of H_2 in the primary circuit is always high (relative to sulfur), the most likely chemical species in the coolant is H_2S, as a result of the following equilibrium reaction:

$$2H_2 + S_2 = 2H_2S \qquad \Delta F_o = -9.8 \text{ kcal/mole at } 700 \text{ K} \quad . \qquad (2\text{-}16)$$

Using this equation, the concentration of the potentially corrosive S_2 can be estimated. The equilibrium constant for this reaction is

$$K = \frac{(P_{H_2S})^2}{(P_{H_2})^2 \, P_{S_2}} \quad . \qquad (2\text{-}17)$$

Since

$$\Delta F^o = -RT\ln K \quad , \qquad (2\text{-}18)$$

the partial pressure of S_2 can be calculated using values of P_{H_2S} from the probe analysis (Eq. 2-15) and the known concentration of hydrogen, P_{H_2}.

3. EXPERIMENTAL PROCEDURES AND RESULTS OF INITIAL EXAMINATION

Probe examinations follow the steps below (each step is discussed in detail in the following subsections):

1. Remove from FSV, ship to General Atomic.

2. Visually examine and gross gamma-scan outside of probe.

3. Disassemble and remove tubes.

4. Flow test all tubes.

5. Cut the tubes into 2.54-cm (1-in.) segments.

6. Gamma count tube segments and internal traps.

7. Gamma count other probe parts: graphite, fiberfrax, plenum, flanges, outside sleeve sections.

8. Leach selected tube segments and parts for S-35 and S-89, Sr-90 beta analysis.

9. Analyze data and report.

3.1. PROBE REMOVAL

The reactor was shut down on November 9, 1981. The plateout probe was removed from the steam generator on November 14, 1981 through the PCRV plateout probe penetration using established procedures. The reactor primary coolant was depressurized to near atmospheric pressure prior to removal. The probe removal equipment consisted of a ventilation barrier

(inert atmosphere glove box), probe shipping cask, and associated handling equipment. The ventilation barrier contained all equipment, including the shipping cask, thus providing a controlled atmosphere for the probe and preventing air ingress into the coolant circuit during removal operations. The removal process went smoothly. The probe was not dropped or scraped at the time of removal. Gross activity measurements at FSV showed 125 mr/h beta and 5 mr/h gamma on contact with the hot end of the probe. The cold end showed 230 mr/h beta and 4 mr/h gamma on contact. The probe was fitted with a soft rubber cap to prevent the potential loss of loose material from the diffusion tubes. The probe was then inserted into the shielded shipping cask for transport to General Atomic Company (GA) in San Diego. The cask design prohibited any contact between probe and cask except at the head bayonet type locking flange assembly; thus, the plateout activity in the diffusion tubes and on the external plateout sleeve was not disturbed during shipping.

3.2. VISUAL EXAMINATIONS AND GROSS GAMMA SCAN

Upon arrival at GA on November 19, 1981, the probe was removed from its cask. The probe was dull gray, indicating surface oxidation. Figure 3-1 shows a photograph of the probe immediately after removal from the cask. The gross activity was 2 mr gamma and 100 mr beta at the surface of the probe, confirming the Public Service Company of Colorado measurements. The primary radioactivity was due to the activation products Cr-51, Fe-59, and Co-60. The most abundant fission product, I-131, was concentrated near the cold end of the probe. During the disengagement of the probe from its bayonet locking device in the cask, it was placed upright with the four hot tubes pointing down. After the probe was positioned inside the laboratory hood, the rubber dust cap was removed and inspected. A small quantity (~2 mg) of black granular dust had fallen out of the up-facing T tube (see Fig. 3-2). No loose dust was in any of the other tubes, although it was later determined that the T, B, R, and L fiberfrax traps were slightly discolored with a black dust. The C tube fiberfrax contained (by visual examination) much more dust than the other tubes (see Fig. 3-3). (The C tube was later discovered to be partially plugged.)

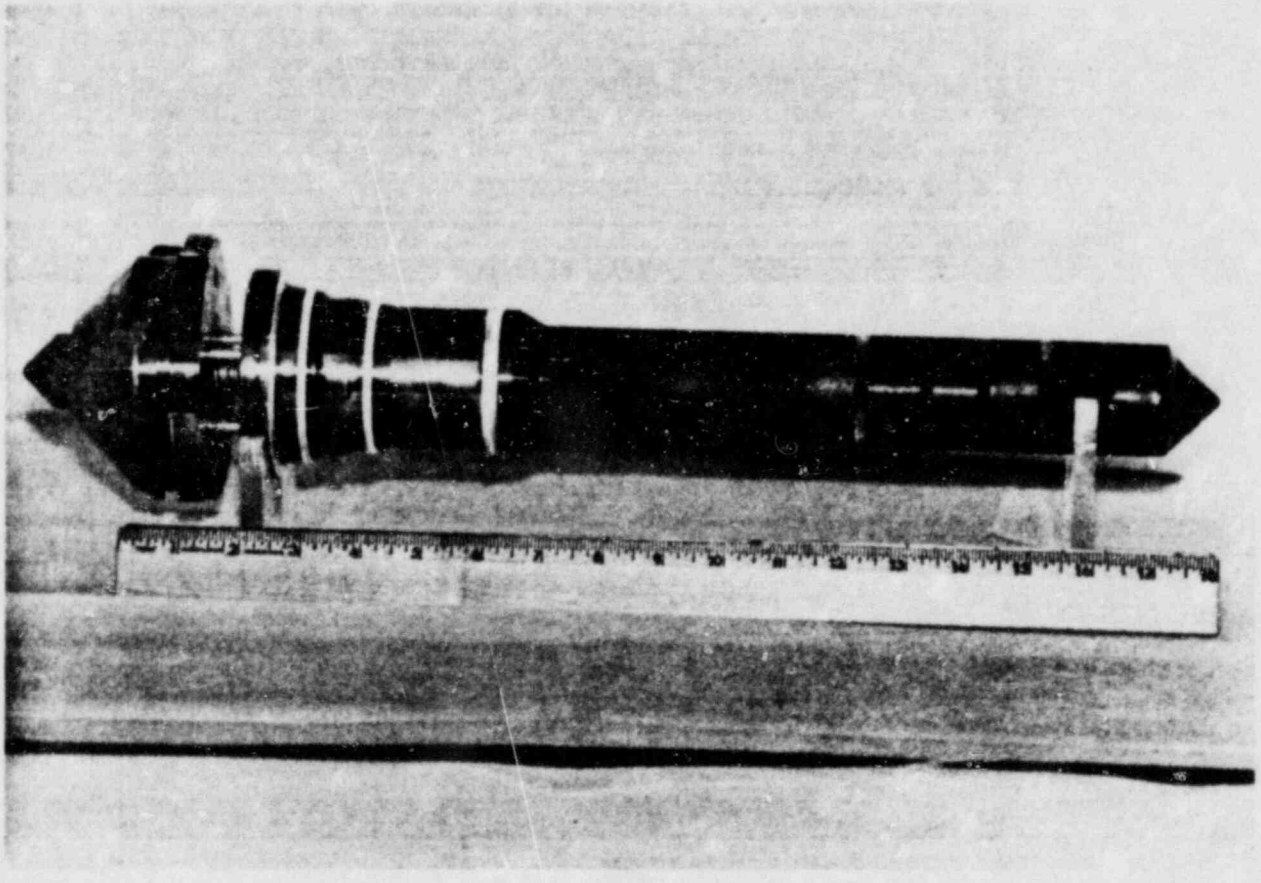

Fig. 3-1. Plateout probe upon arrival at GA

Fig. 3-2. Loose granular dust from the T tube

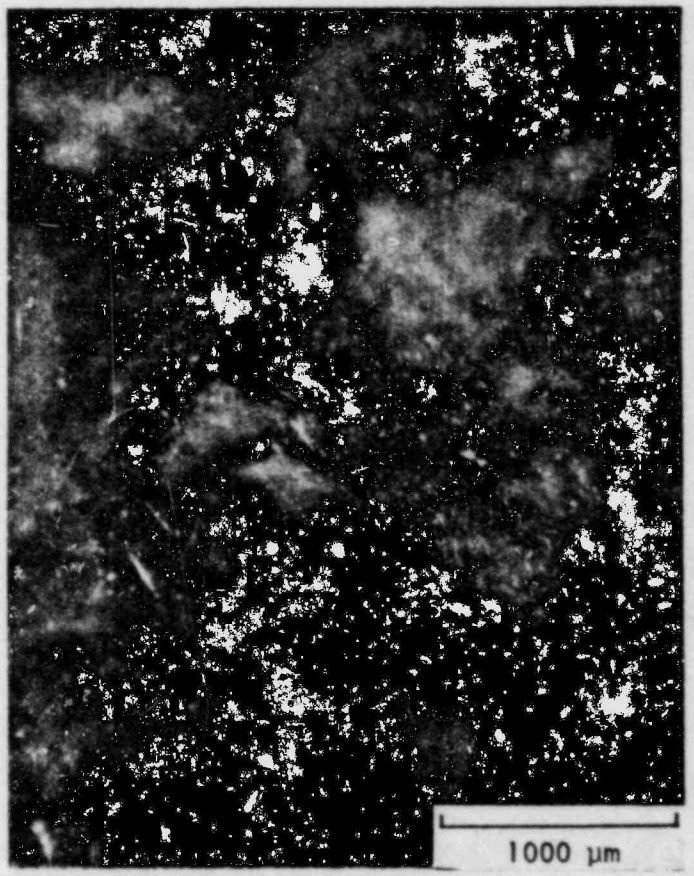

Fig. 3-3. Fiberfrax filter from the C tube containing some black dust

3.3. PROBE DISASSEMBLY

The plateout probe was disassembled as follows:

1. The body barrel and external plateout sleeve were girdle cut circumferentially at the weld junction between barrel and probe tip. This allowed removal of all four hot gas diffusion tubes (still attached to the probe tip) from the graphite sheath. The cold gas diffusion tube was removed similarly by cutting at the weld joint between diffusion tube inlet and probe head nut. Once the probe tip and diffusion tubes were removed from the probe, the external plateout sleeve was removed from the barrel.

2. After separation from the probe, the diffusion tubes were detached from the probe tip by cutting each tube at the base of the tip, thus leaving the inlet section (~3 mm) of each tube attached to the tip. All four inlet sections were then separated from the probe tip by core drilling the tip with a hole saw. The individual tubes were then flow calibrated, as described in Section 3.4.

3. The five diffusion tubes were sectioned into 2.54-cm (1-in.) long segments for radioassay to determine the fission product plateout profile and total activity within the tube. Sectioning was accomplished by cutting with a pair of diagonals (wire cutters). This technique crimped the end of each tube segment, preventing loss of any loose dust particles. The control tip sintered metal filter was cut at the last segment with a tubing cutter. This allowed removal of the individual trap components for radioassay including (in order of flow direction) large fiberfrax, charcoal, small fiberfrax, and control tip segment. See Fig. 2-3 for trap details.

4. The external sleeve was sectioned for metallographic examinations and fission product analysis.

5. Certain internal and external parts were wiped with tissue moistened with dilute acid. The wipes were radioassayed by gamma counting.

6. The internal graphite sleeve and fiberfrax insulation were removed for gamma scanning.

3.4. FLOW CALIBRATION OF DIFFUSION TUBES

The individual diffusion tubes were checked for flow resistance over a wide range of differential pressure for comparison to the initial as-built calibration. Figure 3-4 shows the apparatus used; for the low flow rates involved, a bubble meter was substituted for the wet test meter. The tube calibrations are given in Figs. 3-5a through 3-5e, along with the original as-built calibration data. In the T, B, R, and L tubes, the flow rates were on the low side of the original calibration, but were acceptable. The C tube, Fig. 3-5e, shows a greatly diminished flow rate. Recalling that the C tube fiberfrax filter was visibly discolored with black dust, the C tube was concluded to have been almost totally plugged during its service in the reactor. A final check on the flow resistance of the C tube control tip was performed to ensure that the blockage was not in the as-built tip. The control tip flow shown in Fig. 3-5e lies above the calibration range and indicates that the flow blockage was indeed in the fiberfrax filter section. Why the C tube became plugged and the other tubes did not is not known.

Calculation of Tube Flow Rates at Reactor Conditions

The flow in the individual tubes is controlled by the sintered metal filter or control tip. Under these conditions, Darcy's Law for flow through porous media applies:

$$Q = \frac{B_o A \, \Delta P}{\mu \, L} \quad , \qquad (3\text{-}1)$$

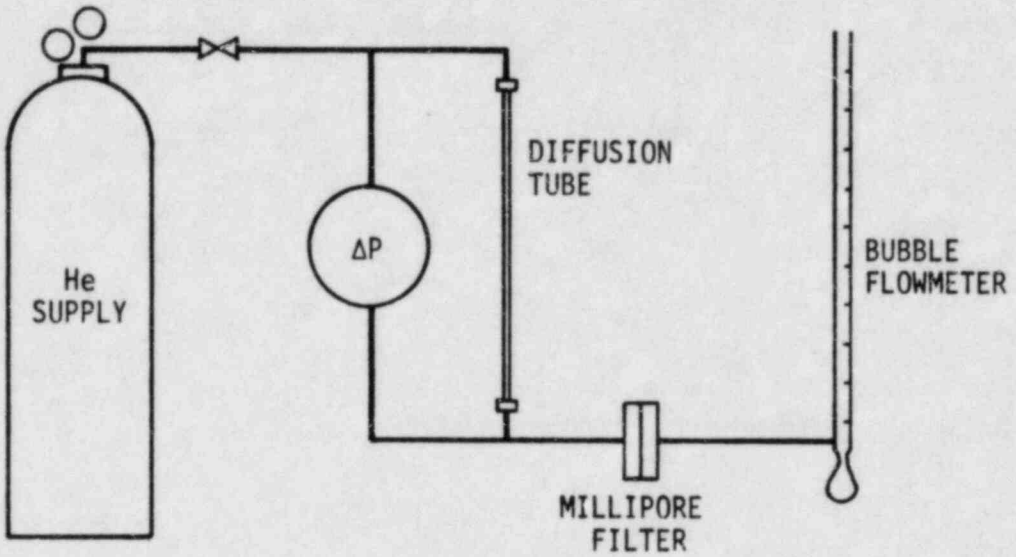

Fig. 3-4. Apparatus for diffusion tube flow calibrations

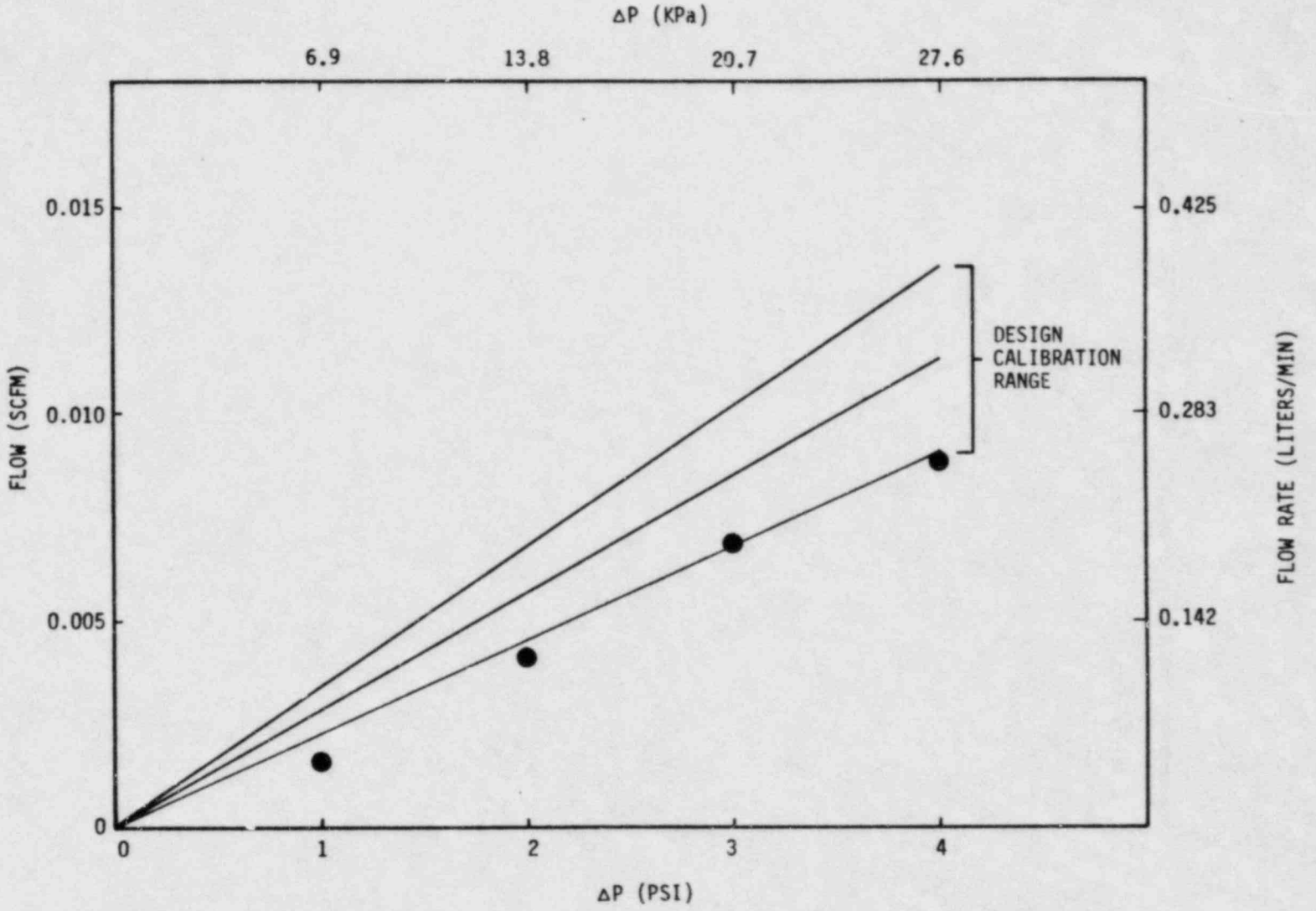

Fig. 3-5. Flow calibration of diffusion tubes: (a) top tube, T (Sheet 1 of 5)

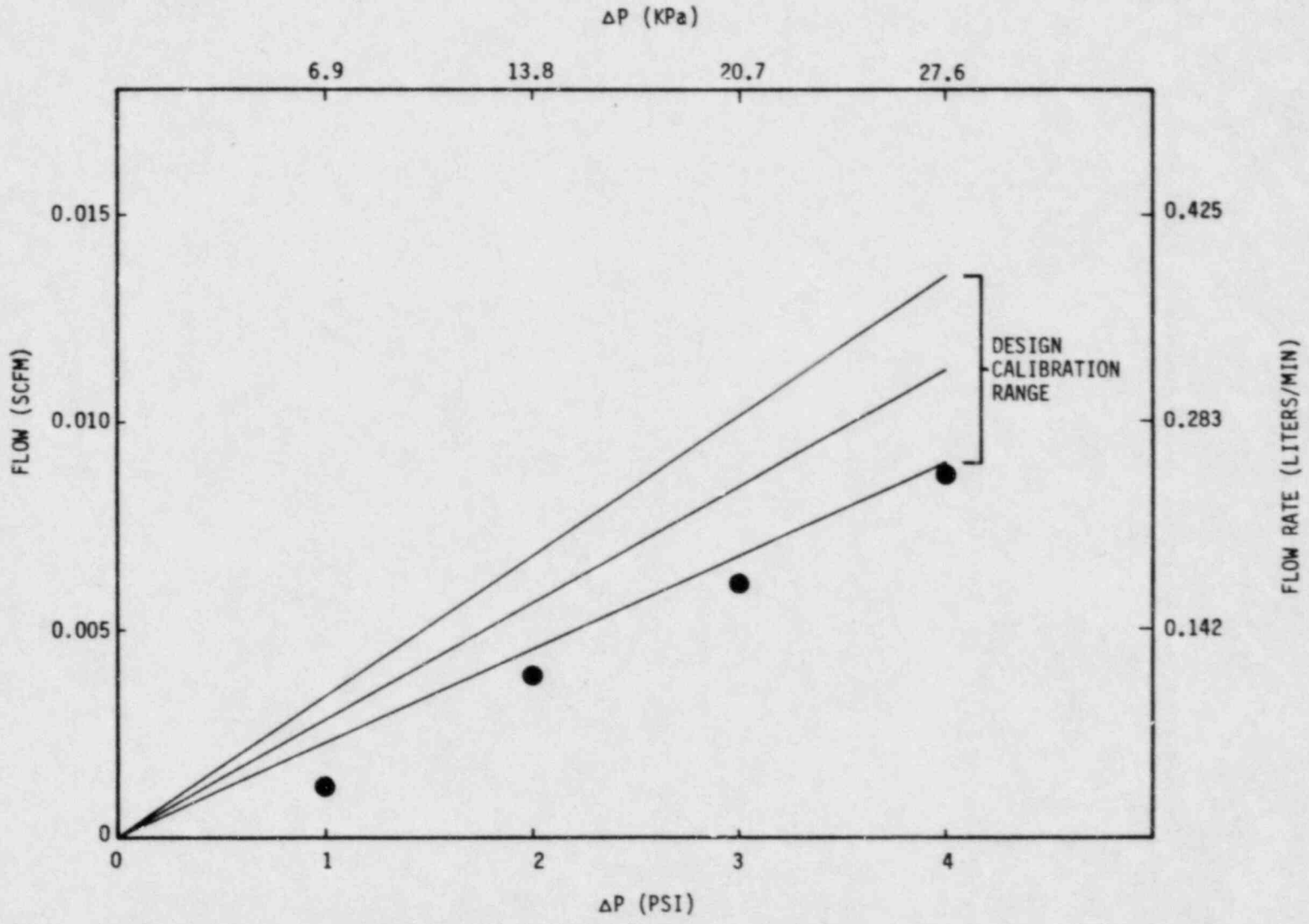

Fig. 3-5. Flow calibration of diffusion tubes: (b) right tube, R (Sheet 2 of 5)

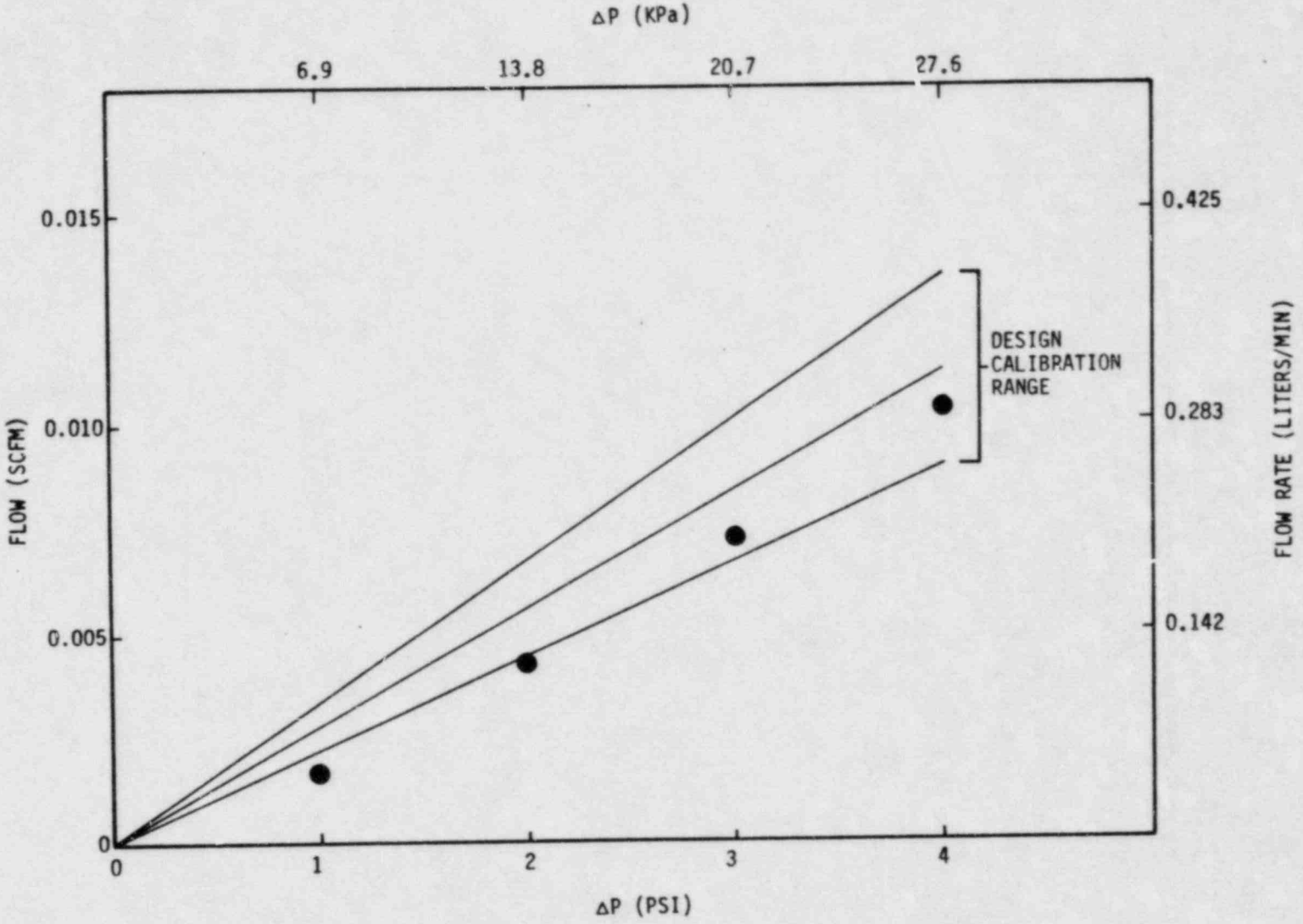

Fig. 3-5. Flow calibration of diffusion tubes: (c) bottcm tube, B (Sheet 3 of 5)

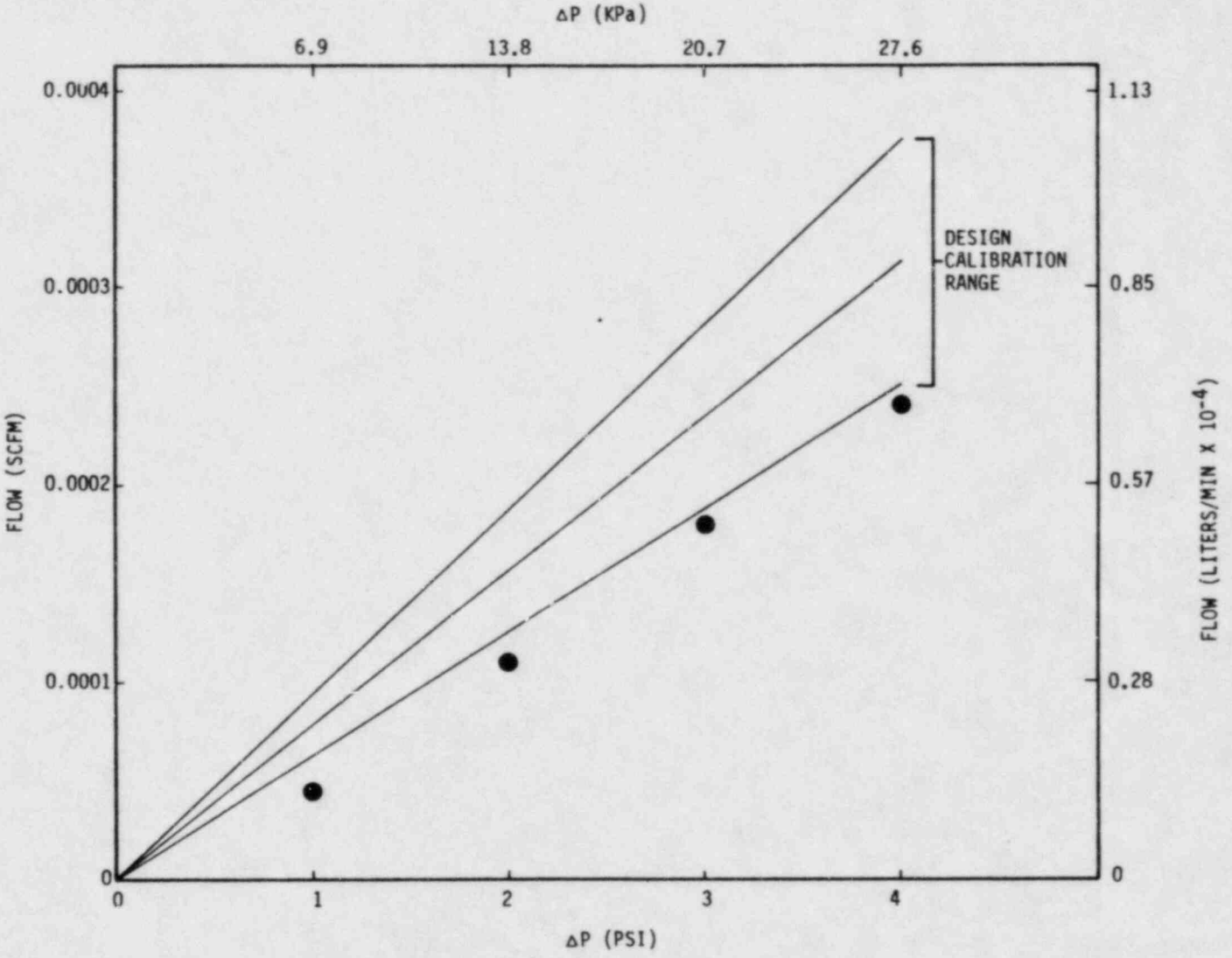

Fig. 3-5. Flow calibration of diffusion tubes: (d) left tube, L (Sheet 4 of 5)

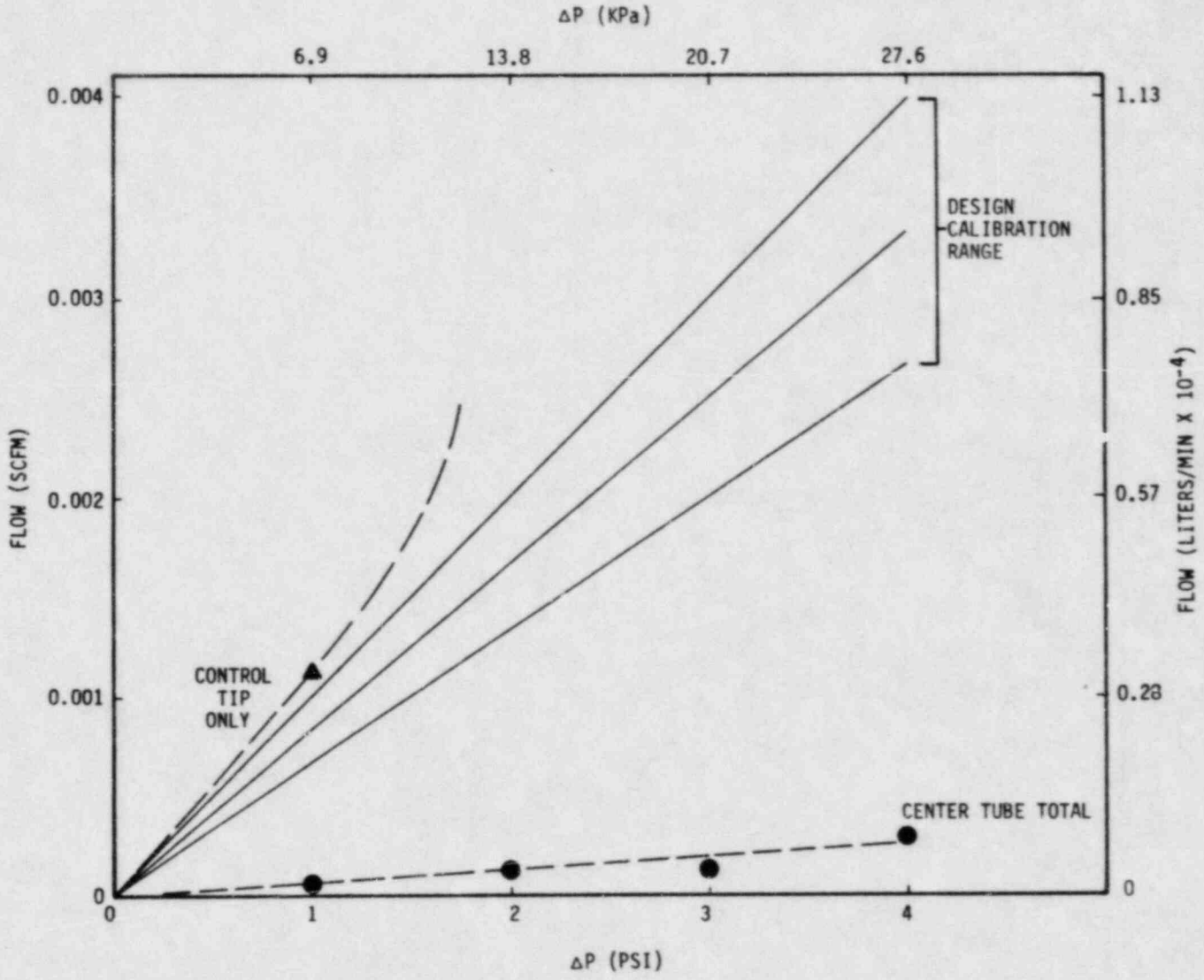

Fig. 3-5. Flow calibration of diffusion tubes: (e) center tube, C (Sheet 5 of 5)

where Q = volumetric flow rate,

B_o = specific permeability,

A = cross section area of tube,

ΔP = pressure drop,

μ = dynamic viscosity,

L = length of porous media.

B_o is a function only of the structure of the sintered metal filter; therefore the flow rate in the reactor Q_r can be calculated from the calibration flows by the following equation:

$$\frac{Q_r}{Q_c} = \frac{\mu_c}{\mu_r} \frac{\Delta P_r}{\Delta P_c} \quad . \tag{3-2}$$

Viscosity, μ, is proportional to $T^{0.678}$, where T = K. If the ΔP in the flow calibration is the same as the reactor, then

$$\frac{Q_r}{Q_c} = \frac{T_c}{T_r}^{0.678} \quad \text{at constant } \Delta P \quad . \tag{3-3}$$

At 70% power, the ΔP_{SGen} was 17 kPa (2.5 psi) and ΔP_{total} was 34 kPa (5 psi). Since most of the reactor operation was at 70% power, a constant ΔP of 17 kPa (2.5 psi) across the hot tubes and 34 kPa (5 psi) across the cold tube was assumed for all calculations. For the hot side, a temperature of 724°C (1335°F) was used and 340°C (655°F) was assumed for the cold side. Using the measured Q_c at 16°C (60°F), tube flow rates, Q_r, were calculated (see Table 3-1). The appendix gives details on the calculations.

3.5. RADIOCHEMICAL ANALYSIS

All diffusion tube segments and acid wipes from other probe components were sealed into 2-dram polyvials and gamma counted. The 2-dram vial is the standard counting geometry wherein "counts" are converted to curies. Some parts, including the external sleeve, the internal graphite sleeve, and cold

TABLE 3-1
DIFFUSION TUBE FLOW PARAMETERS

Parameter	T	B	R	L	C
Lab calibration at 16°C (60°F)[a] (cm^3/s)	2.6	2.7	2.35	0.068	0.18
Volume flow (reactor) (cm^3/s)	1.1	1.2	1.0	0.029	0.10
Volume flow (STP) reactor (cm^3 STP/s)	14.6	15.9	13.2	0.38	2.1
Mass flow reactor (mg/s)	2.6	2.7	2.3	0.068	0.38
Velocity reactor (cm/s)	9.2	10	8.3	0.24	1.0
Delay time (s)	3.6	3.3	4.0	138	40

[a] C tube at 34 kPa (5.0 psi) ΔP. T, B, R, and L tubes at 17 kPa (2.5 psi) ΔP. See Table A-3 for sample calculations.

end flanges, were gamma scanned using nonstandard geometry. Gamma counting was accomplished utilizing a Ge(Li) detector with a photopeak resolution of 2.5 keV full width and half maximum height for a reference Co-60 1330 keV photopeak. The detector was calibrated using National Bureau of Standards traceable standards with 2-dram vial geometry. All gamma spectra obtained using the standard geometry were analyzed to determine the concentration in microcuries per sample of resolvable photopeaks using the Nuclear Data Model 6600 computer and appropriate software. The gamma scan of the graphite sleeve was converted to microcuries per inch of graphite by crushing segments of the graphite into powder which could be inserted into the standard 2-dram polyvial configuration.

After gamma counting, selected tube segments, traps and external sleeve samples were acid leached to remove all radioactivity. The leach solutions were then analyzed for the pure beta-emitting isotopes Sr-89, Sr-90, and S-35 using established procedures. The strontium method is based on an acid separation technique that culminates in the isolation of the insoluble $SrCO_3$. The precipitates were then immediately counted for their Sr-89 activity using a proportional beta counter. At this point, because the Sr-90/Sr-89 ratio is low, the Sr-90 beta activity does not interfere with the Sr-89 count.

The samples were recounted a few days later to obtain a higher count which resulted from the growth of Y-90 ($t^{1/2}$ = 60.4 h), the daughter of Sr-90. A computer method involving simultaneous differential equations allows the Sr-90 count rate to be calculated. Most of these samples, however, contained too little Sr-90 (in the presence of large Sr-89 counts) for accurate analysis using the above method. For this work, the Y-90 was separated cleanly from all of the Sr-89/Sr-90 carbonate precipitates. The Y-90 was then analyzed separately to obtain quantitative Sr-90 activities. The Y-90 samples were checked for purity by counting each three times over several days. The beta activities decayed with the proper 60-h half-life, indicating that no contamination occurred from other activities.

The S-35 was analyzed after selected tube segments were dissolved with acid, followed by separations to isolate S-35. The method involved several separation steps to remove contamination by beta-emitting species, followed by a final precipitation of the S-35 as $BaSO_4$, which was beta counted.

Each S-35 precipitate was checked for contamination by gamma counting. No gamma emitting isotopes were found. The beta energy of each $BaSO_4$ precipitate was checked using a standard aluminum absorber. In all samples, the percent transmittance of the beta rays through the absorber was within 1.5% of the specified transmittance, confirming that the observed beta activity was S-35.

4. EXPERIMENTAL RESULTS

Table 4-1 lists all the radioisotopes found on and inside the probe. The nuclides of greatest activity were caused by in-situ activation of the metallic components in the probe. These activities include Cr-51, Co-60, Fe-59, and Mn-54. The presence of these nuclides in such great abundance all but swamped the activity of the fission products which were present in low concentrations, and made their analysis much more difficult. The only nuclides that originated in the reactor core that were measurably present in all tube segments were the fission products Cs-137, Ba-140, I-131, Sr-89, and Sr-90 and the activation products Cs-134 and S-35. All of these nuclides are gaseous (i.e., iodine and sulfur) or have gaseous precursors.

Trace amounts of Ce-141, Ce-144, Zr-95, and Nb-95 were found in some of the spectra in which long counts (15 h) were obtained. These nuclides have gaseous precursors whose half-lives range from 0.8 to 1.7 s. The fission product Ag-110m was present in trace amounts on the outside of the probe and in some of the tube segments. Ag-110m was found in large abundance on the silver-coated O-rings located outside the probe and inside the thrust cavity (see Fig. 2-2). The silver in the O-rings was apparently activated due to the low neutron flux at the probe location. The only radionuclide in measurable concentration which was neither gaseous nor had a gaseous precursor was Pa-233, the activation product of Th-232.

Table 4-2 lists the amounts of fission products and S-35 found in the diffusion tubes. Predicted amounts are also listed for comparison. The I-131 prediction was based on iodine monitor data. The appendix gives details on the calculations. Predictions of cesium, barium, and strontium release were based on precursor (krypton or xenon) transport alone using measured R/B's (or extrapolated in the case of Xe-140 and Sr-90).

TABLE 4-1
NUCLIDES FOUND ON PROBE: RELATIVE ABUNDANCES AND SOURCES

Nuclides Found on Probe	$t_{1/2}$	Relative Concentration on Probe[a]	Gaseous Precursor	$t_{1/2}$	Source
Cr-51	27.8 days	VH	--		In situ activation probe materials (Cr-50 $^{n,\gamma}$ Cr-51)
Co-60	5.27 yr	VH	--		In situ activation probe materials (Co-59 $^{n,\gamma}$ Co-60)
Fe-59	45 days	H	--		In situ activation probe materials (Fe-58 $^{n,\gamma}$ Fe-59)
Mn-54	280 days	H	--		In situ activation probe materials (Fe-54 ^{n,p} Mn-54)
S-35	85 days	VH	S-34	Stable	S-34 $^{n,\gamma}$ S-35
I-131	8.05 days	H	--		Fission product
Sr-89	51 days	L	Kr-89	3.2 min	Fission product
Sr-90	28 yr	VL	Kr-90	32 s	Fission product
Cs-134	2.2 yr	VL	Xe-133	5.27 days	Xe-133 + Cs-133 $^{n,\gamma}$ Cs-134
Cs-137	30 yr	L	Xe-137	3.9 min	Fission product
Ba-140	12.8 days	VL	Xe-140	16 s	Fission product
Pa-233	27 days	L	--	--	Th-232 $^{n,\gamma}$ Pa-233
Ce-141	32.5 days	T	Xe-141	1.7 s	Fission product
Ce-144	285 days	T	Xe-144	0.8 s	Fission product
Ag-110m	253 days	T	--	--	Fission product, also activation of silver O-rings
Ru-106	1 yr	T	--	--	Fission product
Nb-95	35 days	T	Kr-95	<1 s	Fission product
Zr-95	65 days	T	Kr-95	<1 s	Fission product

(a)VH = concentration greater than 1.0 μCi/tube found in all spectra; H = concentration greater than 0.1 μCi/tube found in all spectra; L = concentration greater than 0.01 μCi/tube found in most spectra; VL = greater than 0.001 in most spectra; T = trace quantities found occasionally.

TABLE 4-2
DIFFUSION TUBE FISSION PRODUCT INVENTORIES (μCi)[a]

	T Tube		B Tube		R Tube		L Tube		C Tube	
Nuclide	Observed	Predicted	Observed	Predicted	Observed	Predicted	Observed	Predicted	Observed	Predicted
I-131	0.56	102[b]	0.58	112	0.55	93	0.036	2.6	0.045	15
Cs-137	0.018	0.0032[c]	0.019	0.0032	0.017	0.0032	0.0059	0.0027	0.0048	0.005
Cs-134	0.0040	—	0.0044	—	0.0043	—	t[g]	—	t	—
Ba-140	0.012	0.008[d]	0.006	0.008	0.0018	0.008	t	—	t	—
Sr-89	0.07	0.048[e]	NA[h]	—	NA	—	0.018	0.038	0.065	0.071
Sr-90	0.003	0.0014[f]	NA	—	NA	—	0.0005	0.0003	0.0008	0.0016
S-35	NA	—	NA	—	2.0	—	NA	—	NA	—

(a) Total tube inventories include amounts in traps. All activities decayed to reactor shutdown, 11/9/81.
(b) I-131 predicted amount based on iodine monitor data. See Table A-7.
(c) Cs-137 predicted amount based on measured precursor R/B. See Table A-3.
(d) Ba-140 predicted amount based on assumed precursor R/B. See Table A-5.
(e) Sr-89 predicted amount based on measured precursor R/B. See Table A-4.
(f) Sr-90 predicted amount based on assumed precursor R/B. See Table A-3.
(g) t means only trace amount detected in occasional tube segments. Total tube inventory not possible.
(h) NA means tube segments not fully analyzed, preventing total inventory calculation. The NA tubes were retained for archival purposes.

Table 4-3 lists quantities of fission products found in other probe locations including the graphite sleeve, probe plenum, cold side flanges, and outer sleeve.

Of particular interest is the relatively high concentration of fission products in the plenum area and in the graphite sleeve. These high concentrations prompted investigations into the possibility of helium leakage past the silver-plated O-ring seals. Figure 2-3 shows two O-rings around the probe body which seal the plenum area from hot and cold side helium. A third O-ring seal surrounds the C tube in the thrust cavity. The first O-rings were bright and shiny and appeared to have effected their intended seal. The third ring in the thrust cavity was corroded and probably was not an effective seal for helium. The helium from the cold side and fission products are surmised to have leaked past this seal and contaminated the plenum area. This leak could not have affected the tube flows; however, it allowed contamination of the inside of the probe, which further confused the analysis.

Figures 4-1 through 4-3 plot concentrations of fission products versus length for the diffusion tubes. Figures 4-1a through 4-1e have I-131, Cs-137, and Cs-134 plotted together. Figures 4-2a through 4-2e have Sr-89, Sr-90, and Ba-140 isotopes. Figure 4-3 is a plot of S-35 on three tubes. Figures 4-4a through 4-4d are plots of activities on the graphite sleeve. Figures 4-5a through 4-5e show in-situ activation products on diffusion tubes. Figure 4-6 shows both activation and fission products on the outside of the probe sleeve.

4.1. IODINE MEASUREMENTS

Information on iodine behavior in the primary circuit has been obtained using all four methods listed in Table 2-1. The methods are (1) total released (or plated out) from xenon R/B, (2) total plated out from decay study during shutdown, (3) amount circulating from iodine monitor, and (4) amount circulating and plated out from plateout probe. All of these

TABLE 4-3
FISSION PRODUCTS INSIDE AND OUTSIDE PLATEOUT PROBE

	Inside Probe (μCi)			Outside Probe (μCi/cm^2)	
Nuclide	Graphite	Fiberfrax	Plenum	Hot Side Sleeve	Cold End Flange
I-131	0.54	0.10	0.044	NA	0.002
Cs-137	0.069	0.018	0.0034	0.001	0.0004
Cs-134	0.01	Trace	0.0019	0.0005	0.0001
Ba-140	Trace	Trace	Trace	0.003	0.0015
Sr-89	NA	NA	NA	0.008	NA
Sr-90	NA	NA	NA	0.00017	NA
S-35	NA	NA	NA	0.01	0.7
Pa-233	0.61	--	0.13	Trace	0.0003
Ag-110m	0.047	--	--	--	--
Ce-141	--	--	--	Trace	--
Ce-144	0.025	--	--	Trace	--
Ru-106	--	--	--	Trace	--
Nb-95	--	--	--	Trace	--
Zr-95	--	--	--	Trace	--
Eu-154	--	--	--	Trace	--

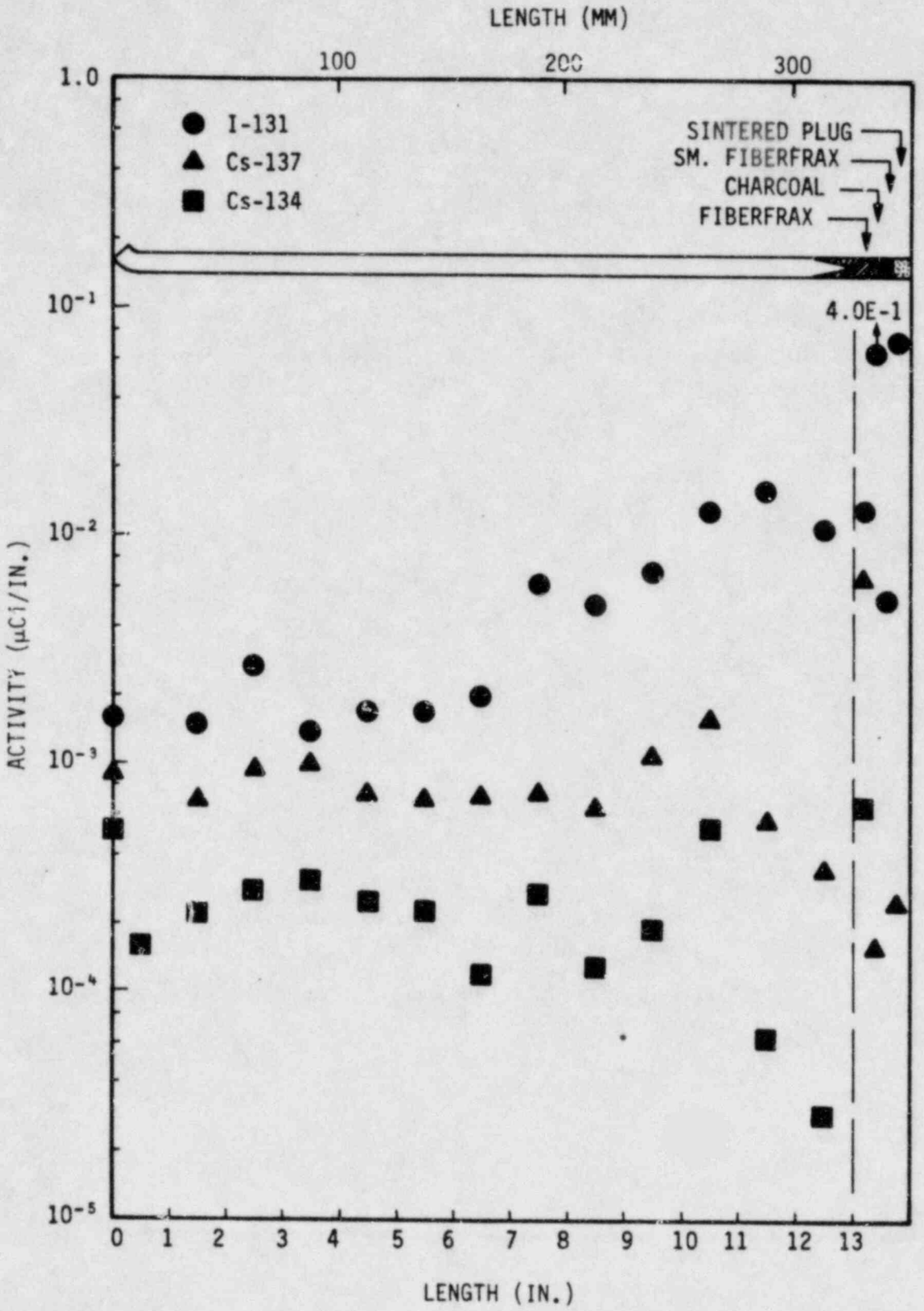

Fig. 4-1. Axial concentrations of I-131, Cs-137, and Cs-134 in diffusion tubes: (a) top diffusion tube (Sheet 1 of 5)

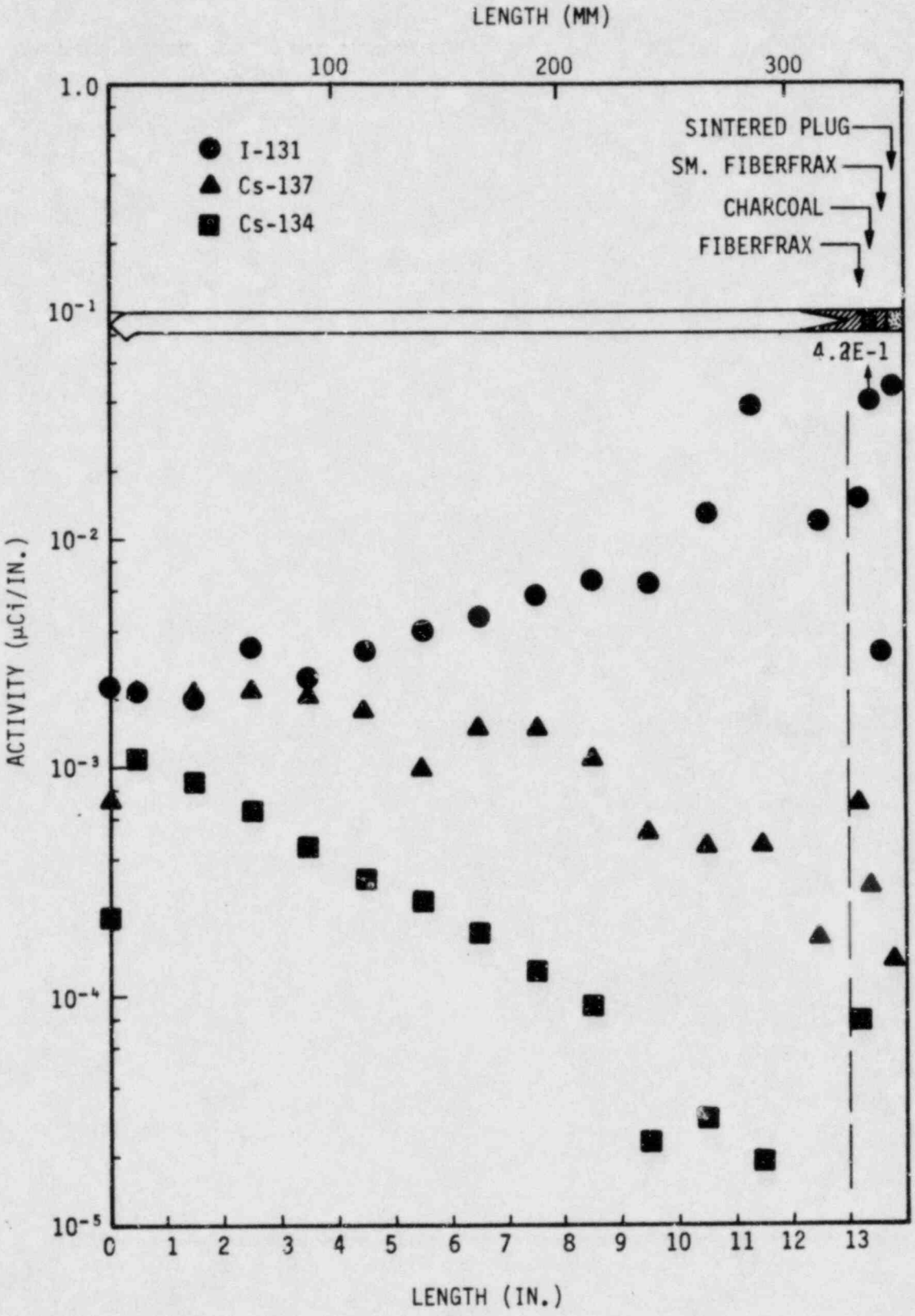

Fig. 4-1. Axial concentrations of I-131, Cs-137, and Cs-134 in diffusion tubes: (b) bottom diffusion tube (Sheet 2 of 5)

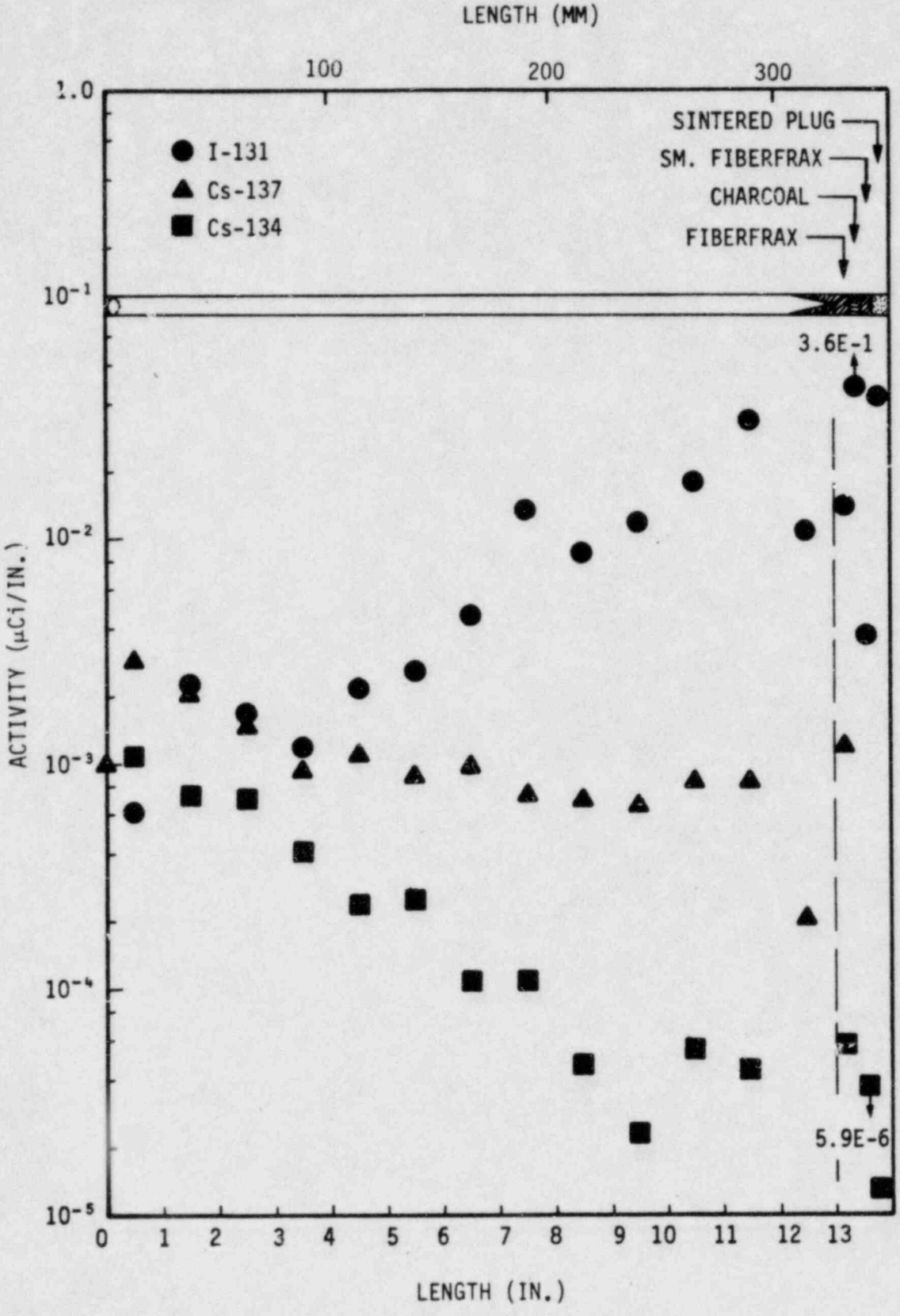

Fig. 4-1. Axial concentrations of I-131, Cs-137, and Cs-134 in diffusion tubes: (c) right diffusion tube (Sheet 3 of 5)

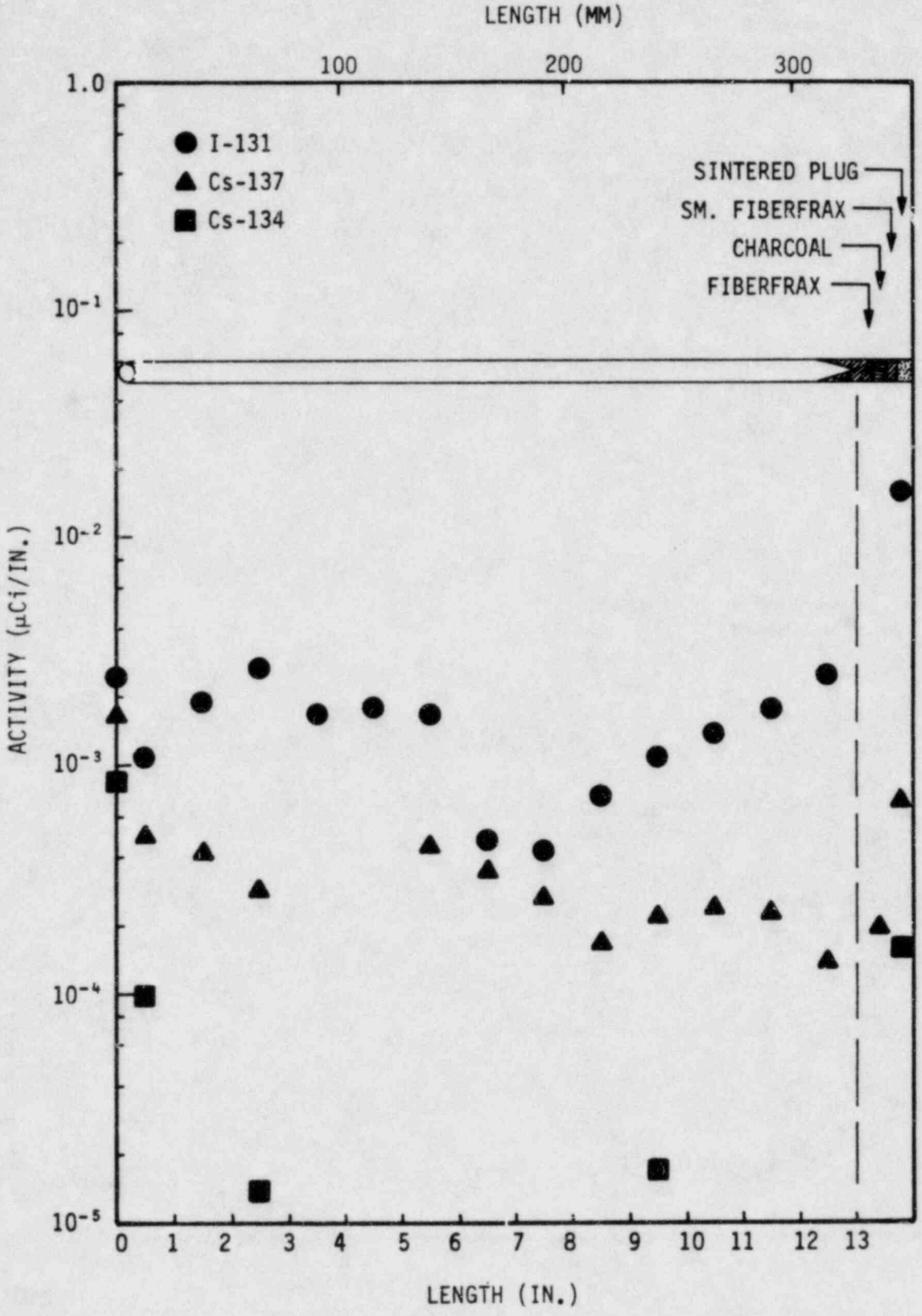

Fig. 4-1. Axial concentrations of I-131, Cs-137, and Cs-134 in diffusion tubes: (d) left diffusion tube (Sheet 4 of 5)

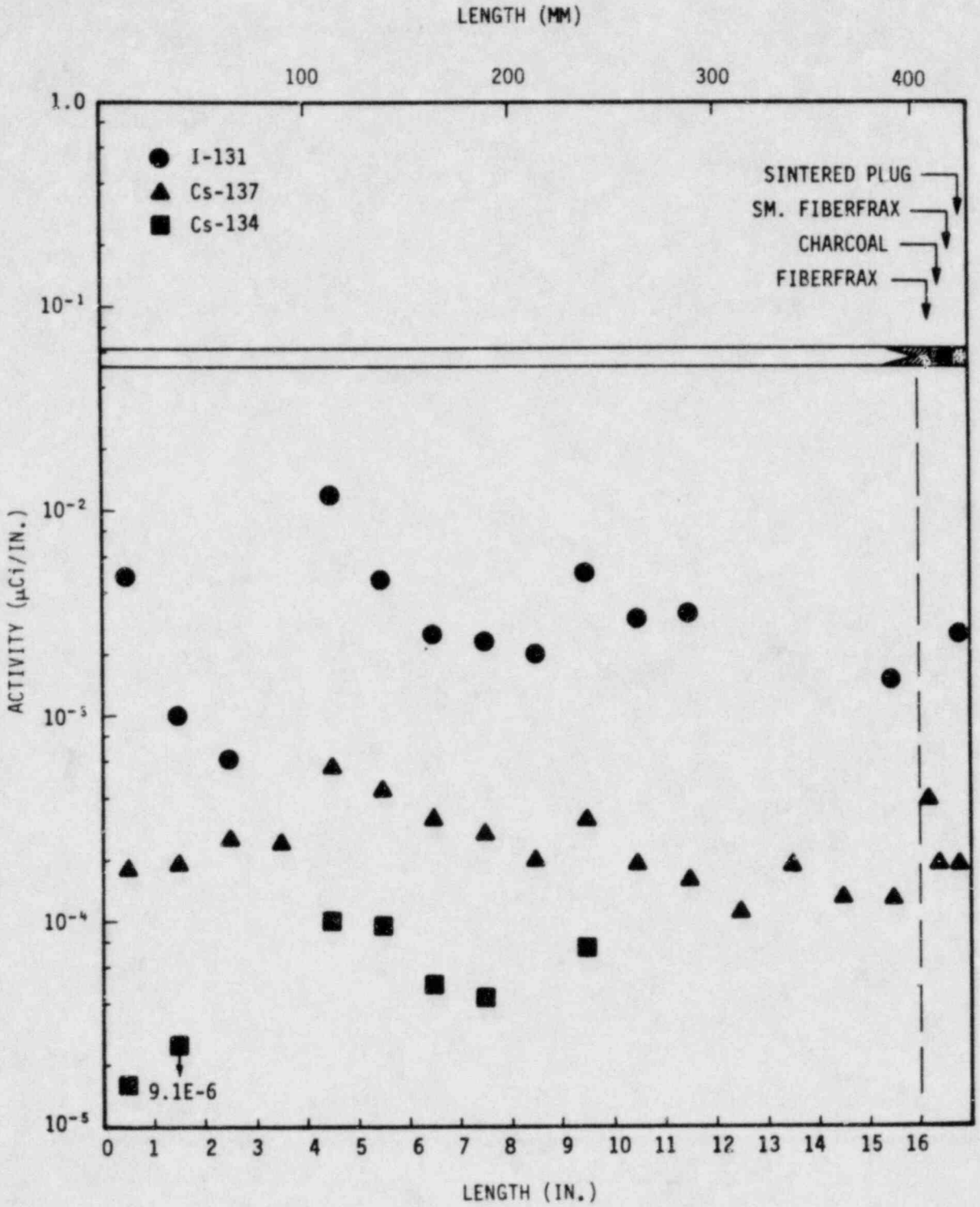

Fig. 4-1. Axial concentrations of I-131, Cs-137, and Cs-134 in diffusion tubes: (e) center diffusion tube (Sheet 5 of 5)

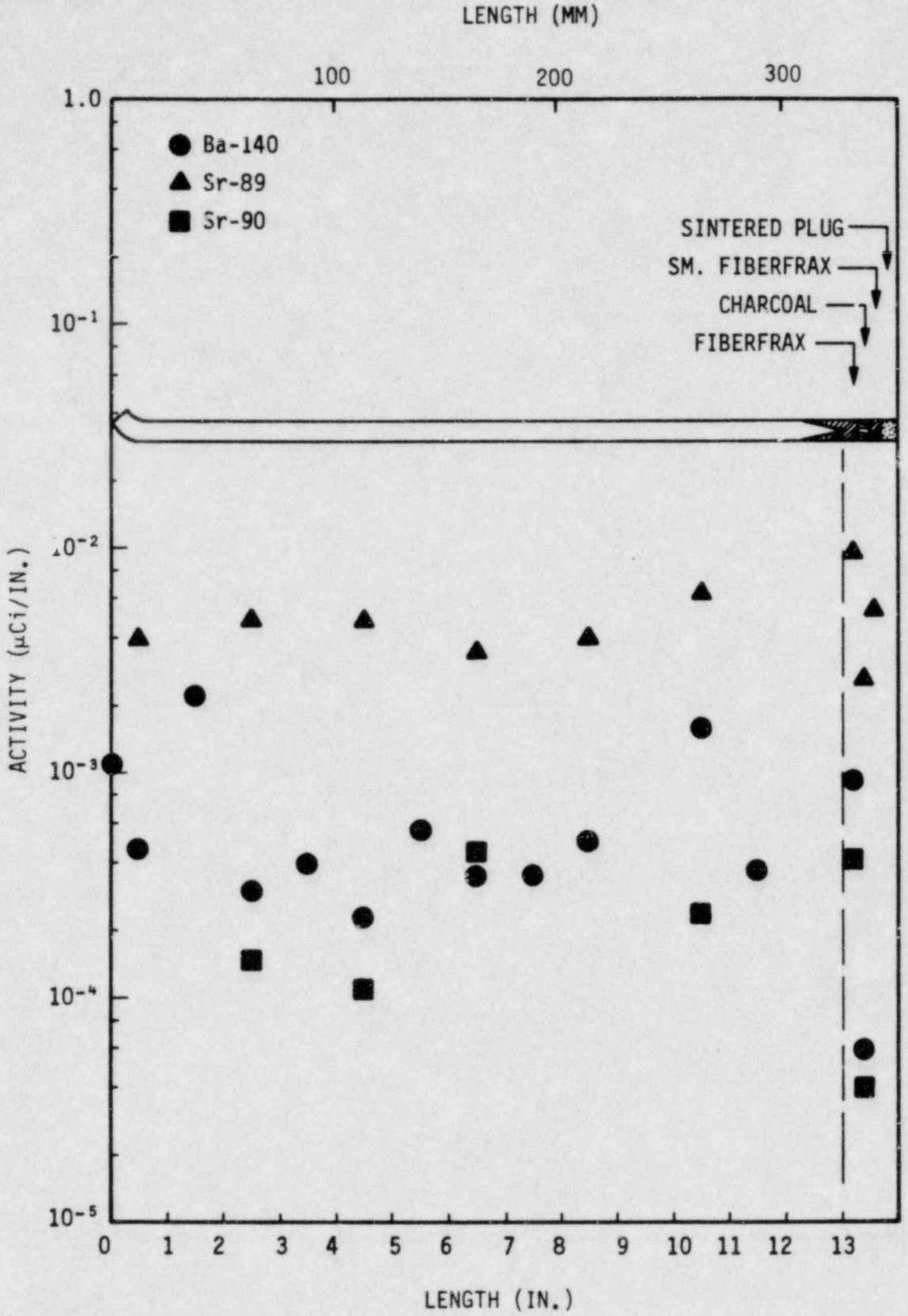

Fig. 4-2. Axial concentrations of Sr-89, Sr-90, and Ba-140 in diffusion tubes: (a) top diffusion tube (Sheet 1 of 5)

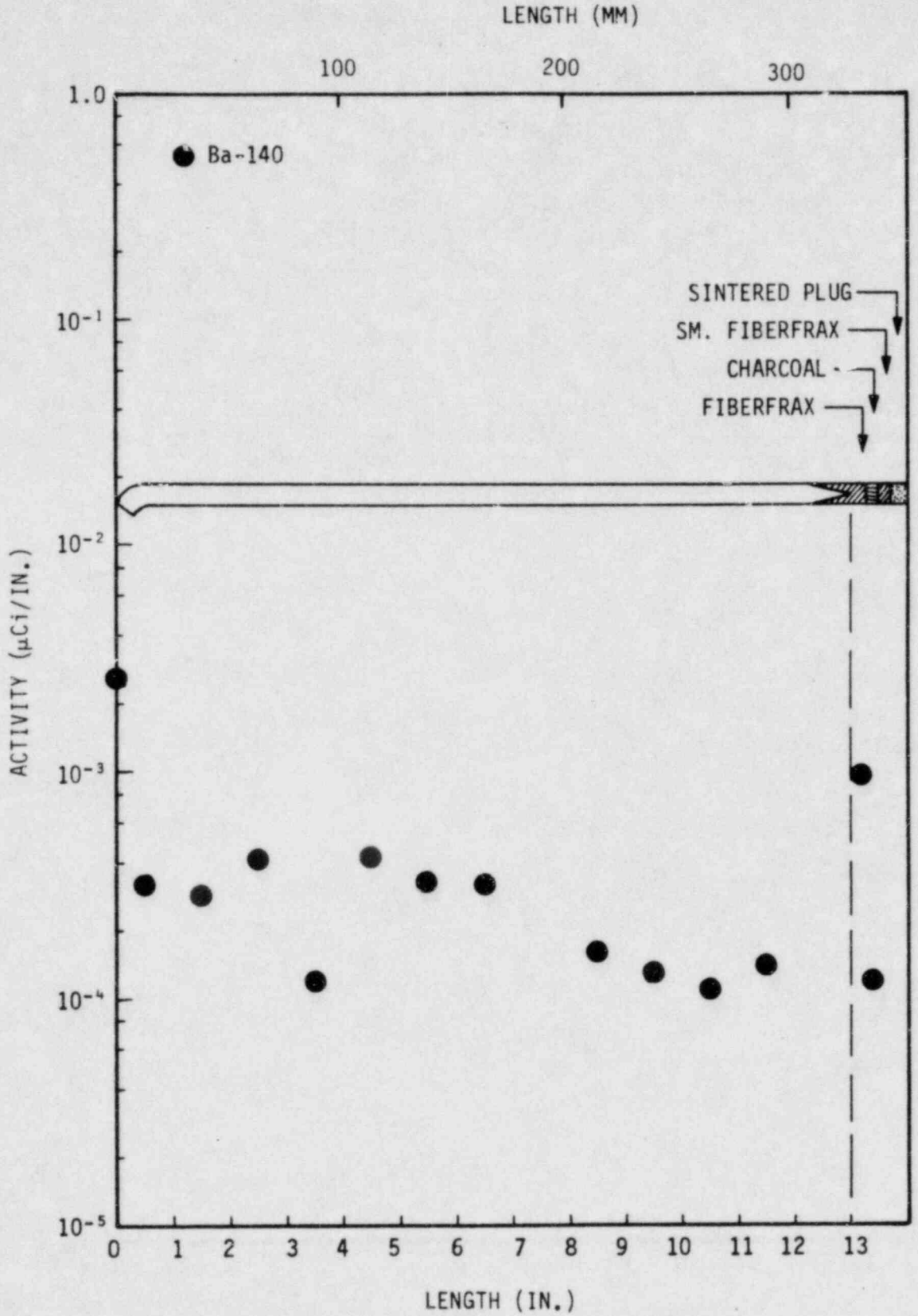

Fig. 4-2. Axial concentrations of Sr-89, Sr-90, and Ba-140 in diffusion tubes: (b) bottom diffusion tube (Strontium analyses were not performed on bottom tube.) (Sheet 2 of 5)

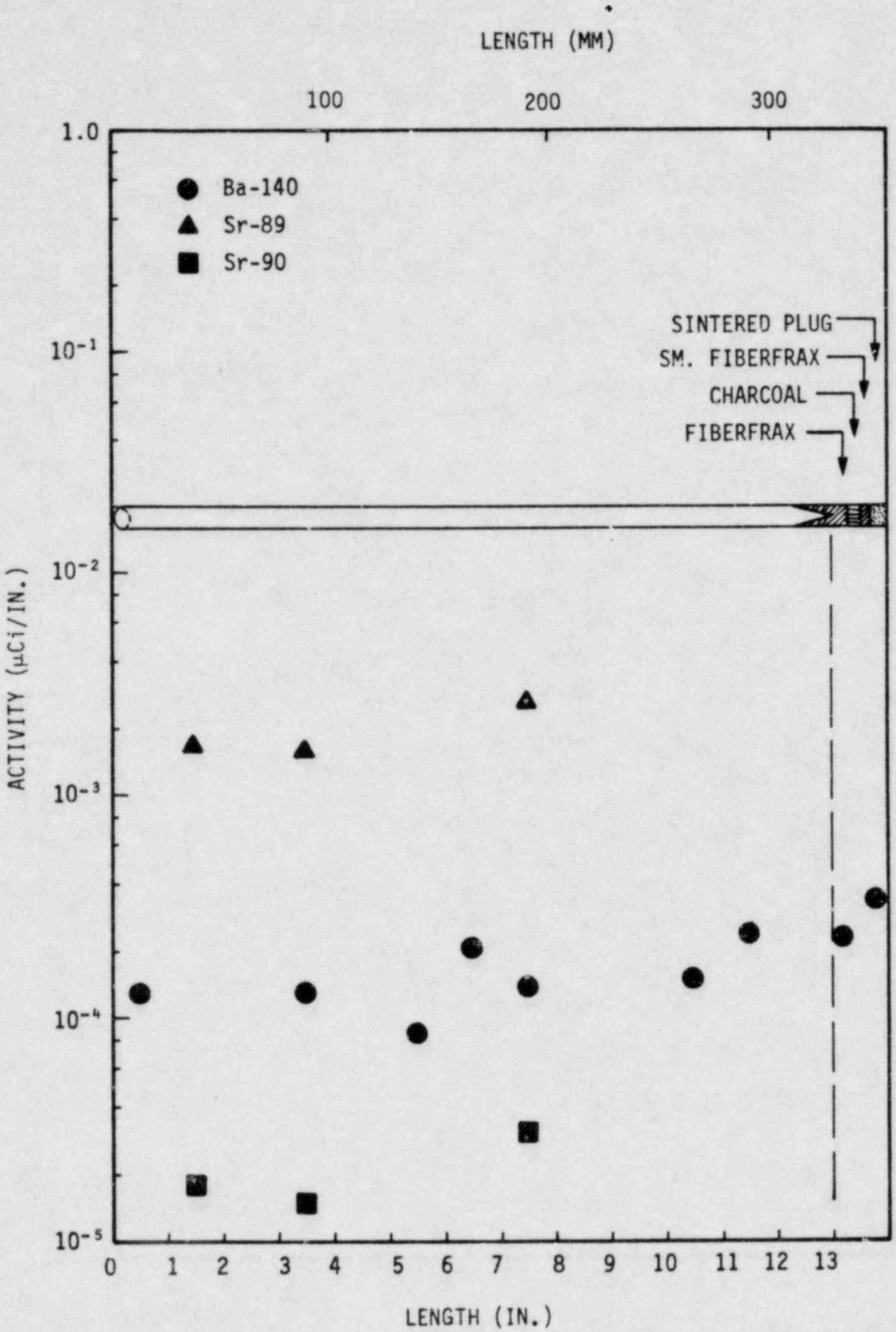

Fig. 4-2. Axial concentrations of Sr-89, Sr-90, and Ba-140 in diffusion tubes: (c) right diffusion tube (Sheet 3 of 5)

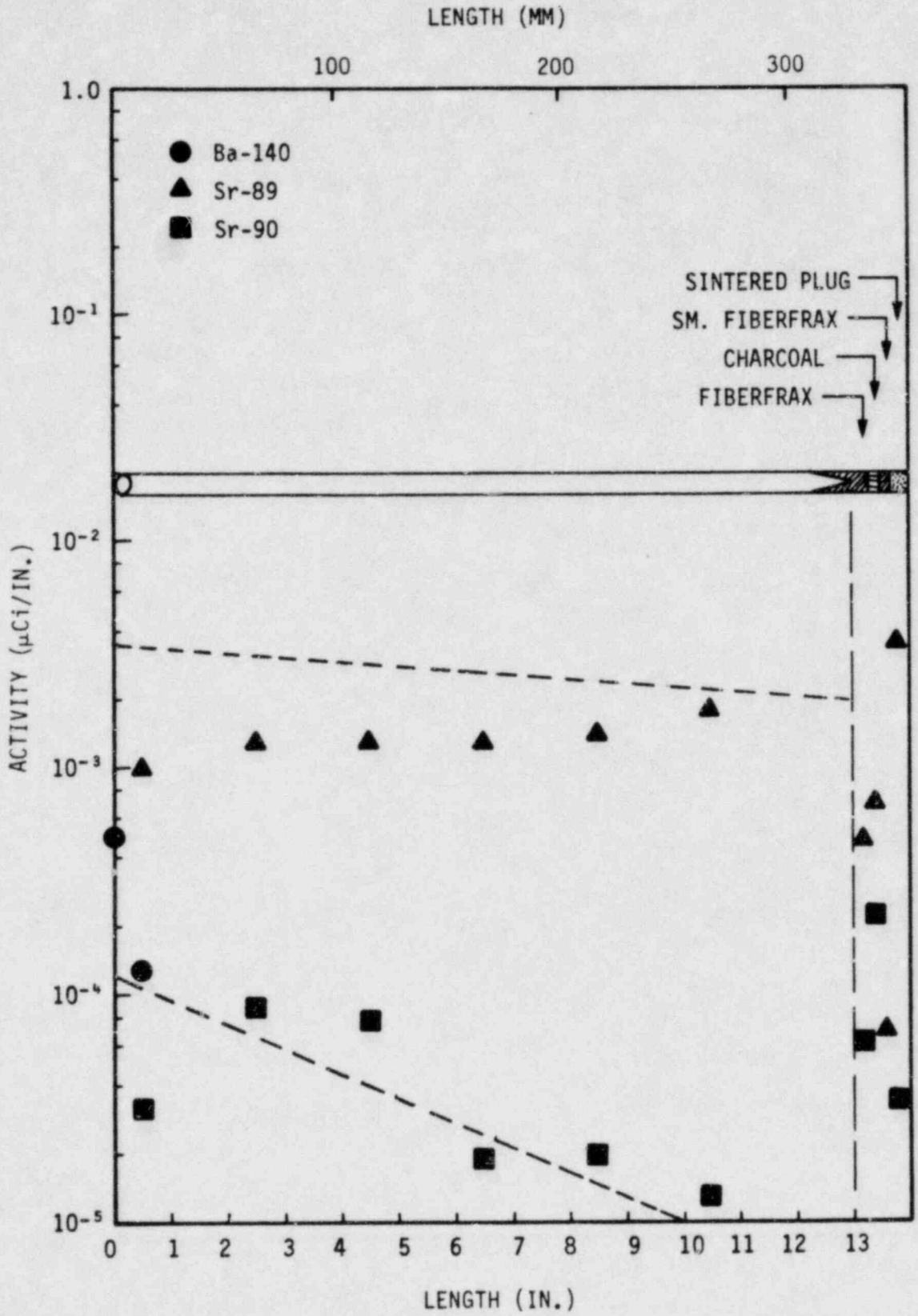

Fig. 4-2. Axial concentrations of Sr-89, Sr-90, and Ba-140 in diffusion tubes: (d) left diffusion tube. The dashed lines are predicted based on decay of Kr-89 and Kr-90. (Sheet 4 of 5)

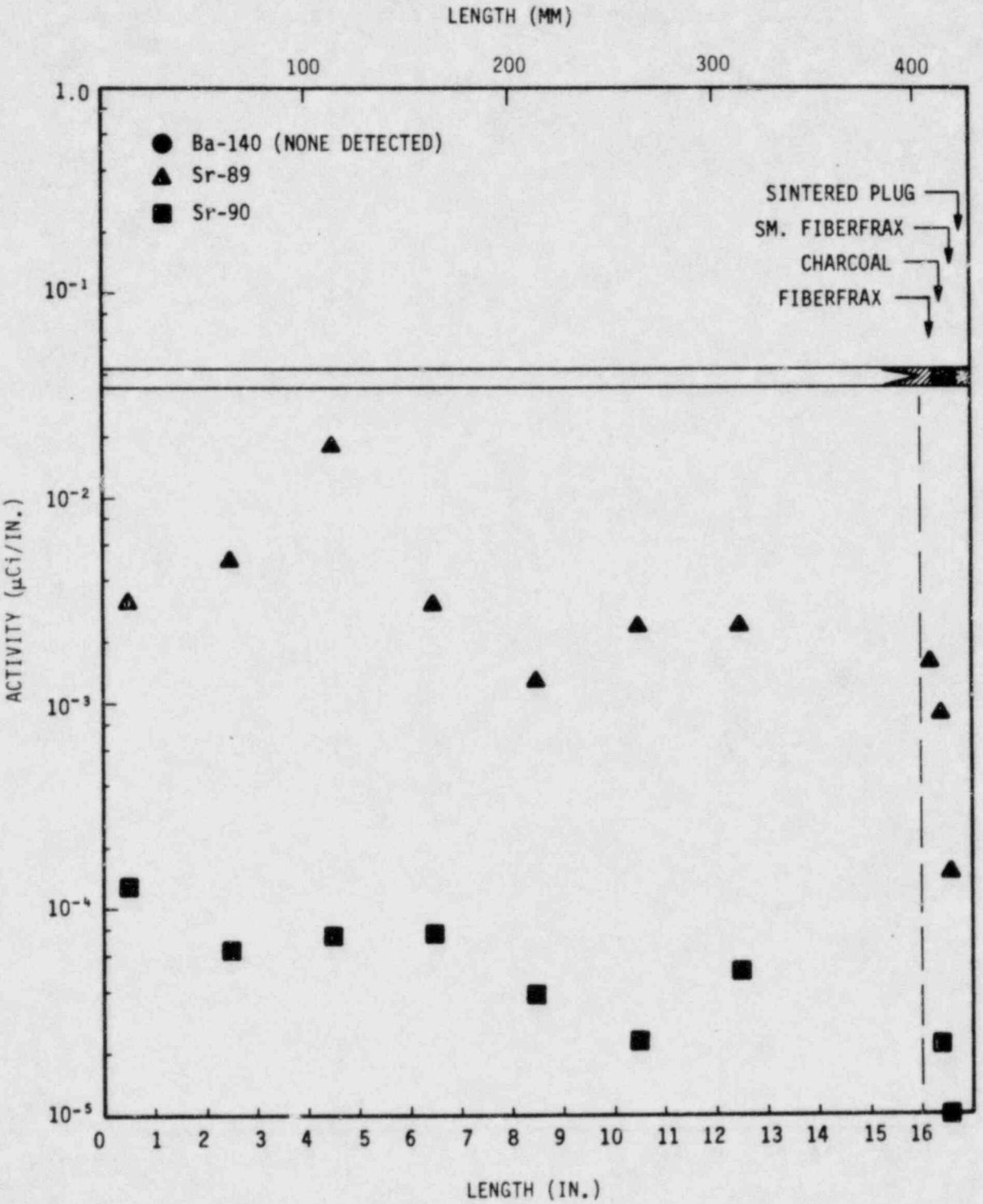

Fig. 4-2. Axial concentrations of Sr-89, Sr-90, and Ba-140 in diffusion tubes: (e) center diffusion tube (Sheet 5 of 5)

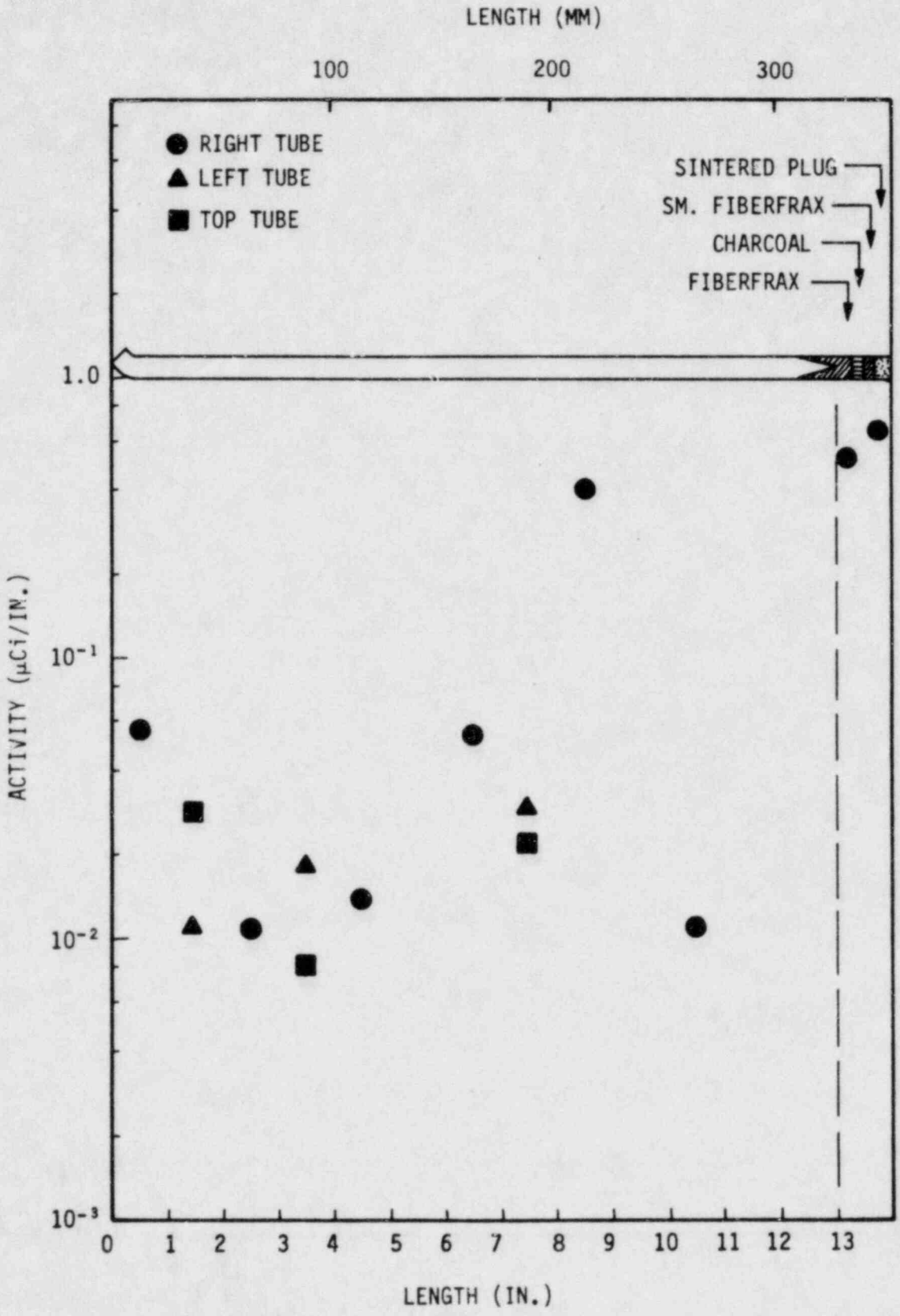

Fig. 4-3. Axial concentrations of S-35 in diffusion tubes

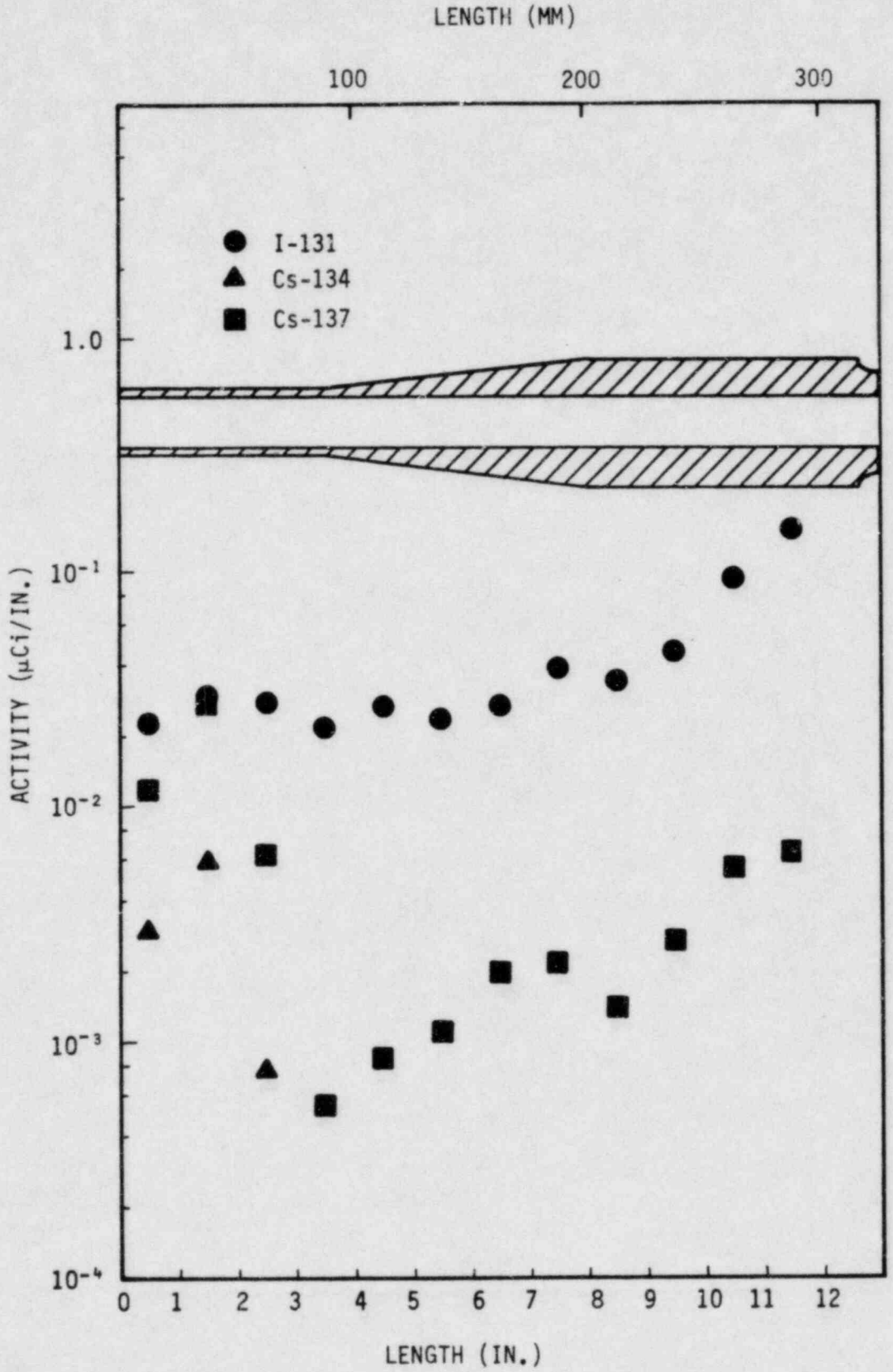

Fig. 4-4. Axial concentrations of nuclides in the internal graphite sleeve: (a) I-1313, Cs-134, and Cs-137 (Sheet 1 of 4)

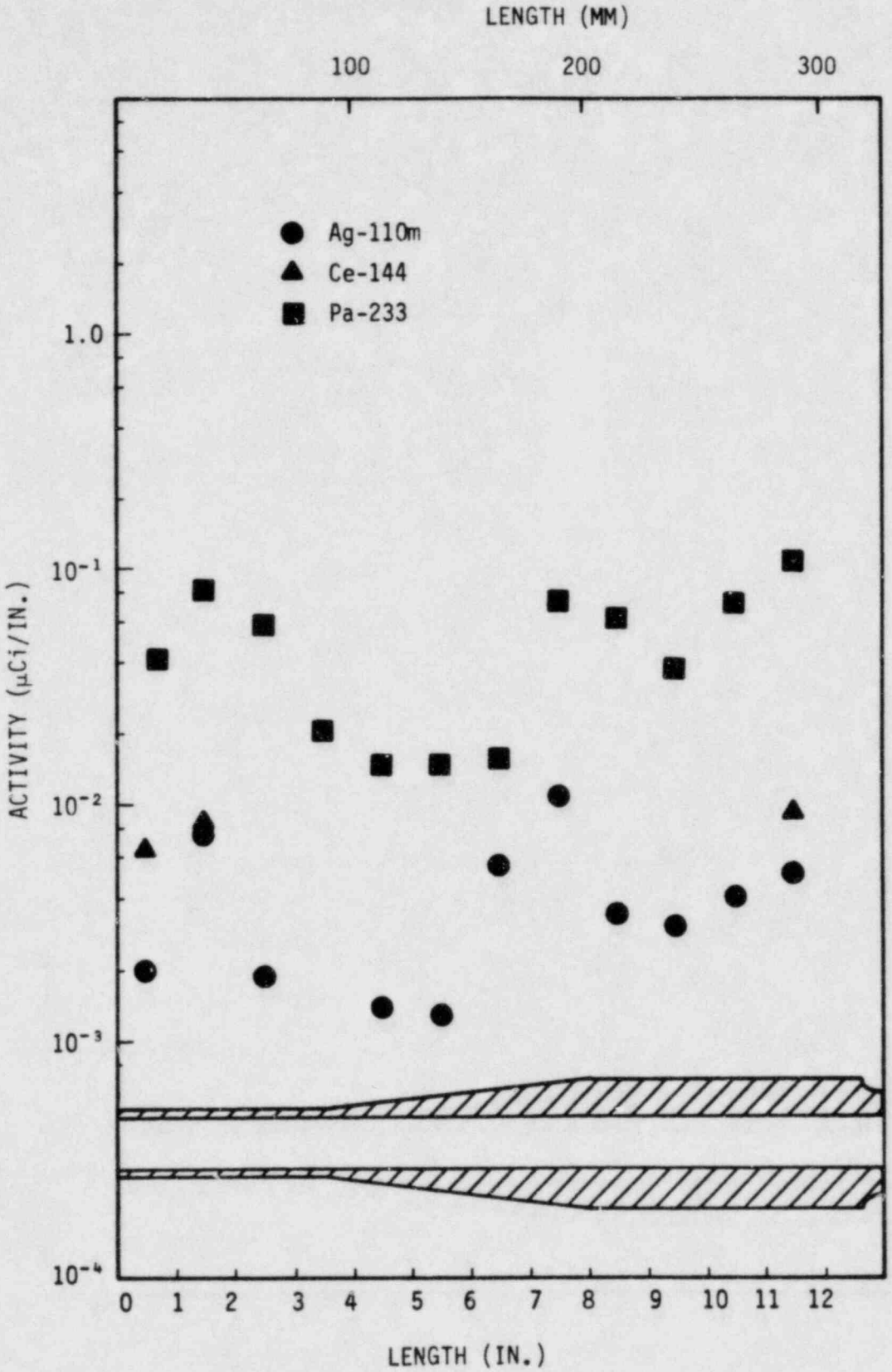

Fig. 4-4. Axial concentrations of nuclides in the internal graphite sleeve: (b) Ag-110m, Ce-144, and Pa-233 (Sheet 2 of 4)

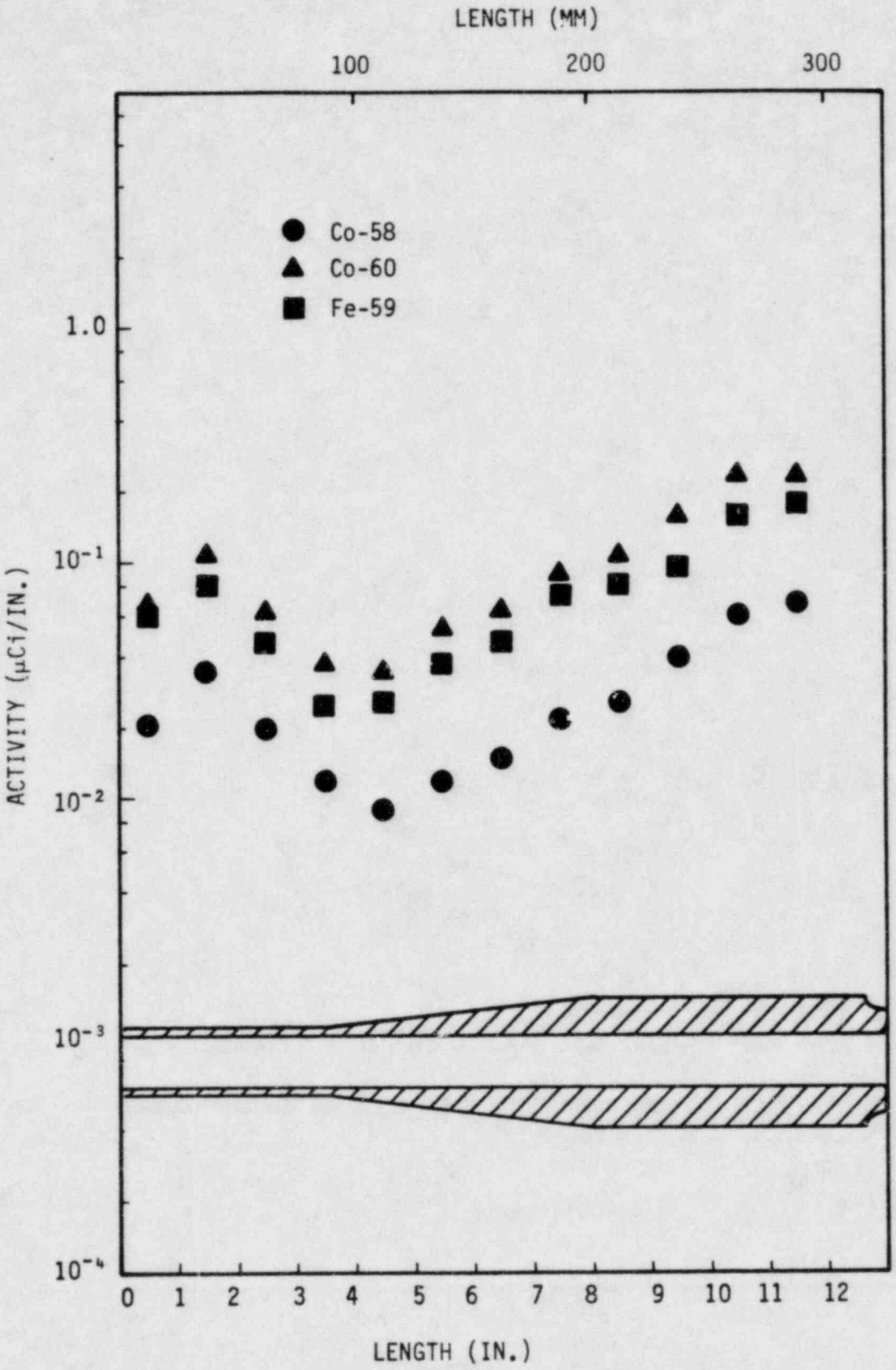

Fig. 4-4. Axial concentrations of nuclides in the internal graphite sleeve: (c) Co-58, Co-60, and Fe-59 (Sheet 3 of 4)

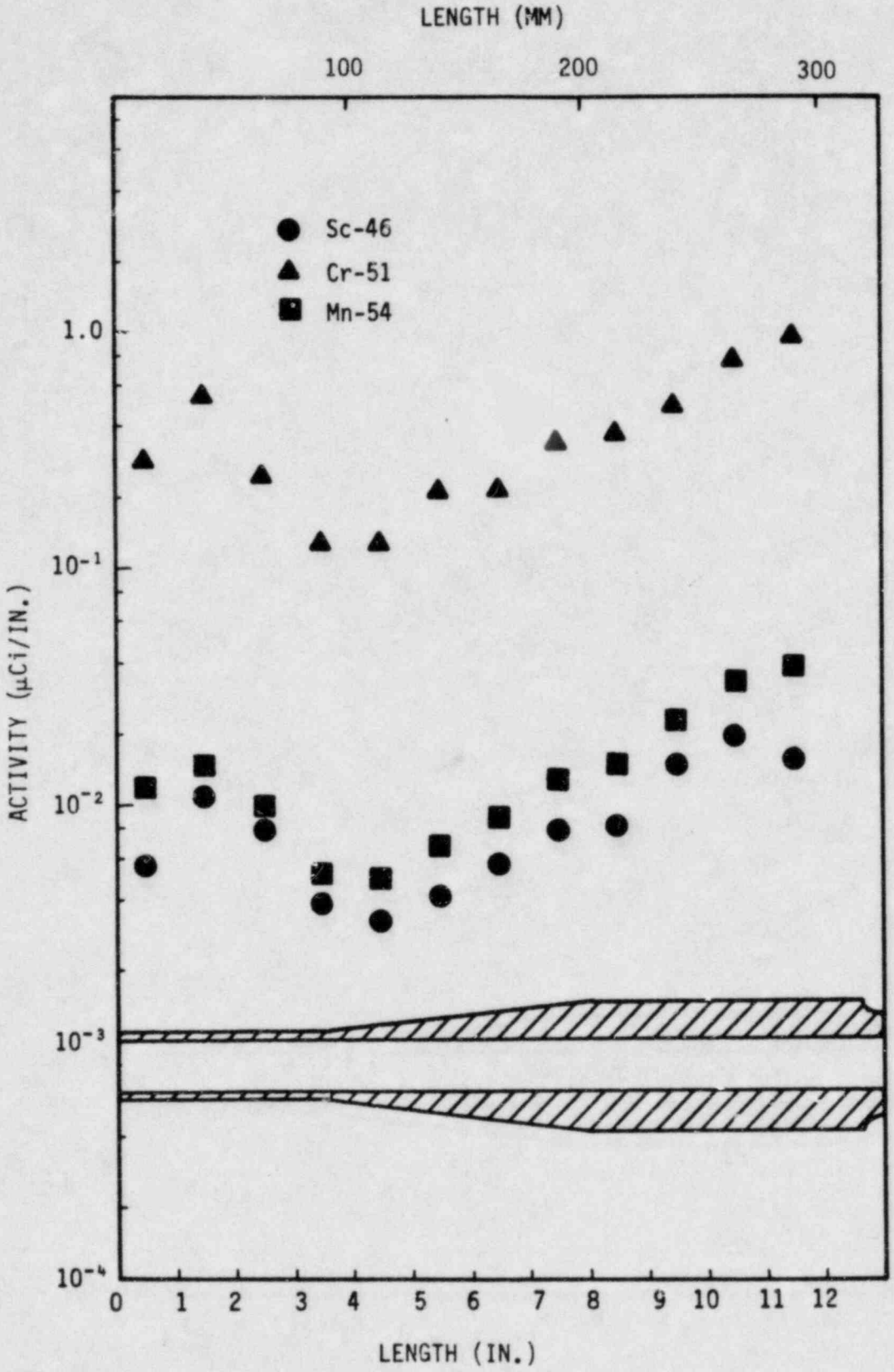

Fig. 4-4. Axial concentrations of nuclides in the internal graphite sleeve: (d) Sc-46, Cr-51, and Mn-54 (Sheet 4 of 4)

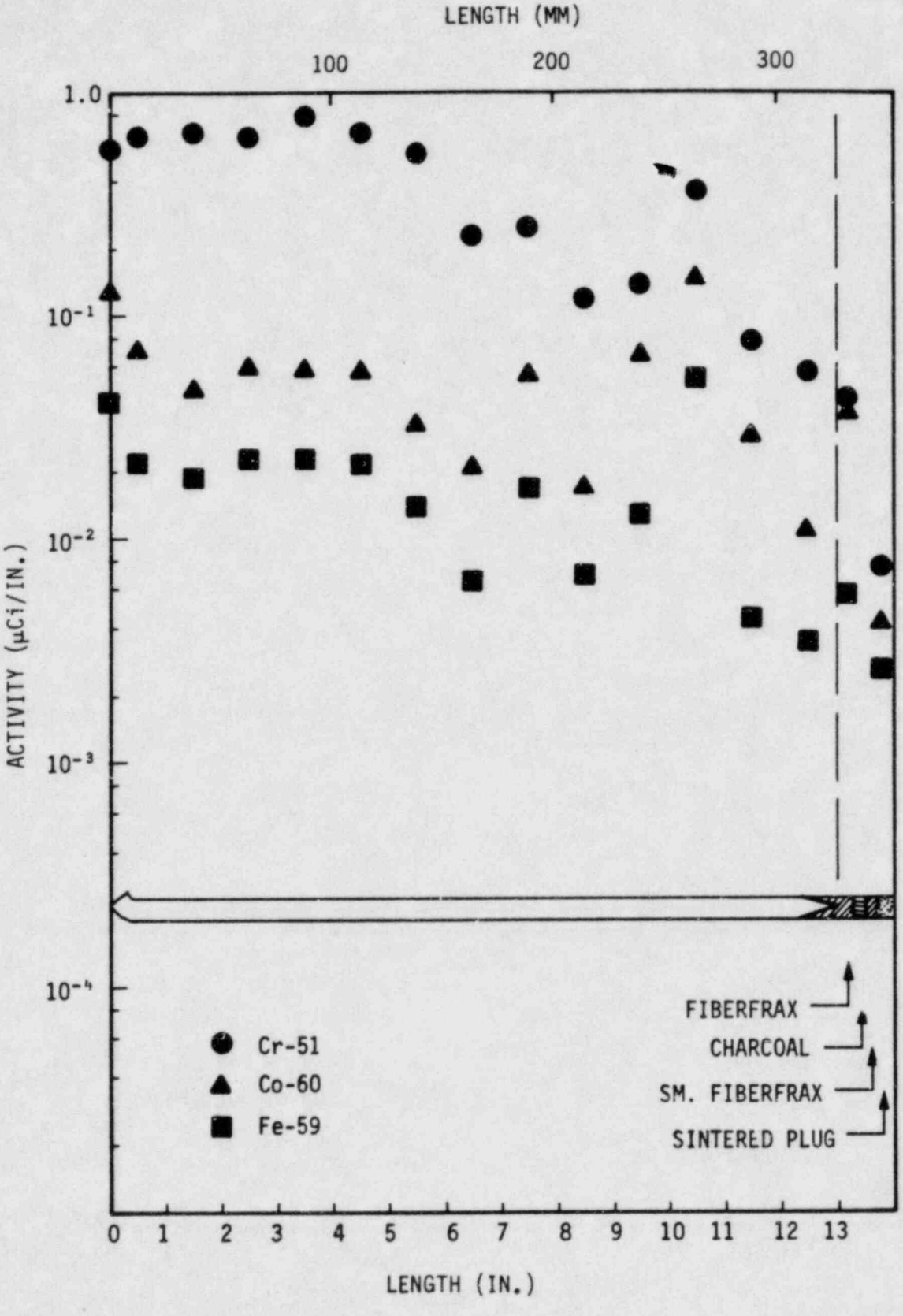

Fig. 4-5. Axial concentrations of activation products in diffusion tubes: (a) top diffusion tube (Sheet 1 of 5)

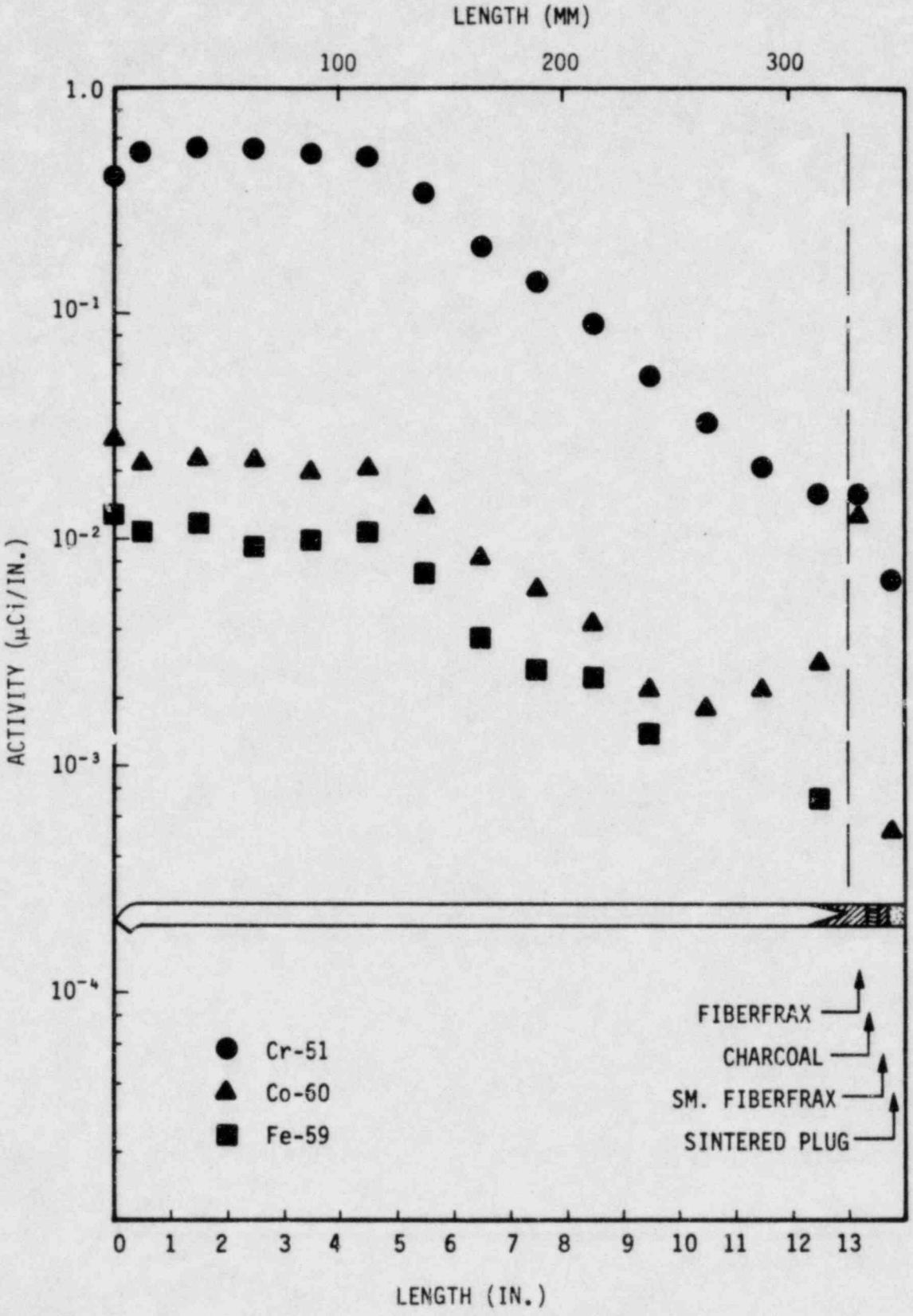

Fig. 4-5. Axial concentrations of activation products in diffusion tubes: (b) bottom diffusion tube (Sheet 2 of 5)

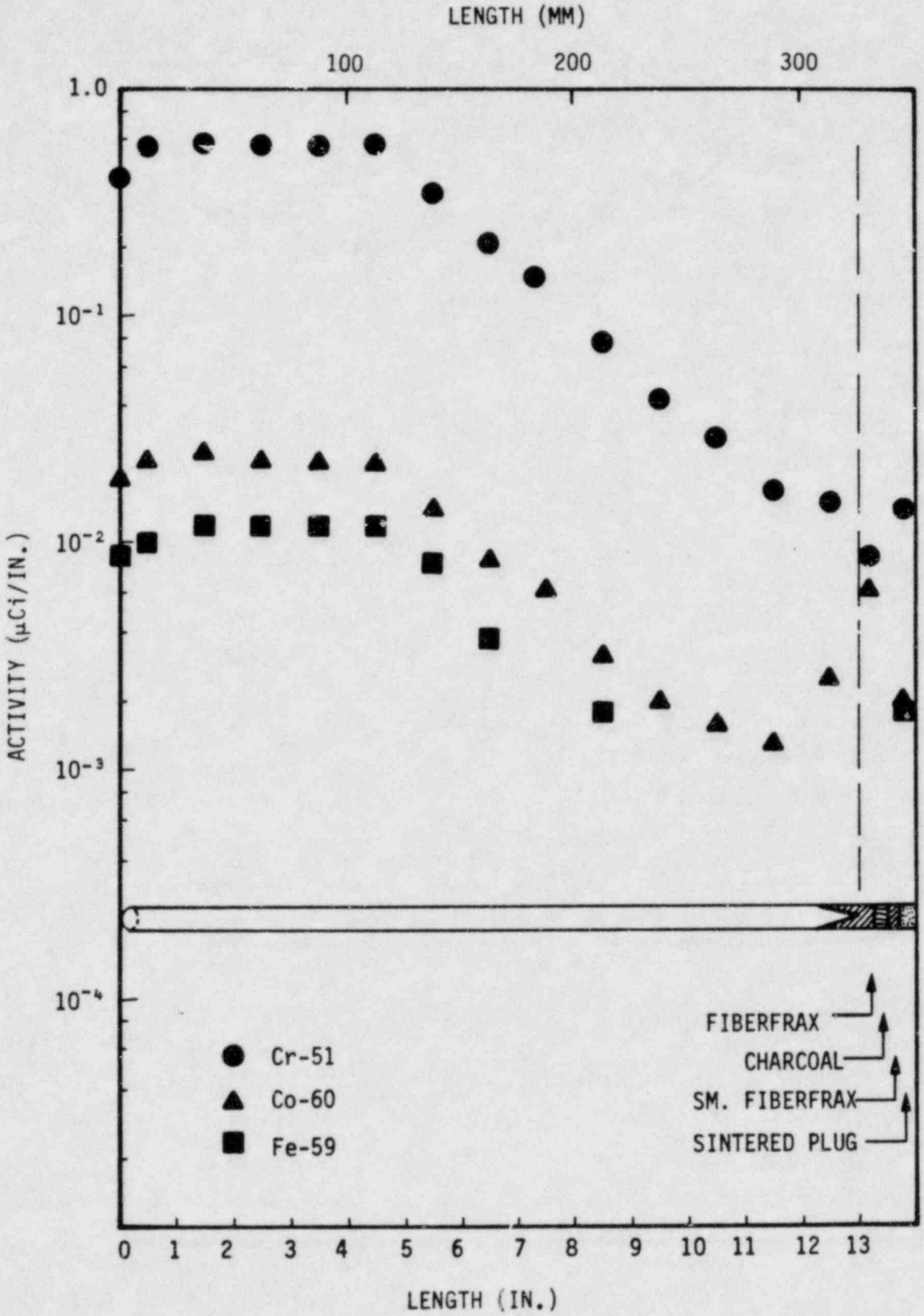

Fig. 4-5. Axial concentrations of activation products in diffusion tubes: (c) right diffusion tube (Sheet 3 of 5)

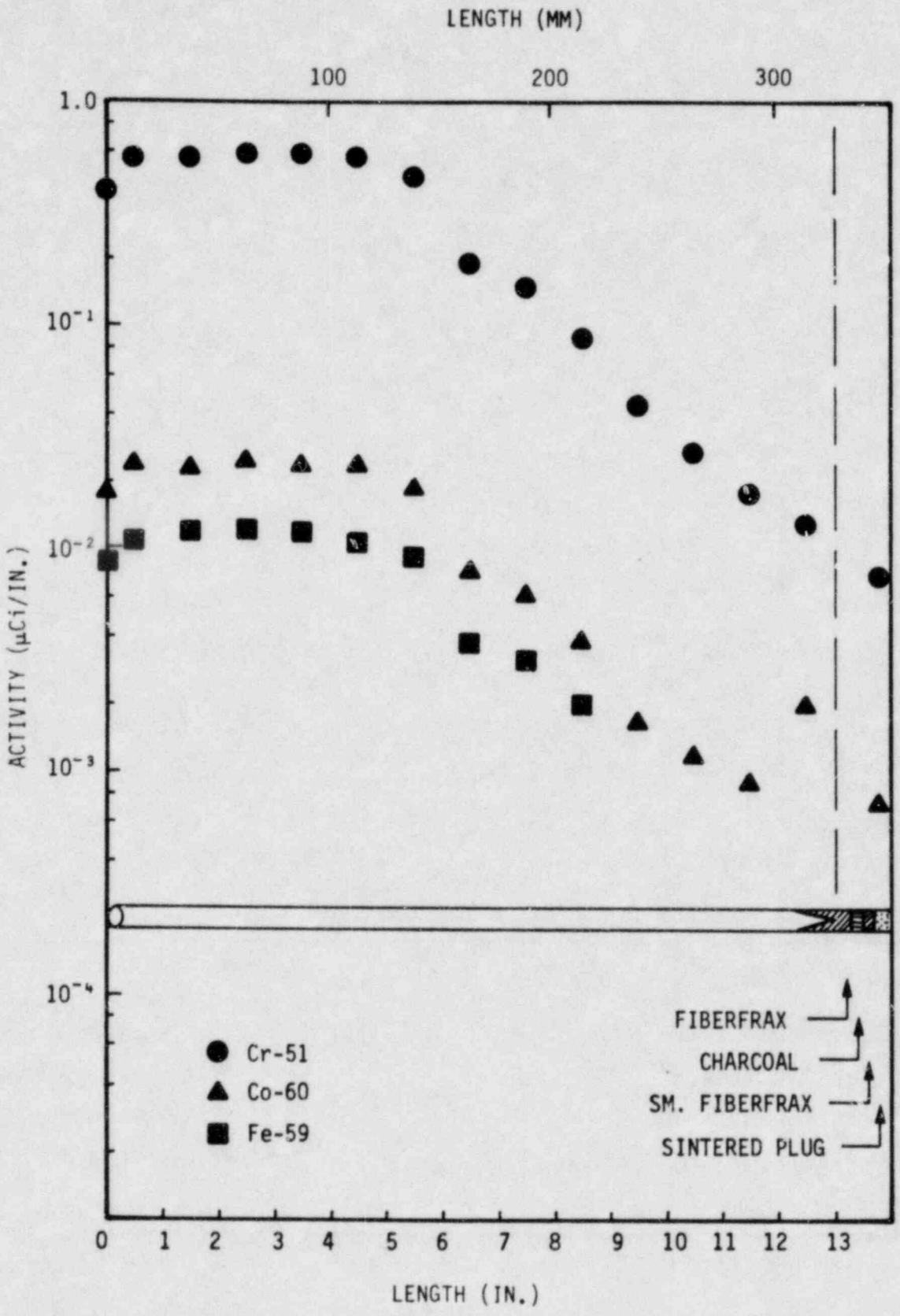

Fig. 4-5. Axial concentrations of activation products in diffusion tubes: (d) left diffusion tube (Sheet 4 of 5)

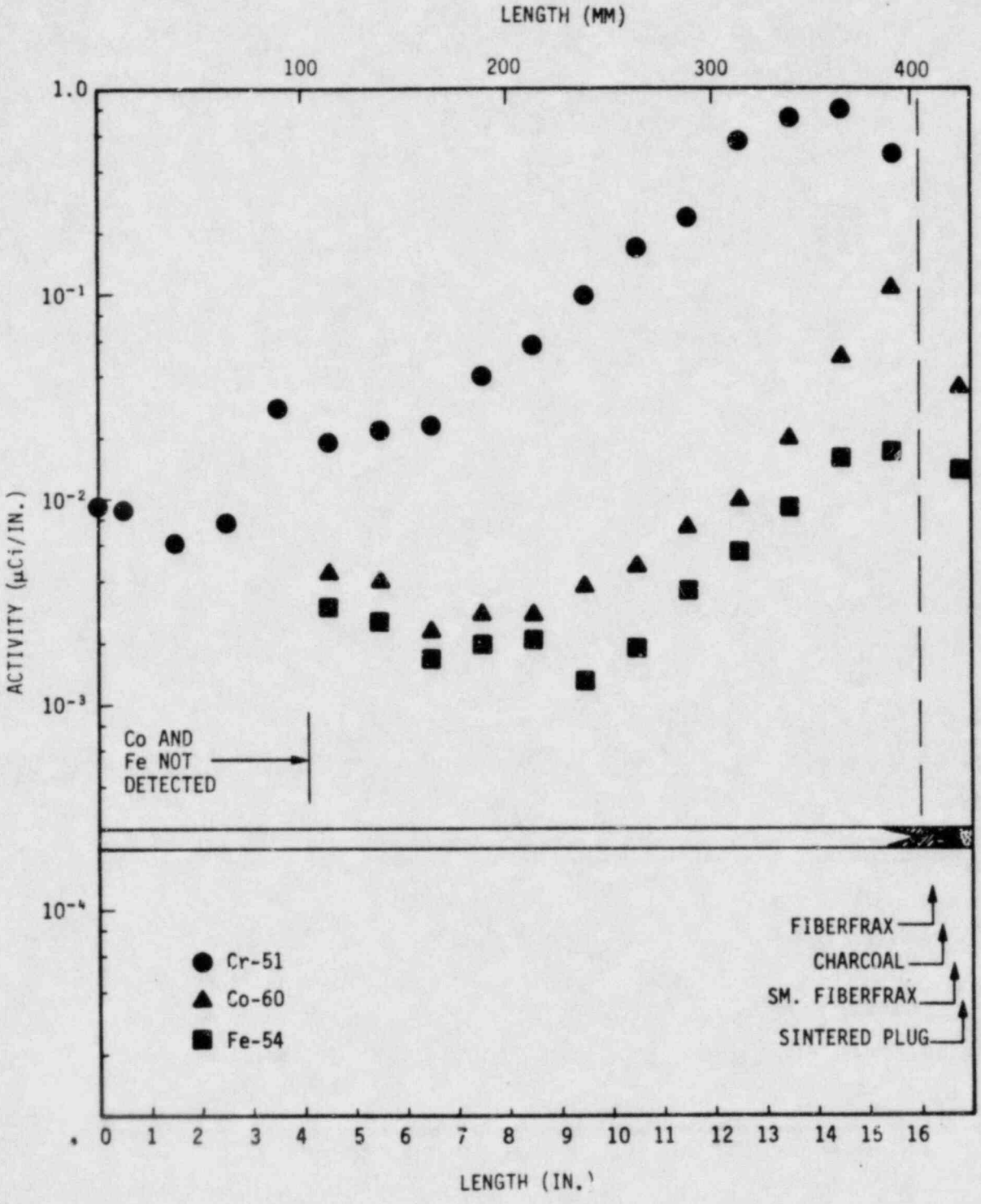

Fig. 4-5. Axial concentrations of activation products in diffusion tubes: (e) center diffusion tube (Sheet 5 of 5)

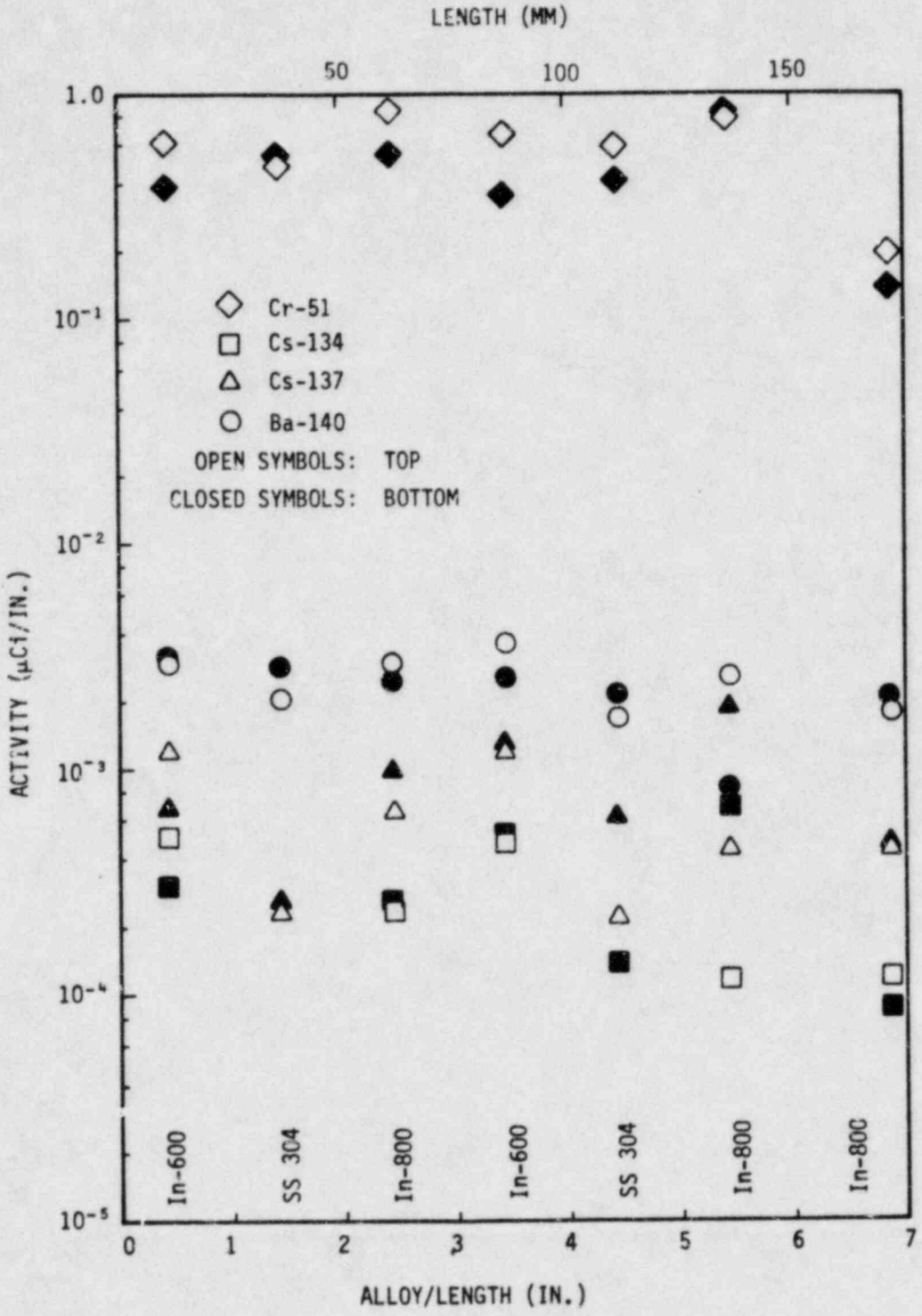

Fig. 4-6. Plateout on probe sleeve. Plateout of Cs-134 and Cs-137 on the 304 stainless steel segments was lower than on the Inconel 600 and Inconel 800 segments

methods and results are discussed to demonstrate compliance with Technical Specification LCO 4.2.8.

4.1.1. Iodine Plateout from Xenon R/B

The plateout of iodine in the primary circuit is assumed to be virtually equal to the total released from the core. The total iodine released from the core is determined from xenon R/B measurements, assuming that iodine release is similar to xenon.

Figure 4-7 plots krypton and xenon R/B versus $t^{1/2}$ for 70% power during cycles 1, 2, and 3. The R/B of any iodine isotope can be obtained from the xenon line. Table 4-4 lists the plateout of iodine isotopes calculated from their respective R/B.

4.1.2. Iodine Plateout from Iodine Decay Study

Total iodine in the primary circuit was measured on May 13 through 15, 1981 at the end of cycle 2. This test continuously monitored the daughter products Xe-133 and Xe-135 in the helium coolant following reactor shutdown. The total concentration of iodine in the primary circuit was calculated from the xenon data. During the shutdown period, the primary circuit conditions were stable and constant and were therefore ideal for this test.

The experimental method was to gamma-count helium grab samples at intervals for a total of 119 h after reactor shutdown. During the first 19 h, no samples were obtained while the purification system was removing the xenon and krypton activity in the coolant that had been directly released from the core.

The data which are plotted in Fig. 4-8 show a classic case of radioactive transient equilibrium [that is, the decaying parents (iodine) have apparent half-lives longer than the daughters (xenon)]. Of course, the radioactive half-lives of the iodine parents are shorter than those of the

Fig. 4-7. R/B of xenon, krypton, and iodine versus half-life for cycles 1, 2, and 3

TABLE 4-4
CALCULATED AND OBSERVED PLATEOUT OF I-133 AND I-135 AT 70% POWER AT END OF CYCLE 2[a]

	I-135	I-133
Observed plateout[b] (Ci)	94	187
Calculated plateout[c] (Ci)	129	204
Iodine R/B[d]	2.9×10^{-6}	5.5×10^{-6}
Xenon R/B[e]	4×10^{-6}	6×10^{-6}

(a) Power was 78% for 4 h prior to shutdown.
(b) Plateout of iodine isotopes measured in decay study, calculated using Eq. 2-7.
(c) Plateout of iodine isotopes calculated from xenon R/B line using Eq. 2-6.
(d) Iodine R/B calculated from actual iodine plateout using Eq. 2-6.
(e) R/B of xenon line at the $t^{1/2}$ of I-135 and I-133.

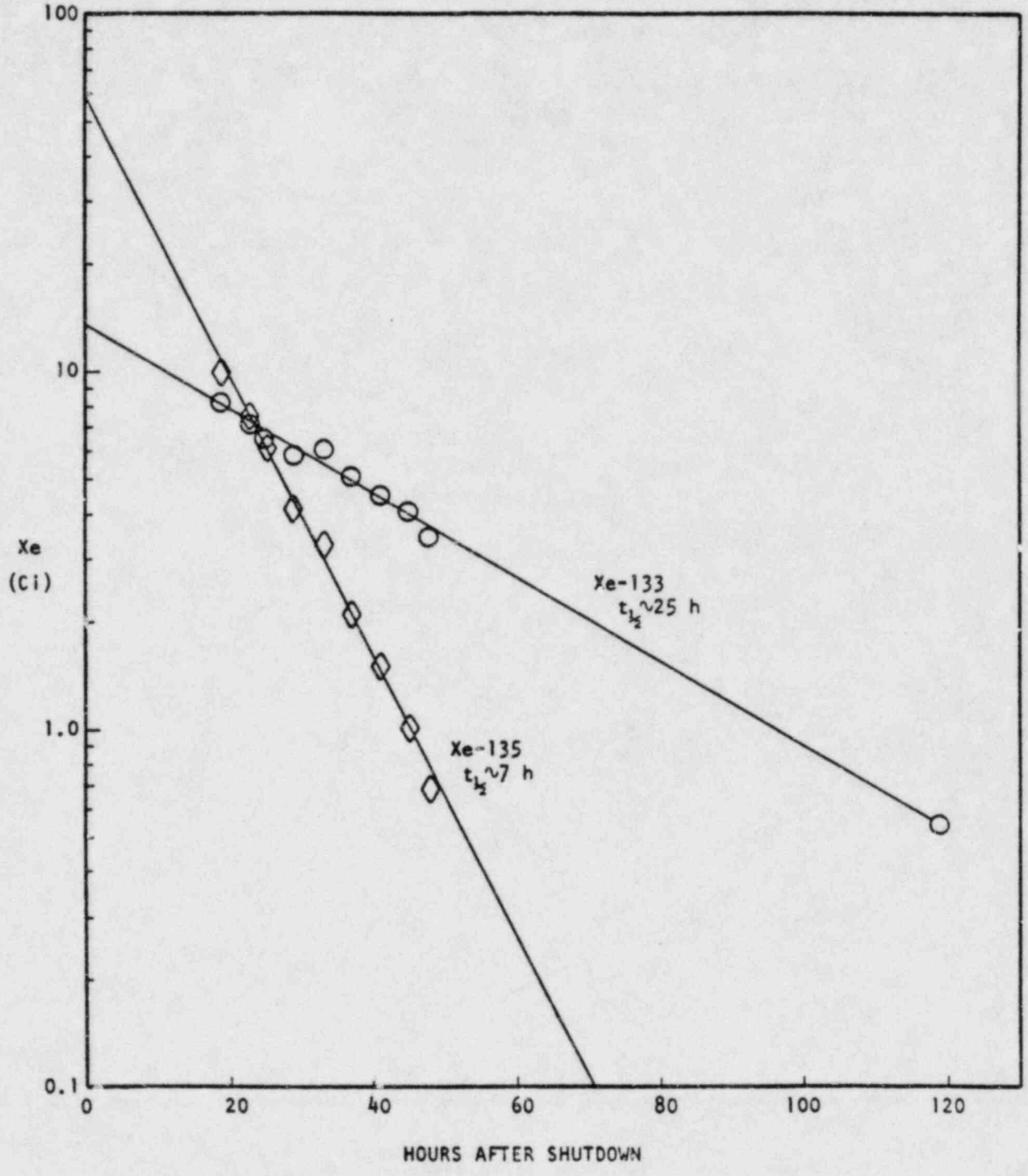

Fig. 4-8. Iodine decay study: FSV, May 13, 1981

xenon daughters. Because of constant purification cleanup, however, the apparent half-life of xenon is shorter than iodine. For such a case, the slope of the xenon activity versus time should reflect the half-life of the parent iodine species. The Xe-135 data showed an apparent $t^{1/2}$ of about 7 h, whereas I-135 $t^{1/2}$ = 6.7 h. The Xe-133 data indicated $t^{1/2}$ = 25 h and I-133 = 21 h. The iodine parent was calculated from these data using Eq. 2-7.

Table 4-4 lists the iodine data. Figure 4-7 plots the iodine R/B data and the xenon and krypton R/B measured at 70% reactor power one day before shutdown. The iodine R/B's are quite close to the xenon line, verifying the assumption that iodine release is similar to xenon at high temperatures.

4.1.3. Circulating Iodine from the Iodine Monitor

The iodine monitor measured the concentration of I-133 and I-135 in the coolant helium on four occasions. Table 4-5 summarizes the data obtained, and Table 4-6 lists the results calculated from the data. Figure 4-9 plots the measured plateout constant r_p versus the decay constant λ. Equation 2-9 predicts the observed direct proportionality of r_p to λ. This allows a means of extrapolating to other iodine species, including I-131 shown in Table 4-6. Table 4-7 lists the calculated concentrations of iodine isotopes in terms of I-131 equivalents. At 70% power, the plateout of I-131 equivalent was about 1% of the limit given by Technical Specification LCO 4.2.8. The circulating I-131 equivalent was only 1.5% of the limit.

4.1.4. Circulating I-131 from Diffusion Tube Data

Figures 4-1a through 4-1e plot I-131 concentration versus tube length in the individual tubes and show Cs-137 and Cs-134 data. In general, the iodine concentrations increase along the tube length with decreasing temperature (see Fig. 2-4 for temperature profile). This is consistent with the behavior of atomic or molecular iodine. Iodine was thought to be associated

TABLE 4-5
IODINE MONITOR DATA FOR FSV REACTOR CYCLES 1 AND 3

Date	Cycle	Power (%)	Coolant Impurities CO/CO_2[a] (ppm)	Cycle EFPD[b]	I-135 R/B[c]	I-135 A_c[d] (Ci)	I-133 R/B[b]	I-133 A_c[d] (Ci)	I-131 R/B[c]
5/18/78	1	65	10/2	80	5.5(-6)	0.795	8.2(-6)	1.839	1.8(-5)
11/20/78	1	63	5/2	139	5.7(-6)	0.750	8.2(-6)	1.890	1.7(-5)
11/27/78	1	64	3/1	143	5.9(-6)	0.897	8.5(-6)	2.34	1.8(-5)
9/29/81	3	70	1.1/0.3	38	2.5(-6)	0.20	3.0(-6)	0.46	4.5(-6)

(a) H_2O below ~1 ppm in all cases.
(b) Effective full-power days.
(c) R/B values for iodine calculated from xenon values.
(d) A_c activity of iodine as measured by the iodine monitor. Data have been multiplied by three to reflect the gamma counting error associated with the cold trap geometry.

TABLE 4-6
CIRCULATING AND PLATED-OUT IODINE IN FSV DURING FUEL CYCLES 1 AND 3
(IODINE MONITOR DATA)

Isotope	$t^{1/2}$ (h)	λ (s^{-1} x 10^6)	Reactor Cycle	R/B (x 10^6)	A_p(a) (Ci)	A_c(b) (Ci)	A_p/A_c	r_p (s^{-1} x 10^4)	τ(%)(c)
134	0.87	220	1(d)	4	139	(0.9)	(160)(e)	(340)(e)	(33)
			3(f)	1.5	57	(0.2)	(300)	(600)	(46)
132	2.29	84	1	6	125	(0.8)	(160)	(130)	(14)
			3	2	46	(0.15)	(300)	(240)	(22)
135	6.7	29	1	5.7	160	0.80	200	57	7
			3	2.5	75	0.20	375	100	10
133	20.7	9.2	1	8.2	250	2.1	120	11	1.4
			3	3.0	100	0.46	217	20	2.0
131	193	0.97	1	17	235	(1.5)	(160)(e)	(1.5)(e)	(0.20)
			3	4.5	68	(0.23)	(300)	(2.7)	(0.28)

(a) A_p = iodine activity plated out.
(b) A_c = iodine activity circulating (in gas phase).
(c) τ = plateout per pass.
(d) Reactor cycle 1 data are average of three measurements (see Table 4-5). Power = 64%, cycle time = 12 s.
(e) Data in parentheses are calculated from r_p and average A_p/A_c obtained from I-133 and I-135 iodine monitor results.
(f) Reactor cycle 3. Power = 70%, cycle time = 10 s.

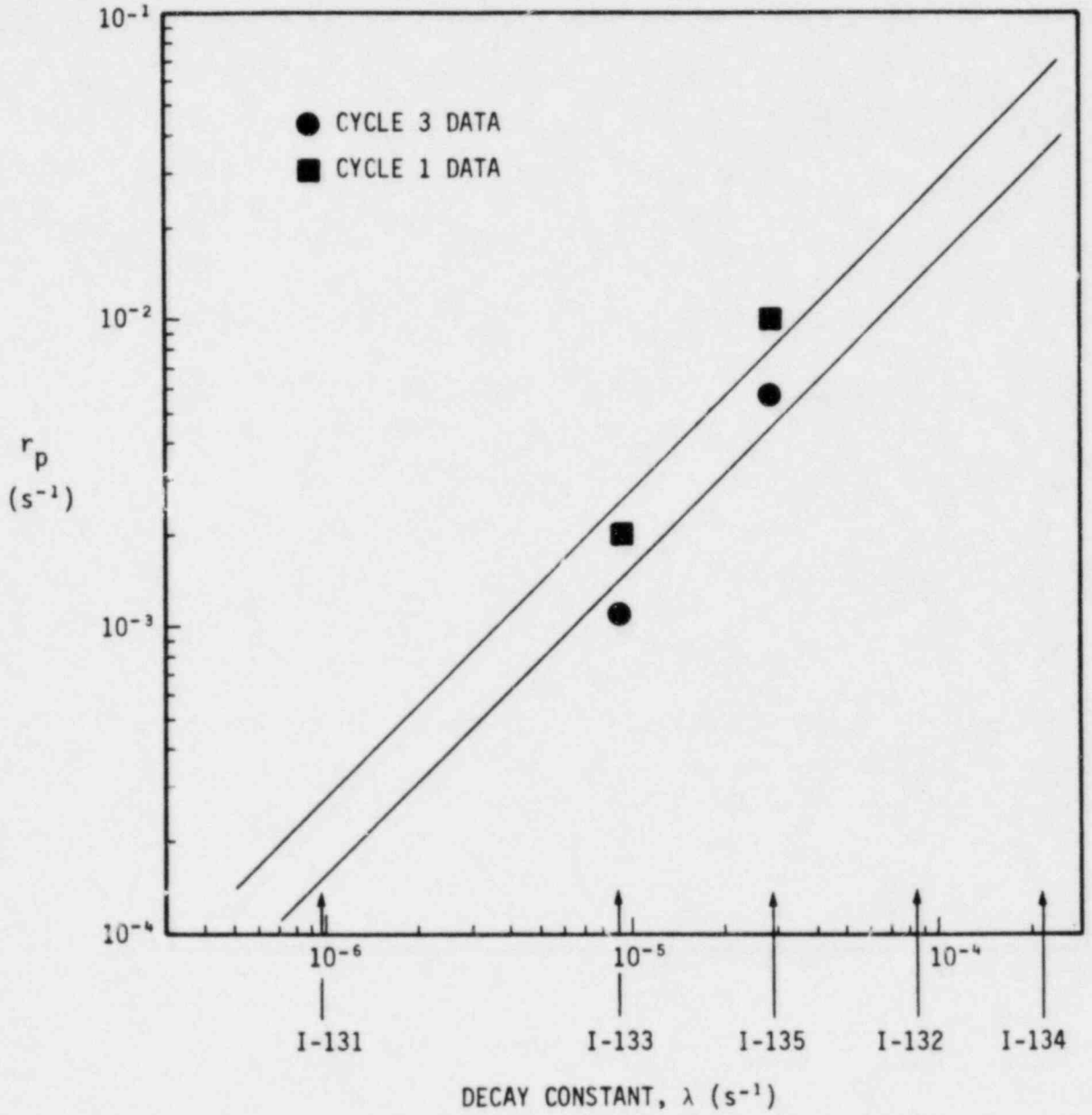

Fig. 4-9. Rate of plateout of iodine, r_p, as a linear function of decay constant, λ

TABLE 4-7
EQUIVALENT I-131 IN FSV DURING CYCLE 3 AT 70% POWER
(BASED ON IODINE MONITOR)

Isotope	E_{131}/E_i[a]	Plateout, A_p		Circulating, A_c	
		Actual	I-131 Eq.[b]	Actual	I-131 Eq.[b]
I-131	1.0	68	68	0.23	0.23
I-132	28	46	1.6	0.15	0.005
I-133	3.76	100	27	0.46	0.12
I-134	58.5	57	0.1	0.2	0.003
I-135	12.1	75	6.2	0.2	0.016
Total		336	103	1.234	0.37
Technical Specification LCO 4.2.8 limits			10,000		24

[a]Ratio of effectivity of I-131 (rem/μCi inhaled) to the effectivity of isotope i.

[b]I-131 equivalent = actual A_p or A_c divided by E_{131}/E_i.

with cesium or other metal fission products to form CsI, BaI, etc. Figure 4-1 shows that the profiles of cesium and iodine do not match. In fact, the cesium profiles tend to decrease with length while the iodine profiles increase. Moreover, most of the iodine activity was found in the charcoal traps, whereas almost no cesium was found in the charcoal. These profiles suggest that CsI was not a major species in the plateout probe. Table 4-2 summarizes the total amounts found in each tube and filter and the predicted amounts based on the concentration of I-131 inferred from iodine monitor data.

Table 4-2 shows a large discrepancy (factor of 200) between the iodine monitor data and the diffusion tube data. This discrepancy could be caused by one or more of three factors: (1) the diffusion tube flow rates in the reactor were lower than the calculated flows by a factor of 200, (2) the diffusion tubes and charcoal traps did not quantitatively collect all iodine entering the tubes, and (3) the iodine monitor data are a factor of 200 too high.

No evidence exists that the diffusion tube flows were grossly in error (with the possible exception of the C tube), especially since the lab flow calibrations for the T, B, R, and L tubes agreed well with the original calibrations. The iodine monitor data appear to agree well with theory, and no evidence exists that the iodine monitor is grossly in error.* Until the iodine monitor procedures and analysis are checked, the temporary conclusion is that the diffusion tubes did not quantitatively trap the I-131. Evidence for this conclusion is offered below.

The actual loading of iodine on the tubes in FSV is much lower than was originally envisaged when the probe was designed. For example, if I-131 in

*The iodine monitor could give erroneously high results if, during the xenon collection mode, the sample gas was contaminated with primary coolant gas. Examination of the gamma spectra, however, reveal that only Xe-133 and Xe-135 are in the collection traps. If contamination occurred, other long-lived noble gas isotopes would show up in the spectrum, particularly 4.4-h Kr-85m. No krypton was found in the spectrum.

the tubes is assumed to be at sorption equilibrium, the loading can be compared with known sorption isotherms of iodine on stainless steel. Furthermore, since the probe and diffusion tubes were observed to be uniformly gray, indicating surface oxide deposits, then the comparison should be made with sorption of iodine on oxidized stainless steel. At the time the probe was designed, data on iodine adsorption on oxidized stainless steel were not available. In fact, no iodine sorption data on any material were available at the low vapor pressure [0.1 to 100 mPa (10^{-15} to 10^{-12} atm) iodine] in the reactor coolant. Data were available only on iodine on mild steel or low chromium steel at partial pressures of 0.1 mPa (10^{-9} atm) or higher (Ref. 11). Thus, the predicted iodine adsorption on the diffusion tubes could be much higher than that observed due to the tenuous extrapolations from data on the wrong material and at much higher vapor pressure. Since the start of operation of FSV, iodine sorption isotherms have been measured on oxidized stainless steel at iodine vapor pressure reasonably close to that in FSV. This work was accomplished by the Commissariat a L'Energie Atomique (CEA) at Grenoble, France.

Table 4-8 compares the I-131 loadings found in the probe with the CEA isotherm at two iodine partial pressures, equivalent to the iodine monitor data and the diffusion tube data, respectively. The appendix gives details of these calculations. The measured loadings are quite consistent with the CEA isotherm at the partial pressure measured by the iodine monitor rather than the probe. This result suggests that the monitor correctly measured circulating iodine concentration. Table 4-8 shows that the apparent tube iodine loadings are slightly lower than the CEA isotherm prediction. Iodine sorption in the reactor could be argued to be somewhat lower than the ideal conditions in the laboratory because of competition for sorption sites by many other species including fission products, sulfur atoms, and the chemical impurities H_2O, CO, CO_2, and CH_4. In addition, differences in material, surface roughness, and oxidation state could cause differences in iodine sorption. Taking all these possible differences into account, the iodine loadings in the probe are deemed to be in remarkable agreement with the CEA isotherm data (assuming that the partial pressure measured by the iodine

TABLE 4-8
COMPARISON OF PLATEOUT PROBE IODINE LOADINGS WITH THE CEA ADSORPTION ISOTHERM FOR OXIDIZED 347 STAINLESS STEEL

Data Source	Iodine ($\mu g/cm^2 \times 10^9$) 700°C	400°C
Diffusion tubes	3 to 6	20 to 70
Probe end flange		80 to 160
CEA isotherm at 60 nPa (6×10^{-13} atm) iodine[a]	7	120
CEA isotherm at 0.3 nPa (3×10^{-15} atm) iodine[b]	0.03	0.6
GA isotherm (Ref. 11) at 60 nPa (6×10^{-13} atm)[c]	0.15	2×10^6

(a) 60 nPa (6×10^{-13} atm) I-131 corresponds to the iodine monitor data; 1×10^{-5} μCi I-131/cm^3 helium at 70% power. See Table A-4.

(b) 0.3 nPa (3×10^{-15} atm) I-131 is calculated from the diffusion tube inventory using Eq. 2-11.

(c) The GA isotherm was for low-chromium (2-1/4 Cr-1 Mo) steel.

monitor is correct). The Ref. 11 isotherm is apparently incorrect. It appears to assume an almost infinite sink for iodine sorption at 400°C.

The low sorption of iodine on the charcoal trap is difficult to explain. Activated carbon adsorbs iodine irreversibly by chemical reaction to form iodide with metallic charcoal impurities such as sodium, potassium, and iron. About 10^{-5} g-moles of metallic impurities is in the small charcoal bed. On the order of 10^{-9} g-moles of total iodine is passed through each tube. The thermodynamic standard free energies are favorable for the formation of sodium and potassium iodides. On this basis, the charcoal traps should have gettered the iodine quantitatively. The kinetics of iodide formation could be hindered by diffusion through surface scales on the metallic impurity granules or by competition with other chemical species including CO, CO_2, H_2O, and H_2S which are all present in much greater concentration than iodine.

Definite evidence of iodine penetration of a charcoal filter was found when the graphite internal sleeve was gamma scanned. This scan indicated substantial amounts of I-131 (see Fig. 4-4). Iodine can adsorb in the hot graphite sections only after passage through the C tube and its internal trap. Substantial amounts of iodine were also in the cold end of the graphite insert. This iodine could have exited from the T, B, R, and L tubes or could have entered the plenum area from the leakage flow mentioned in Section 4.

4.1.5. Calculation of Circulating and Plated-Out Iodine from the Plateout Probe Data

The arguments above indicate that the diffusion tubes and their charcoal traps did not quantitatively collect all the iodine. The above arguments not withstanding, the probe still could have worked correctly and the iodine monitor incorrectly. (As mentioned in Section 4.1.4, the iodine monitor could yield high results if the xenon sample were contaminated with primary coolant helium.) Until the iodine monitor data can be confirmed,

for comparison, this section assumes that the plateout probe is correct and calculates iodine concentrations accordingly.

The concentration of iodine in the helium is calculated from the diffusion tube inventories using Eq. 2-11. Plateout per pass is calculated using Eq. 2-12. Total circuit plateout is calculated from Eq. 2-3 (Table A-4 gives details). (Equation 2-3 is specifically for radioactive dust but is a general equation that can be used for any condensible species, including iodine.) Equations 2-3 and 2-12, however, rely on an accurate knowledge of concentration and flow rate in the hot (T, B, R) tubes and the cold (C) tube. The C tube, however, was known to have been partially plugged sometime during reactor operation; therefore, the C tube data are questionable. Since, however, the half-life of I-131 is eight days, only the last few weeks of reactor operation are important. Therefore, if the C tube is assumed to have been partially plugged prior to September 1981, then the final calibration flow rate given in Table 3-1 may be used. Table 4-9 lists the plateout probe results using Eqs. 2-3, 2-11, and 2-12. It shows the iodine monitor data and the plateout from R/B calculations for comparison.

The amount of I-131 plated out using the probe data and Eq. 2-3 is quite similar to that calculated from the xenon R/B. This result suggests that the probe data are correct, and conversely, that the iodine monitor is incorrect. Of course, compliance with the Technical Specification LCO 4.2.8 is demonstrated with either of the methods for iodine analysis.

4.2. STRONTIUM, CESIUM, AND BARIUM DATA

Isotopes of strontium, cesium, and barium were found to be distributed in the diffusion tubes and on the external surfaces of the probes. Figures 4-1 and 4-2 plot the concentration versus length along the tubes. Table 4-2 lists total quantities found along with predicted amounts. The predicted values are based on transport of krypton and xenon parents through the diffusion tubes and in-situ radioactive decay.

TABLE 4-9
IODINE CONCENTRATIONS IN THE FSV PRIMARY CIRCUIT
USING THE PLATEOUT PROBE RESULTS

	Plateout Probe	Iodine Monitor	R/B Calc.	Technical Specification LCO 4.2.8 Limit
Circulating I-131 A_c (Ci)	0.004(a)	0.2(b)	--	24
Plated-out I-131, A_p (Ci)	33(c)	--	45(d)	10^4
Plateout per pass I-131, τ (%)	50(e)	0.3(e)	--	--

(a)From Eq. 2-11; average concentrations over last two months of operation.
(b)Concentration at 70% power (see Table 4-6).
(c)From Eq. 2-3 (see Table A-6).
(d)From Eq. 2-6 (see Table A-5).
(e)From Eq. 2-12.

By examination of the profiles in Figs. 4-1 and 4-2 and the total tube inventories in Table 4-2, the modes of release and transport and therefore the total primary circuit inventories can be deduced. The next sections discuss these points in detail.

4.2.1. Mode of Release of Strontium, Barium, and Cesium

The metallic fission products strontium, barium, and cesium have xenon and krypton gaseous precursors. The primary mode of release of these metals from the fuel is, therefore, the release of xenon and krypton followed by radioactive decay in the primary circuit to the solid daughters, strontium, barium, and cesium. These three metals, however, are relatively volatile and diffuse easily through pyrocarbon and graphite. Another mode of release, therefore, is termed direct release, which is the diffusion of metal atoms out of failed particles (or diffusion through the coatings of intact particles with failed SiC layers), followed by diffusion through the fuel element webs, and evaporation into the helium stream.

The relative ease of diffusion in carbon materials is Cs > Sr > Ba. Therefore, cesium would be directly released before strontium or barium. The fuel particles have two long-lived cesium isotopes, Cs-134 (2.06 yr) and Cs-137 (29.9 yr). Cs-137 has a Xe-137 (3.9 min) precursor, while Cs-134 is an activation product of stable Cs-133, which in turn has a Xe-133 (5.27 days) parent. The ratio of Cs-134 to Cs-137 in the fuel is a known quantity, with curies of Cs-134 predominating over Cs-137 because of its shorter half-life. If this same ratio occurs in the primary circuit, for example at the probe, the cesium atoms could be deduced to be released directly from the fuel. If the ratio at the probe is different, for example if Cs-137 is higher than Cs-134 (because of its gaseous parent), then direct release may be insignificant. Table 4-10 lists the observed ratios of Cs-137 to Cs-134.

The observed ratios of Cs-137 to Cs-134 on the probe and on the circulator are definitely higher than in the fuel. This indicates that the actual release of Cs-137 is relatively larger than that of Cs-134, which is

TABLE 4-10
RATIO OF Cs-137 TO Cs-134 IN FSV PRIMARY CIRCUIT

	T Tube	B Tube	R Tube[b]	External Sleeve(c)	Circulator C-2101[a] Cycle 1	Circulator C-2101[a] Cycle 2	FSV Fuel 1 Yr	FSV Fuel 2 Yr
Cs-137/ Cs-134	4.5	4.3	4.0	3.4	5.8	4.3	0.4	0.5

(a) Circulator gamma scans on February 1, 1979 and July 23, 1981.
(b) Cs-134 was too low in the L and C tubes for quantification.
(c) Average of nine measurements (see Fig. 4-6).

to be expected because of its xenon parents. The transport of Cs-134 is discussed in Section 4.2.2.

From these data, it is concluded that little or no direct release of cesium atoms from the core has occurred. Because cesium diffuses more readily than strontium or barium, no direct release of barium or strontium follows. This conclusion is important because it means that the only way that the key isotope Sr-90 was released during the first two fuel cycles was via its Kr-90 precursor.

4.2.2. Mode of Transport of Strontium, Barium, and Cesium

As discussed in Section 2.3.1, condensible fission products have three possible modes of transport (see Fig. 2-7): (1) vapor transport (the steep dashed line in Fig. 2-7), (2) aerosol or particulate transport (the nearly horizontal dashed line), and (3) precursor transport (the solid line). As Figs. 4-1 and 4-2 show, vapor transport for all metallic species can be immediately ruled out, since the axial profiles are all relatively flat with virtually no indication of depletion near the tube entrance.

The observed profiles and inventories indicate a definite precursor transport for some isotopes in some tubes and a combination of precursor and aerosol transport in other tubes. Of course, these statements and this analysis depends on the knowledge of tube flow rates and on the concentration of the xenon and krypton parents (based on grab sample data) in the coolant. For the time being, assume that both of these factors are reasonably accurately known (i.e., that the tube flow parameters in Table 3-1 are correct and that the primary coolant xenon and krypton grab sample data are correct).

As discussed in Section 2.3, the delay times in the T, B, and R tubes are such that flat profiles (i.e., little decay) would be expected for precursor transport. Therefore, in those tubes, the only way to distinguish precursor transport from aerosol transport would be to compare the totals

found with the predicted values based on precursor alone, as was done in Table 4-2.

The L or low flow tube was specifically designed to distinguish aerosol transport from precursor transport. Also, since the C tube was apparently partially plugged, it should also serve as a low flow tube in this regard. (The C tube data are somewhat questionable, however, since when it became plugged is unknown.)

The dashed lines in Fig. 4-2d are calculated based on precursor delay and decay in transit in the L tube. Precursor transport is evident in the Sr-90 data but not in the Sr-89 profile. In the T tube (Fig. 4-2a), however, the measured Sr-90 content is higher than would be predicted by precursor transport alone. In this case, some of the Sr-90 could have been attached to dust particles. The low concentration of Sr-90 in the trap is difficult to explain. If a significant fraction of the tube Sr-90 inventory was in fact attached to particulates, then the fiberfrax traps would be assumed to have accumulated more Sr-90.

In the same tubes, the Sr-89 profiles are flat, as they should be, because the Kr-89 parent has a half-life of 3.2 min and would not deplete to an appreciable extent due to radioactive decay in any of the tubes. The L tube is an exception, with an expected 60% depletion (see Fig. 4-2).

Table 4-2 shows the measured inventories of Sr-89 and Sr-90 to be all relatively close to the calculated precursor inventories, with the possible exception of Sr-90 in the T tube, as mentioned earlier.

The Cs-137 data give other indications of particulate transport. Figures 4-1a through 4-1e show the axial profiles for Cs-137 to be relatively flat. Yet the total Cs-137 transported (see Table 4-2) is higher than from Xe-137 decay by factors of from 1.6 for the L tube and 4 for the T, B, and R tubes. Transport via aerosol particles could explain this phenomenon. (This assessment is made even though the traps did not accumulate high concentrations of Cs-137. See the section below on Cs-134.)

Since the flow rate in the L tube was so low (1/38 of the T, B, and R tubes), the higher flow tubes could be argued to have sampled entrained dust particles more efficiently than the low flow tube.

The case for Ba-140 is less clear. In Table 4-2, the T tube indicated dust transport to be important, while the B and R tubes did not. (Note that the Ba-140 count rates were quite low and therefore are considerably more uncertain than the Cs-137 data.)

Data on two other isotopes yield the most compelling evidence for transport of radionuclides via dust particles. First, the refractory species Pa-233 was observed on and in the probe (see Table 4-1). This isotope was found inside the diffusion tube outlet plenum in relatively high concentrations. In Fig. 2-2, the only flow path to the plenum is either the normal one, through the diffusion tubes and traps, or via leakage from the cold side past the silver O-rings in the thrust cavity. (Section 4 discusses this apparent leak.) Either pathway is quite tortuous and suggests that aerosol particles following those flow paths would be quite stable and/or of small diameter.

The other convincing argument for radioactive aerosols is that Cs-134 was observed in the diffusion tubes. Cs-134 is an activation product of stable Cs-133, which is a decay product of Xe-133. Cs-134 could, in principle, result from direct activation of Cs-133 on the probe (Cs-133 could have been transported to the probe by its Xe-133 precursor). The neutron flux at the probe and the concentration of Cs-133 are far too low, however, to produce measurable amounts of Cs-134 by direct neutron activation on the probe.

Rather, activation to produce Cs-134 must have occurred in the reactor core where the neutron flix is high. This implies that direct release of Cs-134 atoms occurred followed by attachment to aerosol particles. Figure 4-10 shows another possible mechanism. In this mechanism, xenon and krypton are released from failed particles or tramp uranium and diffuse through

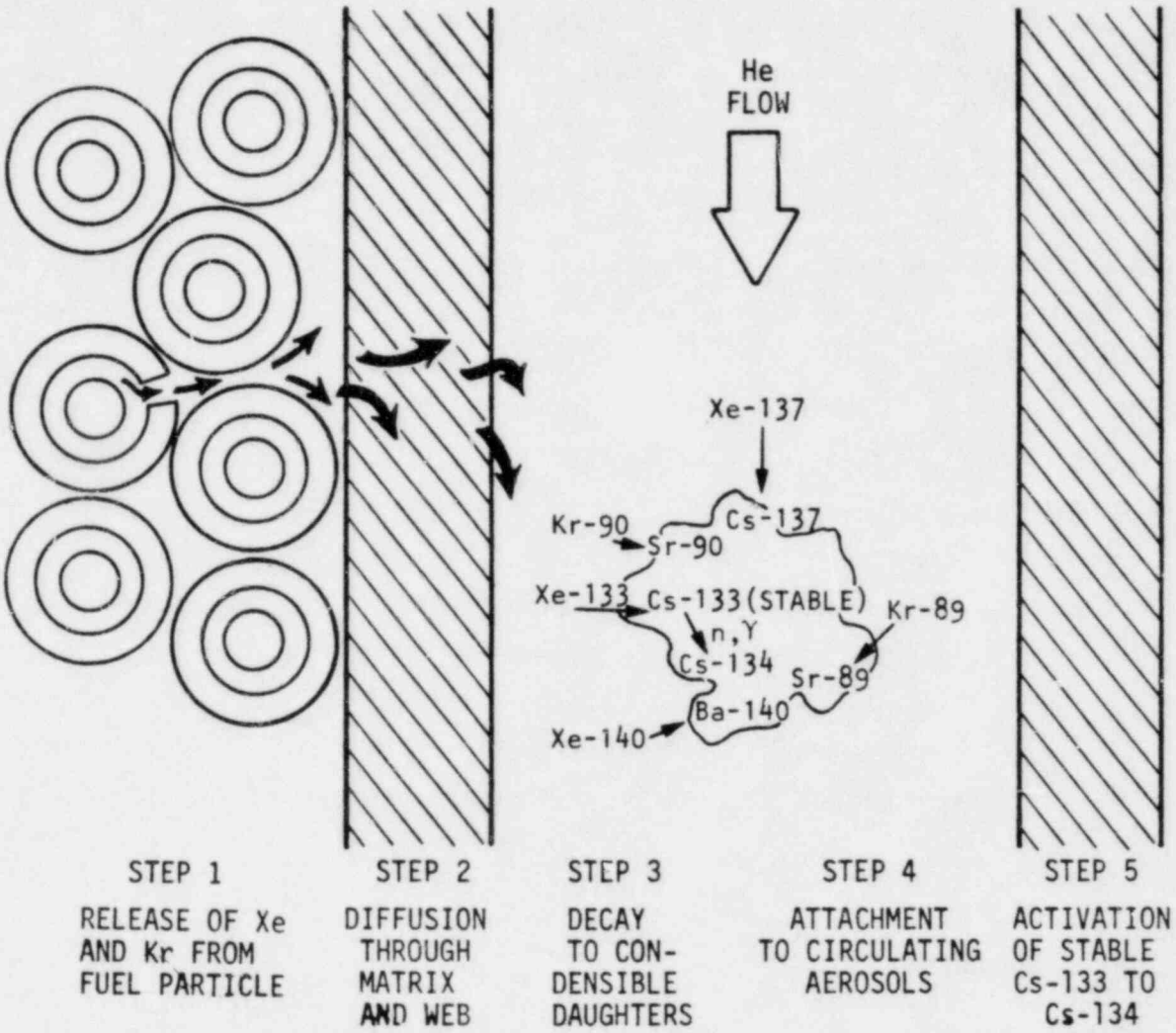

Fig. 4-10. Mechanism for transport of radioactive particles

the graphite web to the primary coolant. They decay in the primary circuit, mainly in the lower cavity which contains about one-half of the total helium inventory and where most of the circuit delay occurs. The daughter products of xenon and krypton are long-lived species of strontium, cesium, and barium, including stable Cs-133.

At the low temperature in the lower cavity, these metal atoms would readily adsorb onto the first surface they happen to collide with, including aerosol particles. Aerosol particles with a diameter of less than 1 μm would tend to be quite stable and could circulate many times around the loop. Cs-133 on stable particles would be activated to Cs-134 during passage through the core. In this way, Cs-134 along with the other metallic isotopes, would be transported to the probe. The only other explanation for the presence of Cs-134 on the probe is that it got there by atomic Cs-134 vapor. As explained above, the diffusion tube concentration profiles are not steep; this rules out the existence of cesium, barium, and strontium vapor in the primary circuit. In addition, as discussed in Section 4.2.1, the direct release of cesium, barium, and strontium atoms from the fuel was apparently small.

To summarize, significant fractions of metallic species of cesium, barium, and strontium are concluded to be attached to aerosol particles. Since the fiberfrax traps did not accumulate much metallic activity, this conclusion is less convincing. The discussion above argued, however, that Cs-134, having no gaseous precursor, can only be transported to the probe by dust or aerosol particles. Yet the traps did not accumulate large concentrations of Cs-134. The Cs-134 aerosol particles must be concluded to be so small that they simply did not accumulate in the fibrous trap. If this is true, then the same could be true for the other metallic species believed to be transported on dust particles.

The following observations are drawn on mode of transport:

1. Direct transport of metal vapor to date is ruled out.

2. Strontium isotopes appear to be transported largely via their krypton precursors with some aerosol transport indicated.

3. Cs-137 appears to be transported largely on dust particles.

4. Trap inventories are generally lower than expected, diminishing the argument for dust transport.

5. Transport of Pa-233 and Cs-134 to the probe can only occur via dust particles. The Cs-134 in the traps was low, proving that the traps did not efficiently remove the stable aerosol particles.

6. The concentrations of Sr-90 and Ba-140 in the diffusion tubes are consistent with R/B of 32-s Kr-90 and 14-s Xe-140 on the R/B versus $t^{1/2}$ line extrapolated in straight line fashion (see Fig. 4-7).

4.2.3. Calculation of Primary Circuit Inventories of Cesium, Barium, and Strontium

Equations 2-3 and 2-4 calculate the total amount of the condensible species cesium, barium, and strontium in the primary circuit. Equation 2-4 calculates the amount in the circuit from gaseous precursor decay. Since direct release of the metals is small, Eq. 2-4 calculates the total inventory in the circuit.

Equation 2-3 utilizes the T diffusion tube data after subtracting out the precursor contribution. The remaining amount is assumed to be transported on dust particles. Table 4-11 lists the results. The calculations show that Cs-137 and Sr-90 are virtually totally associated with the dust particles, while substantial fractions of Ba-140 and Sr-89 were on dust. (All Cs-134 is on dust, because no gaseous precursor contribution exists.)

TABLE 4-11
TOTAL CIRCUIT ACTIVITIES OF
CESIUM, BARIUM, AND STRONTIUM
(Ci)

Isotope	Total Circuit[a]	On Dust[b]	FSAR[c] 30-yr Design Values
Cs-137	1.3	1.9	5460
Cs-134	(0.5)[d]	0.5	--
Ba-140	2.2	0.5	543
Sr-89	18.3	2.9	618
Sr-90	0.66	0.2	280[e]

[a]The total in the circuit was calculated from Eq. 2-4 (see Tables A-7, A-8, A-9), based on gaseous precursor decay in the circuit (except Cs-134).

[b]The curies on dust were calculated from Eq. 2-3 using the T tube inventory (see Table A-6).

[c]Final Safety Analysis Report.

[d]No Cs-134 precursor contribution exists; Cs-134 therefore is virtually all on dust.

[e]Technical Specification LCO 4.2.8 limit.

4.2.4. Measurements of Cesium and Barium Outside of the Probe

A metal sleeve was welded to the outside of the probe specifically to provide samples for metallurgical examination (see Ref. 1). The sleeve was constructed from alternating 2.54-cm (1-in.) long rings of 304 stainless steel, Inconel 600, and Incolloy 800 alloys, all welded together. Figure 2-5 shows the as-manufactured sleeve, and Fig. 3-1 shows its appearance after exposure in the reactor. In Fig. 3-1, the welds between the rings are clearly visible.

The first six rings protruded into the primary coolant stream and therefore were exposed to identical conditions of temperature, flow rate, coolant impurities, dust content, and fission product concentrations. The seventh ring was inside the plenum shroud (see Fig. 2-3) and therefore was not exposed to the identical flow conditions as the first six rings. Consequently, the seventh ring data are not used in the following comparison.

The sleeve was sectioned by cutting 1-cm wide strips from the top and bottom. The strips were then cut into 1-cm long samples. Each sample therefore was about 1 cm^2 of surface area.

Prior to metallurgical examinations, the samples were gamma counted. The results of the counts are given in Fig. 4-6 where concentrations of barium, cesium, and chromium isotopes are plotted versus length. The interesting feature of these data is that in the first six rings Cs-134 and Cs-137 show significantly less plateout on the 304 stainless steel than on the Inconel 600 and Incolloy 800. No differences were found in the plateout of fission product Ba-140 and the activation product Cr-51.

Since the exposure conditions were identical, the difference in cesium plateout must be due to surface conditions, either differences in roughness or in the chemical composition of the oxide scales on the alloys. Since the 304 stainless steel contains less nickel and more iron than the other alloys, chemical differences in the oxide surface may have occurred and therefore affected the adsorption of cesium atoms.

Another explanation, according to Ref. 1, is that the 304 stainless steel sleeve samples showed evidence of spalling, whereas the Inconel 600 and Incolloy 800 alloys did not. Surface spalling occurring occasionally throughout reactor life would lower the surface concentration of long-lived species like Cs-137 (30 yr) and Cs-134 (2.3 yr), relative to the other "non-spalled" alloys. Spalling would not affect the concentration of activation products like Cr-51 because in-situ activation would not be surface oriented. Therefore, the Cr-51 concentration would be relatively constant. Moreover, if spalling of the 304 stainless steel did not occur during the last two to three months of operation, then the concentration of the short-lived Ba-140 would be constant from sample to sample.

4.3. SULFUR DATA

The probe has been analyzed to obtain data on circulating and plated-out S-35. Selected diffusion tube segments were dissolved, and sections of the outer sleeve and cold end flange were leached. These solutions were then subjected to the radiochemical analysis for S-35 content (see Section 3.5). Table 4-12 shows the results of the analyses. Figure 4-3 plots concentration versus length of tube. In general, the plot shows increasing sulfur deposition with tube length or decreasing temperature. This is consistent with preferred adsorption at lower temperatures of gaseous sulfur species such as H_2S, S_2, or SO_2. As mentioned in Section 2.3.5, the most likely species is H_2S, since the concentration of H_2 is always several thousand to 1 million times higher than that of the sulfur impurity.

Table 4-12 shows that the total amount of S-35 in the R tube was about 2 μCi and that more than half was in the charcoal trap and sintered plug. Assuming that the tube and traps quantitatively removed the H_2S, the concentration of S-35 in the helium can be calculated using Eq. 2-13. Furthermore, assuming that the source of the S-35 was fuel matrix (which means that the S-35 was formed in situ by activation of S-34), the concentration or partial pressure of natural sulfur (H_2S) in the coolant can be calculated. Finally, the partial pressure of S_2 is calculated from Eqs. 2-16 and 2-17.

TABLE 4-12
S-35 CONCENTRATIONS IN DIFFUSION PROBE

Segment No.	S-35 (μCi)			
	R Tube[a]	T Tube	L Tube	C Tube
1	0.056	--	--	--
2	~0.03[b]	0.028	0.011	0.052
3	0.011	--	--	--
4	~0.012[b]	0.008	0.018	0.048
5	0.014	--	--	--
6	~0.03[b]	--	--	--
7	0.054	--	--	--
8	~0.1[b]	0.022	0.029	0.0045
9	0.40	--	--	--
10	~0.1[b]	--	--	--
11	0.011	--	--	--
Traps	0.56	--	--	--
Sintered plug	0.65	--	--	--
Total	~2.0			

(a) Tube loading at ~700°C = 0.007 μCi/cm^2
Tube loading at 400°C = 0.04 μCi/cm^2
Cold flange 30.3 μCi or 0.67 μCi/cm^2
Outer sleeve R-2 0.122 or 0.01 μCi/cm^2
Outer sleeve R-4 0.069 or 0.007 μCi/cm^2
Outer sleeve R-6 0.095 or 0.01 μCi/cm^2

(b) These tube segments were not analyzed, values given are interpolated.

This is important because the partial pressure of S_2 dictates whether sulphidation corrosion occurs. Table 4-13 lists the calculation of sulfur concentrations. The concentration of S_2 in the circuit is <0.01 fraction of the threshold for sulphidation corrosion. Reference 1 discusses this in more detail.

4.4. ANALYSIS OF IN-SITU ACTIVATION PRODUCTS

The main activity on the probe and in the diffusion tubes was due to activation products. Most of this was the result of in situ neutron activation of iron, chromium, cobalt, and nickel in the stainless steel as a result of the low neutron flux at the probe location. Some of the activation products were apparently on dust particles (that is, they could be removed by wiping and/or they were found in areas of the probe where in situ activation was less likely, for example in the internal graphite sleeve). Figures 4-5a through 4-5e show axial concentrations of Cr-51, Fe-58, and Co-60 in the diffusion tubes. Other activities not shown include Mn-54 and Co-58. Figure 4-4 shows activation products in the graphite sleeve inside the probe body.

Table 4-14 lists the activation products in the tubes and outer sleeve and internal parts of the probe. The predicted amounts in the tubes are based on in situ activation, using a neutron flux of 1.4×10^7 n/cm^2/s. This flux was calculated assuming neutron streaming into the steam generator cavity.

The concentrations of the activation products Cr-51 and Fe-59 in the B, R, and L tubes are quite close to the calculated amounts, assuming direct neutron activation. The T tube in every case contained more activation than the other tubes. This suggests that either the neutron flux was higher on the top (not likely) or that the up-facing T tube intercepted more radioactive dust than the other tubes. Comparing the total activation product in

TABLE 4-13
SULFUR SPECIES IN PRIMARY CIRCUIT

R tube inventory S-35	2 μCi
S_{nat}/S-35 (Eq. 2-14)[a]	2.8×10^5
$H_2S_{(nat)}$ partial pressure (Eq. 2-15)[b]	0.35 mPa (3.5×10^{-9} atm)
S_2 partial pressure (Eqs. 2-16, 2-17, and 2-18)[b]	0.5 μPa (5×10^{-12} atm)
Sulfur plateout on probe	
Hot side	0.06 μg/cm^2
Cold side	4.2 μg/cm^2
Total sulfur plateout in circuit[c]	30 Ci S-35 168 g S_{nat}

---

[a] Lower limit value since the major source is assumed to be the fuel matrix or core graphite.

[b] Lower limit values since the R tube is assumed to have quantitatively gettered the H_2S.

[c] Total sulfur plated-out calculated assuming that the sulfur plateout on all surfaces at <400°C (~4×10^7 cm^2) is equal to cold-side probe concentration of 4.2 μg/cm^2.

TABLE 4-14
ACTIVATION PRODUCT INVENTORIES

Nuclide	Observed or Calculated	Diffusion Tubes[a] T	Diffusion Tubes[a] B, R, L[b] Average	Diffusion Tubes[a] C	Graphite Sleeeve
Cr-51, μCi (total)	Observed	5.3	3.8	2.7	4.8
Cr-51, μCi/cm[c]	Observed	0.27	0.21	0.25	--
Cr-51, μCi/cm[d]	Calculated	0.28	0.28	0.28	--
Co-60, μCi (total)	Observed	0.75	0.17	0.27	1.3
Co-60, μCi/cm[c]	Observed	0.028	0.009	0.021	--
Co-60, μCi/cm[d]	Calculated	0.003	0.003	0.003	--
Fe-59, μCi (total)	Observed	0.26	0.083	0.08	0.92
Fe-59, μCi/cm[c]	Observed	0.01	0.004	0.006	--
Fe-59, μCi/cm[d]	Calculated	0.003	0.003	0.003	--

[a]Diffusion tubes were made of 304 stainless steel having the following constituent percent: Cr = 19.0, Mn = 1.55, Fe = 69.8, Co = 0.065, Ni = 9.4, Mo = 0.15. Analyses were made by x-ray fluorescence at General Atomic Company.

[b]Activation products of the B, R, and L tubes were virtually identical.

[c]Average μCi/cm found in first 15.24 cm (6 in.) of the probe which extended into the hot coolant stream exposed to the neutron streaming.

[d]μCi/cm calculated using a neutron flux of 1.4×10^7 n/cm^2/s.

the graphite sleeve with the tubes reveals a larger than expected inventory in the graphite, based solely on direct activation of the graphite impurities, iron, chromium, and cobalt, which are normally in the parts per million range or less. This suggests that radioactive dust particles contaminated the graphite.

5. CONCLUSIONS

Remarks and conclusions on each of the stated objectives are provided below.

5.1. COMPLIANCE WITH TECHNICAL SPECIFICATION LCO 4.2.8

Table 5-1 summarizes the data on iodine and strontium to demonstrate compliance with Technical Specification LCO 4.2.8.

As explained in the text, the plateout probe and the iodine monitor have a discrepancy with respect to circulating iodine. Until this is resolved, the iodine monitor data can be used, since it provides the higher value of circulating iodine.

5.2. SULFUR VAPOR PRESSURE

The vapor pressures of H_2S and S_2 in the primary circuit were calculated from the R tube inventory assuming the following:

1. The tube quantitatively gettered the H_2S.
2. The tube flow rates were correct.
3. The source of the H_2S was the fuel matrix.
4. The species S_2, H_2S, and H_2 are in thermodynamic equilibrium:

$$P_{H_2S} = 0.35 \text{ mPa } (3.5 \times 10^{-9} \text{ atm}) \quad .$$

$$P_{S_2} = 0.5 \text{ µPa } (5 \times 10^{-12} \text{ atm}) \quad .$$

The concentration of S_2 is too low for deleterious sulphidation in the FSV circuit. This is confirmed by the corrosion analysis in Ref. 1.

TABLE 5-1
STRONTIUM AND IODINE ACTIVITIES IN PRIMARY CIRCUIT

	Plateout Probe	Iodine Monitor	R/B Calculation	Technical Specification LCO 4.2.8 Limit
Circulating I-131	0.004	0.6	--	24
Plateout I-131	33	--	45	10,000
Plateout Sr-90	0.4	--	0.4	280

5.3. METALLIC CORROSION

Metallic corrosion of the outer sleeve was virtually nonexistent, as reported in Ref. 1.

5.4. CONCENTRATION OF OTHER FISSION PRODUCTS

The only fission products found on the probe were cesium, barium, and strontium. All of these have gaseous precursors. The concentrations found were low (totalling less than 25 Ci in the circuit), consistent with release and decay of noble gases in the primary circuit.

5.5. CHEMICAL SPECIES AND MODE OF TRANSPORT

The ratio of Cs-137 to Cs-134 was high, indicating little or no direct release of the metals cesium, barium, and strontium. The diffusion tube profiles were not steep, ruling out metallic vapors. The profiles and inventories of cesium, barium, and strontium showed a combination of noble-gas precursor and dust transport.

The fact that the internal traps did not accumulate larger amounts of activity diminishes the argument for dust transport. Cs-134 and Pa-233, however, have no gaseous precursors and therefore were totally transported to the probe on dust particles. These facts suggest that the dust particles were extremely small, in the aerosol category, and therefore were not efficiently removed by the traps and/or filters.

5.6. ACTIVATION PRODUCTS

The quantities of some activation products indicate that in situ activation of probe materials (chromium, cobalt, and iron) occurred. The estimated neutron flux of 1.4×10^7 n/cm^2/s is appropriate for the probe location. Some activation product concentrations were higher than expected, however, indicating a dust transport mechanism.

6. ACKNOWLEDGMENTS

The original probe design was pioneered by F. Vanslager and R. Lansley of General Atomic Company. Vanslager also delineated most of the calculational analysis used in this report. D. Hanson, N. L. Baldwin, and D. Alberstein later updated Vanslager's original documents and paved the way for the logical radiochemical work and analytical interpretations to follow.

The probe disassembly, flow testing, gamma scanning, and general radiochemical sleuthing was performed by John Greenwood with assistance from Tom Crockett, Dale Hill, and Mark Hiatt. Dale Hill performed most of the gamma counting and interpretation of the gamma spectra. Mark Hiatt performed the radiochemistry on strontium, and Diane Fleischman was responsible for the sulfur analyses. The success of the laboratory effort is due largely to the careful planning by N. L. Baldwin and methodical and painstaking work by John Greenwood and the others.

This study could not have been conducted without the help of the Public Service Company of Colorado, which owns and operates the FSV reactor. Their support and timely comments are appreciated.

Finally, thanks are given to D. Alberstein, D. Jensen, D. Hanson, and O. M. Stansfield who provided valuable editorial assistance.

All of the efforts of the co-workers are gratefully acknowledged.

7. REFERENCES

1. Johnson, W. R., "Metallographic Examination of Plateout Probe Sleeve," General Atomic Report GA-A-16800, to be published.
2. Vanslager, F. E., "Proposed Analysis and Interpretation of the Fort St. Vrain Plateout Probes," USAEC Report GAMD-9768, General Atomic Company, August 1970.
3. Hanson, D. L., N. L. Baldwin, and D. Alberstein, "Fort St. Vrain Plateout Probes," General Atomic Report GA-A14402, October 1977.
4. Busch, D. D., "The Nature of Condensible Fission Products in an HTGR Environment," USAEC Report GA-6957, General Dynanics, General Atomic Division, April 15, 1966.
5. Gormley, P. G., and M. Kennedy, "Diffusion from a Stream Flowing Through a Cylndrical Tube," Proc. Roy. Irish Acad. A 52, 163-169 (1949).
6. Browning, W. E., Jr., and R. D. Ackley, "Diffusional Characterization of Millimicron Radioactive Aerosols and Their Removal from Reactor Gases," in "Nuclear Safety Program Semiannual Progress Report for the Period Ending December 31, 1962," Oak Ridge National Laboratory Report ORNL-3401, March 8, 1963, p. 44.
7. Roos, B. W., "On the Dispersion of a Substance in a Stream Flowing Through a Cylindrical Tube," General Dynamics, General Atomic Division Report GA-6733, October 1, 1965.
8. Vanslager, F. E., et al., "Fission Product Transport in HTGR Systems - A Summary," General Atomic Report GA-10073, April 22, 1970.
9. Scheffel, W. J., N. L. Baldwin, and R. W. Tomlin, "Operating History Report for the Peach Bottom HTGR. 1. Reactor Operating History," ERDA Report GA-A13907, v. 1, General Atomic Company, August 31, 1976.
10. Mellor, J. W., "Comprehensive Treatise on Inorganic and Theoretical Chemistry," Longmans, Green and Company, London, May 1936.

11. Hoinkis, E., "A Review of the Adsorption of Iodine on Metals and its Behavior in Loops," USAEC Report ORNL-TM-2916, Oak Ridge National Laboratory, May 1970.

APPENDIX

SAMPLE CALCULATIONS

TABLE A-1
SUMMARY OF RADIONUCLIDE PARAMETERS

Gaseous Fission Product Precursors and Metallic Daughters
Kr-89 (3.2 min) → Rb-89 (15.4 min) → Sr-89 (50.5 days) → Y-89 (stable)
Kr-90 (32 s) → Rb-90 (2.7 min) → Sr-90 (28 yr) → Y-90 (64.3 h) → Zr-90 (stable)
Xe-137 (3.9 min) → Cs-137 (30 yr) → Ba-137m (2.57 min) → Ba-137 (stable)
Xe-140 (13.6 s) → Cs-140 (66 s) → Ba-140 (12.8 days) → Kr-140 (40.2 h) → Ce-140 (stable)
Gaseous Fission Product Precursors and Metallic Activation Products
Xe-133 (5.3 days) → Cs-133 (stable) $\xrightarrow{n,\gamma}$ Cs-134 (2.3 yr) → Ba-134 (stable)
Iodine Fission Products and Xenon Daughters
I-131 (8.05 days) → Xe-131 (stable)
I-133 (20.7 h) → Xe-133 (5.27 days)
I-135 (6.7 h) → Xe-135 (9.17 h)

TABLE A-2
FISSION PRODUCT PARAMETERS

	$t_{1/2}$	λ (s^{-1})	Fraction Fission Yields	
			U-235	U-233
Kr-90	32 s	2.15×10^{-2}	0.0505	0.045
Sr-90	29 yr	7.6×10^{-10}	0.059	0.069
Kr-89	3.2 min	3.65×10^{-3}	0.046	0.054
Sr-89	50.5 days	1.59×10^{-7}	0.049	0.063
Xe-140	13.6 s	5.1×10^{-2}	0.037	0.015
Ba-140	12.8 days	6.3×10^{-7}	0.063	0.065
Xe-137	3.8 min	3.0×10^{-3}	0.061	0.060
Cs-137	30.1 yr	7.3×10^{-10}	0.062	0.068
Xe-133	5.27 days	1.5×10^{-6}	0.067	0.060
Cs-133	stable	--	0.067	0.060
Cs-134	2.06 yr	1.07×10^{-8}	--	--
I-131	8.05 days	9.7×10^{-7}	0.029	0.036
I-133	20.7 h	9.2×10^{-6}	0.067	0.060
I-135	6.7 h	2.9×10^{-5}	0.063	0.049

TABLE A-3
SAMPLE CALCULATIONS OF FLOW PARAMETERS

Q_c for T tube laboratory calibration at 16°C (60°F), 0.1 MPa (1 atm) pressure, and 34 kPa (5 psi), ΔP = 2.6 cm^3 He/s.

Q_r flow in the reactor (Eq. 3-3):

$$Q_r = Q_c \left(\frac{T_c}{T_R}\right)^{0.678} = 2.6 \left(\frac{288}{997}\right)^{0.678} = 1.1 \text{ cm}^3\text{/s} \quad .$$

Volume flow in reactor at STP:

$$1.1 \text{ cm}^3\text{/s} \times \frac{273}{997} \times 47.5 \text{ atm} = 14.6 \text{ cm}^3\text{/s} \quad .$$

$$\text{Mass flow in reactor} = \frac{14.6 \times 4 \text{ g-mole}}{22{,}400 \text{ cm}^3\text{/mole}} = 2.6 \times 10^{-3} \text{ g/s} \quad .$$

$$\text{Velocity in tube T} = \frac{1.1 \text{ cm}^3\text{/s}}{0.12 \text{ cm}^2} = 9.1 \text{ cm/s} \quad .$$

$$\text{Delay time in tube T} = \frac{4 \text{ cm}^3 \text{ vol}}{1.1 \text{ cm}^3\text{/s}} = 3.6 \text{ s} \quad .$$

TABLE A-4
CALCULATIONS OF IODINE VAPOR PRESSURE

$$P_{I-131} = \frac{A_c \times C_1 \times C_2 \times P_{He}}{V_\ell \lambda NA} ,$$

where A_c = circulating I-131 ($\mu Ci/cm^3$),
V_ℓ = loop volume 2.1×10^{10} cm^3 STP,
C_1 = 3.7×10^4 dps/μCi,
C_2 = 22,400 cm^3 STP/mole He,
P_{He} = 46 atm,
λ = 9.7×10^{-7} s^{-1},
NA = Avogadro's No. (6×10^{23} atoms/mole).

$$P_{I-131} = \frac{0.23 \times 10^6 \ \mu Ci \times 3.7 \times 10^4 \times 22{,}400 \times 46}{2.1 \times 10^{10} \ cm^3 \times 9.7 \times 10^{-7} \times 6 \times 10^{23}}$$

$$= 0.7 \text{ nPa } (7 \times 10^{-13} \text{ atm}) .$$

TABLE A-5
SUMMARY OF CALCULATIONS OF TOTAL PLATEOUT IODINE IN DIFFUSION TUBES AT SHUTDOWN, NOVEMBER 9, 1981

Dates at Power 1981	% Power/ R/B[a] x 10^6	t_1/ t_2 x 10^{-5}	A_i, Circuit Total[b] I-131 Plateout (Ci)	A_c, I-131 Circulating[c] (Ci)	Expected I-131 in Tubes[d] (μCi) T	B	R	L	C
11/7 + 11/9	100/5.0	2.2/0	22	0.37	50	55	46	1.3	7.2
11/4 + 11/6	70/4.5	1.7/2.2	11	0.23	20	22	18	0.5	2.9
10/9 + 10/27	30/3.5	16/11	23	0.10	19	21	17	0.5	2.8
8/5 + 10/9	70/4.5	56/26	75	0.23	13	14	12	0.3	1.9
Total at 11-9-81			45	0.37	102	112	93	2.6	14.8

[a] R/B extrapolated from xenon line cycle 3, Fig. 4-7, and adjusted for reactor levels.
[b] Total plateout for each time increment is calculated from Eq. 2-6. A total of 45 Ci is decayed to reactor shutdown on November 9, 1981.
[c] Circulating or gas phase I-131 is calculated from Eq. 2-8 assuming that the rate of plateout, r_p, is constant.
[d] I-131 in diffusion tubes is calculated from Eq. 2-11.

Sample Calculations:

$$A_i = 0.85\ P\bar{\gamma}\ R/B\ (1 - e^{-\lambda t_1}) \quad . \qquad \text{Eq. 2-6}$$

At 100% power, $A_i = 0.85\ 842 \times 10^6\ 0.032\ 5 \times 10^{-6}\ (1 - e^{-9.7 \times 10^{-7}\ 2.2 \times 10^5})$.

$$A_i = 22\ \text{Ci} \quad .$$

$$A_c = \frac{0.85\ P\ R/B\ \bar{\gamma}\ [1 - e^{-(\lambda + \gamma_s + \gamma_p)t}]}{1 + (r_s + r_p)/\lambda} \quad . \qquad \text{Eq. 2-8}$$

At 100% power, $A_c = \dfrac{0.85\ 842 \times 10^6 \times 5 \times 10^{-6} \times 0.032\ [1 - e^{-(9.7 \times 10^{-7} + 3.3 \times 10^{-5} + 2.7 \times 10^{-4})\ 2.2 \times 10^5}]}{1 + (3.3 \times 10^{-5} + 2.7 \times 10^{-4})/9.7 \times 10^{-7}}$.

$$A_c = 0.37\ \text{Ci} \quad .$$

$$I_x = \frac{A_c\ F_x}{\lambda\ V_\ell}\ (1 - e^{-\lambda t_1})\ e^{-\lambda t_2} \quad . \qquad \text{Eq. 2-11}$$

At 100% power, T tube $I_T = \dfrac{0.37 \times 10^{-6}\ \mu\text{Ci}\ 14.5\ \text{cm}^3/\text{s}}{9.7 \times 10^{-7} \times 2.1 \times 10^{10}\ \text{cm}^3}\ (1 - e^{-9.7 \times 10^{7}\ \ 2.2 \times 10^{8}})$.

$$I_T = 50\ \mu\text{Ci} \quad .$$

TABLE A-6
CALCULATION OF CIRCUIT CONCENTRATIONS OF IODINE AND DUST-BORNE METALLIC FISSION PRODUCTS USING EQ. 2-3

	Top Tube (μCi)			C Tube (μCi)			Circuit
Isotope	Total	- Precursor	= Dust	Total	- Precursor	= Dust	Ci on Dust
Cs-137	0.018	0.0032	0.0148	0.0048	0.005	0	1.9
Ba-140	0.012	0.008	0.004	—	—	—	0.5
Sr-89	0.07	0.048	0.022	0.065	0.071	0	2.9
Sr-90	0.003	0.0014	0.0016	0.0008	0.0016	0	0.2
I-131(a)	0.56	—	—	0.045	—	—	33(a)

(a)Iodine is not associated with dust, but Eq. 2-3 is used for this calculation since it is a condensible species.

Sample calculation:

$$M_{t_{dust}} = \left(\frac{M_{h_{dust}}}{f_h} - \frac{M_{c_{dust}}}{f_c} \right) F_R \quad . \qquad \text{Eq. 2-3}$$

Cs-137

$$M_{t_{dust}} = \left(\frac{1.48 \times 10^{-2}}{2.6 \times 10^{-3}\ g/s} - 0 \right) 3.4 \times 10^{5}\ g/s$$

$$= 1.9 \times 10^{6}\ \mu Ci \text{ or } 1.9\ Ci \quad .$$

I-131

$$\text{I-131 circuit} = \left(\frac{0.56}{2.6 \times 10^{-3}} - \frac{0.045}{0.38 \times 10^{-3}} \right) 3.4 \times 10^{5}\ g/s$$

$$= 33 \times 10^{6}\ \mu Ci \text{ or } 33\ Ci \quad .$$

TABLE A-7
CALCULATIONS[a] OF Cs-137 AND Sr-90 FROM RELEASE AND DECAY OF Xe-137 AND Kr-90

Isotope	Power Level (%)	R/B	EFPD	Time at Power[b] (s)	M_{gt} Eq. 2-4 (Ci)	M_{gx} Tube Inventories Eq. 2-5 (nCi) T,B,R	L	C
Xe-137/	30	7×10^{-7}	0 to 80	2.3×10^{7}	0.15	—	—	—
Cs-137	70	3×10^{-6}	80 to 408	4.0×10^{7}	1.12			
Total					1.27	3.2	2.7	5
Kr-90/	30	6×10^{-7}(c)	0 to 80	2.3×10^{7}	0.11	—	—	—
Sr-90	70	7×10^{-7}(c)	80 to 408	4.0×10^{7}	0.50			
Total					0.66	1.4	0.46	1.6

(a)Calculations assume that the first 80 EFPD were at 30% power and the remaining 328 EFPD were at 70%.

(b)Time at power (s) = EFPD x 8.64 x 10 s/day ÷ power.

(c)The Kr-90 R/B's were extrapolated from the R/B versus $t^{1/2}$ lines. The calculated Sr-90 values are, therefore, probably upper limits.

Typical Calculations:

$$M_{gt} = G\,(1 - e^{-\lambda m t})(e^{-\lambda m t_2}) \quad \text{where } G = 0.85\,\bar{\gamma}\,R/B\,P \quad . \qquad \text{Eq. 2-4}$$

$$M_{gt} = (0.85)(842 \times 10^{6} \times 0.70\ W)(0.060)(1.3 \times 10^{-6})\,(1 - e^{-7.3 \times 10^{-10}\ 4 \times 10^{7}\ s}) \quad .$$

M_{gt} = 1.12 Ci Cs-137 [the $(e^{-\lambda m t_2})$ term is neglected for long-lived Sr-90 and Cs-137] .

$$M_{gx} = \frac{M_{gt}\,F_x\,(1 - e^{-\lambda g \tau_x})}{\lambda g\,V_t} \quad \text{using T tube flow of } 14.6\ cm^3\ \text{STP/s} \quad . \qquad \text{Eq. 2-5}$$

$$M_{gx} = \frac{1.27\ Ci\ 14.6\ cm^3/s\,(1 - e^{-3 \times 10^{-3}\ 3.6})}{3 \times 10^{-3}\ 2.1 \times 10^{10}\ cm^3} = 3.2 \times 10^{-9}\ Ci \text{ or } 3.2\ nCi \text{ in T tube} \quad .$$

TABLE A-8
CALCULATIONS[a] OF Sr-89 FROM GASEOUS PRECURSOR Kr-89

Dates at Power 1981	Power (%)	t_1 ($s \times 10^5$)	t_2 ($s \times 10^5$)	R/B $\times 10^6$	Kr-89, G_1 (Ci)	Sr-90, M_{gt} Eq. 2-4 (Ci)	M_{gx} Tube Inventories Eq. 2-5 (nCi)		
							T,B,R	L	C
11/7 → 11/9	100	2.2	0	1.8	64	2.25	—	—	—
11/4 → 11/6	70	1.7	2.2	1.3	31	0.82	—	—	—
10/9 → 10/27	30	16	11	1.0	10.7	2.0	—	—	—
8/5 → 10/9	70	56	26	1.3	31	12.1	—	—	—
4/10 → 5/12	70	28	150	1.3	31	1.0	—	—	—
1/20 → 3/20	70	24	200	1.3	31	0.4	—	—	—
10/30 → 12/31 (1980)	70	52	213	1.3	31	0.6	—	—	—
Total						19.2	48	38	71

[a]Separate calculations using Eqs. 2-4 and 2-5 for the power operation listed in columns 1 and 2.

Typical Calculations:

$$M_{gt} = 0.85\ P\ \bar{\gamma}\ R/B\ (1 - e^{-\lambda m t_1})(e^{-\lambda m t_2}) \quad . \qquad \text{Eq. 2-4}$$

For 100% power, $M_{gt} = (0.85)(842 \times 10^6)(0.05)(1.8 \times 10^{-6})(1 - e^{-1.6 \times 10^{-7}\ 2.2 \times 10^5}) = 2.25$ Ci

$(t_2 = 0)$.

$$M_{gx\ (T\ tube)} = \frac{M_{gt}\ F_x\ (1 - e^{-\lambda g \tau_x})}{\lambda g\ V_\ell} = \frac{19.2\ \text{Ci}\ 14.6\ (1 - e^{-0.0365 \times 3.6})}{0.00365\ 2.1 \times 10^{10}} = 4.8 \times 10^{-8}\ \text{Ci or 48 nCi} \quad . \text{ Eq. 2-5}$$

TABLE A-9
CALCULATIONS OF Ba-140 FROM GASEOUS PRECURSOR Xe-140

Dates at Power 1981	Power (%)	t_1 ($s \times 10^{-5}$)	t_2 ($s \times 10^{-5}$)	R/B[b] Xe-140 $\times 10^7$	Xe-140, Gi (Ci)	Ba-140, M_{gt} Eq.2-4 (Ci)	M_{gx} T,B,R (nCi)
11/7 → 11/9	100	2.2	0	5	10.0	1.3	—
11/4 → 11/6	70	1.7	2.2	4	5.6	0.5	—
10/9 → 10/27	30	16	11.5	3	1.8	0.6	—
8/5 → 10/9	70	56	26	4	5.6	1.0	—
Total						3.4	7.8

[a]Calculations of Ba-140 using Eqs. 2-4 and 2-5 and 1981 power history given in columns 1 and 2.
[b]The R/B of Xe-140 was obtained by extrapolation of the R/B versus $t^{1/2}$ time for cycle 3 given in Fig. 2-8.

Typical Calculations:

$$M_{gt} = 0.85\ P\ \bar{\gamma}\ R/B\ (1 - e^{-\lambda m t_1})(e^{-\lambda m t_2}) \quad . \qquad \text{Eq. 2-4}$$

At 100% power, $M_{gt} = 0.85\ 842 \times 10^6\ 0.028 \times 5 \times 10^{-7}\ (1 - e^{-6.3 \times 10^{-7}\ 2.2 \times 10^5})$

$$= 1.3 \text{ Ci Ba-140} \quad .$$

$$M_{gx\ (\text{Top tube})} = \frac{M_{gt}\ F_x\ (1 - e^{-\lambda \tau_x})}{\lambda g\ V_\ell} \quad . \qquad \text{Eq. 2-5}$$

$$M_{gx} = \frac{3.4 \text{ Ci } 14.6\ (1 - e^{-0.051\ 3.6})}{0.051\ 2.1 \times 10^{10}} = 9.6 \times 10^{-9} \text{ Ci or } 9.6 \text{ nCi} \quad .$$

TABLE A-10
CALCULATIONS OF SULFUR CONCENTRATIONS

$$S\text{-}35_{tot} = \frac{2\ \mu Ci \times 9.4 \times 10^{-8} \times 2.1 \times 10^{10}\ cm^3}{(1 - e^{-9.4 \times 10^{-8}\ 2 \times 10^{7}\ s})\ 13.2} \qquad \text{Eq. 2-13}$$

$$= 352\ \mu Ci\ S\text{-}35\ in\ He \quad .$$

$$\frac{N_s}{Ns\text{-}35} = \frac{9.4 \times 10^{-8}}{4 \times 10^{13} \times 0.042 \times 2.3 \times 10^{-25} (1 - e^{-9.4 \times 10^{-8}\ 2 \times 10^{7}\ s})}$$

$$= 2.86 \times 10^{5} \quad . \qquad \text{Eq. 2-14}$$

$$P_{H_2S} = 2.86 \times 10^{5} \frac{352\ \mu Ci \times 3.7 \times 10^{4}\ dps/\mu Ci \times 46\ atm\ He}{9.4 \times 10^{-8}\ 6 \times 10^{23} \times 8.5 \times 10^{5}\ g\text{-}moles\ He}$$

$$= 0.35\ MPa\ (3.5 \times 10^{-9}\ atm)\ H_2S \quad . \qquad \text{Eq. 2-15}$$

$$P_{S_2} = \frac{\left(P_{H_2S}\right)^2}{\left(P_{H_2}\right)^2 K} = \frac{(3.5 \times 10^{-9})^2}{(1.38 \times 10^{-4})^2\ e^{-9800/1.99(1000)}} \quad .$$

$$= P_{S_2} = 0.47\ \mu Pa\ (4.7 \times 10^{-12}\ atm) \quad . \qquad \text{Eq. 2-16, 2-17, 2-18}$$

GENERAL ATOMIC COMPANY
P. O. BOX 81608
SAN DIEGO, CALIFORNIA 92138